2nd International Workshop on Advanced Materials and Innovative Systems in Structural Engineering: Novel Researches

ISTANBUL
fib CEB-FIP Turkey
IWAMISSE
2019

Proceedings

Editors: Alper Ilki, Yavuz Selim Çavunt

İTÜ   İSTANBUL TEKNİK ÜNİVERSİTESİ 1773   fib CEB-FIP Turkey

Proceedings of IWAMISSE 2019
2nd International Workshop
on Advanced Materials and Innovative Systems in
Structural Engineering: Novel Researches

Editors
Alper İlki
Yavuz Selim Çavunt

September 2019

2nd International Workshop on Advanced Materials and
Innovative Systems in Structural Engineering: Novel Researches
IWAMISSE 2019, Istanbul, Turkey
September 20, 2019

Preface

The Second International Workshop on Advanced Materials and Innovative Systems in Structural Engineering: Novel Researches, IWAMISSE 2019, is co-organised by The International Federation for Structural Concrete Turkey Branch, *fib*-Turkey, and Istanbul Technical University, ITU, on September 20, 2019 at ITU.

The International Federation for Structural Concrete, *fib*, is a not-for-profit association formed by 42 national member groups and approximately 1000 corporate and individual members. The *fib*'s mission is to develop at an international level the study of scientific and practical matters capable of advancing the technical, economic, aesthetic and environmental performance of concrete construction.

Istanbul Technical University (ITU) was established in 1773 and is a state university which defined and continues to update methods of engineering and architecture in Turkey. It provides its students with innovative educational facilities while retaining traditional values, as well as using its strong international contacts to mould young, talented individuals who can compete not only within their country borders but also in the global arena. With its educational facilities, social life and strong institutional contacts, ITU has always been preferred by Turkey's most distinguished students since its foundation and has achieved a justified respect.

The workshop covers the topics of advanced materials and innovative systems in structural engineering with a focus on seismic practices as well as other issues related with steel fiber reinforced concrete, anchors/fasteners, precast structures, and recent advances on different types of structural systems such as reinforced concrete, steel, and reinforced masonry structures.

This event which is organized for the second time will provide a platform for exploring the potential national and international cooperation schemes in terms of research and application on the areas covered within the scope of the workshop.

A part of this workshop is devoted to papers presenting the initial outcomes of the TUBITAK-RCUK Project "Rapid Earthquake Risk Assessment and Post-Earthquake Disaster Management Framework for Substandard Buildings in Turkey" coordinated jointly by Istanbul Technical University and Sheffield University.

This proceeding book contains twelve papers from five countries worldwide. We have no doubt that the up-to-date subjects covered during the workshop will be highly beneficial for the academicians and practitioners in the field. We would like to thank all authors for their contributions to the workshop as well as the members of the International Scientific Committee for their rigorous work for reviewing the papers. We also gratefully acknowledge the support of the sponsoring companies and we express our sincere thanks to organization committee for their tireless efforts in the overall organization of the workshop. Many thanks go as well to undergraduate and graduate students from ITU for their assistance during all stages of the workshop.

Alper Ilki, Yavuz Selim Cavunt

20 September 2019

Organization

Chair

Alper Ilki   Istanbul Technical University
                                               Istanbul / Turkey

Workshop Secretary

Derya Cavunt   Istanbul Technical University
                                               Necmettin Erbakan University
                                               Istanbul / Turkey

Sponsors

International Scientific Committee

Akio Kasuga	Hilmi Luş	Medine Ispir
Beyza Taşkın	Hugo Corres Peiretti	Oğuz Cem Çelik
Cem Demir	Kutay Orakçal	Riadh Al-Mahaidi
David Fernández-Ordóñez	Kypros Pilakoutas	Susumo Kono
Elişan Filiz Piroğlu	Larbi Sennour	Tülay Aksu Özkul
György L. Balazs	Marco Di Ludovico	Ufuk Yazgan
Hasan Hüsnü Korkmaz	Maria Polese	

Table of Contents

Papers

Development of a new seismic damage evaluation system based on the capacity spectrum method

Koichi KUSUNOKI[1], and Masaomi Teshigawara[2]

[1] Professor, Earthquake Research Institute, the University of Tokyo, Tokyo, Japan
[2] Professor, Graduate school of environmental studies, Nagoya University, Nagoya, Japan

ABSTRACT: To reduce further more damage to structures and the number of people displaced from their home due to an aftershock, a quick inspection of damaged buildings is required. However, the buildings require individual inspection by engineers under the present situation. The judgment of the building's safety can vary according to the engineers' experience, and it is time-consuming to investigate every damaged building. This chapter introduces a new real-time residual seismic capacity evaluation system for buildings, currently in development by the corresponding author, which utilizes a few inexpensive accelerometers. The system is based on the capacity spectrum method. This system makes it possible to not only to evaluate the damage level of the instrumented building during the mainshock but to also predict the level of damage resulting from an aftershock of equal magnitude to the mainshock. In order to apply the capacity spectrum method, the response displacement is needed. It is derived from firstly using the wavelet transform method to decompose the measured acceleration, recomposing the acceleration considering only the predominant response, then performing a double integral. The validity of the system is confirmed with the measured accelerations of instrumented buildings during the 2011 Tohoku earthquake and shaking table tests.

1   INTRODUCTION

Once a large shaking intensity earthquake event occurs, many buildings incur severe damage, and consequently, it gives rise to many homeless. The damage level could increase due to an aftershock in some buildings, and enormous harm to the inhabitants in such buildings could occur. On the contrary, some people could get caught up in fear and leave buildings which have enough residual seismic capacity from the engineering point of view. Hence, the number of homeless can increase drastically. In order to determine the further potential for damage in a building due to an aftershock and to reduce the amount of homeless, a quick inspection on the damaged buildings must be conducted soon after the mainshock. However, under the present situation, the buildings have to be investigated one by one by engineers or researchers. For example, 5,068 engineers took 19 days to investigate 46,000 buildings within a damaged area following the 1995 Kobe earthquake (BCJ (1996)). Nineteen days were too long, and yet even more buildings still required investigation.

Moreover, many buildings received a "Caution" level, which meant that further detailed investigation by engineers was required. "Caution" judgment is a gray zone and left many inhabitants afraid of remaining in the building. Furthermore, the current quick investigation system presents a dilemma since buildings only visual observation were performed by engineers at this stage, and hence, this judgment varies according to the engineers' experiences. One

potential approach to assess the safety of buildings quickly is to use information from structural health monitoring devices, and pair it with the equivalent linearization method, which was proposed to evaluate non-linear response by simplifying the multi-degree-of-freedom (MDoF) response down to that of a single-degree-of-freedom (SDoF) system (Freeman (1978), Freeman (2004)). The maximum response during an earthquake can thus be predicted by comparing the performance and demand curves, which are the simplified relationship between restoring force and deformation of SDoF and the relationship between response acceleration and displacement spectra, respectively (Freeman (2004)). If it is possible to calculate the performance and demand curve from a measured acceleration of the basement and of each floor of a structure with cheap accelerometers, and further estimate the residual seismic capacity of a structure by comparing these curves, the problems mentioned in the previous paragraph can be solved.

The absolute response accelerations and relative response displacement on each floor are needed for the performance curve. A certain fixture is generally needed to measure the inter-story drift or the relative response displacement to the basement, which may be obstructive for usage. On the contrary, it is easy to measure accelerations with accelerometers. If displacements could be derived reliably from the accelerations using double integration, the performance curve of structures can be easily measured.

In this chapter, a new real-time residual seismic capacity evaluation system was proposed to address the needs discussed. Furthermore, shaking table tests with steel plane frame was carried out to confirm the validity of the proposed evaluation system.

2   CONFIGURATION OF THE SYSTEM AND OUTLINE OF THE EVALUATION

The proposed system uses one accelerometer on each floor and one judgment machine, as shown in Figure 1. The evaluation method is based on the performance design concept, as shown in Figure 2. The capacity curve in Figure 2 is the relationship between the representative restoring force and representative displacement, which are derived from the measured accelerations and are explained in detail later section 3.2. The demand curve is the relationship between the response acceleration spectrum and response displacement spectrum, which are calculated from the recorded acceleration at the basement of the building. The amount of the damping coefficient needs to be assumed when the demand curve is derived. The damping coefficient for the elastic stage can be assumed as the viscous damping ratio of 5% as "Curve 1" shown in Figure 2. An additional damping effect due to non-linear response can be considered after yielding at point (A) in Figure 2. Since the additional damping effect increases corresponding to the level of building damage, the total damping coefficient increases according to the representative displacement past the yield point (A). Therefore, the demand curve is reduced due to the additional damping effect from point (B) as "Curve 2" in Figure 2. The maximum response during the mainshock is predicted as the intersection of the capacity curve and the reduced demand curve (Curve 2), point (C) in Figure 2. In practice, the maximum response can be predicted using the measured acceleration from the sensors.
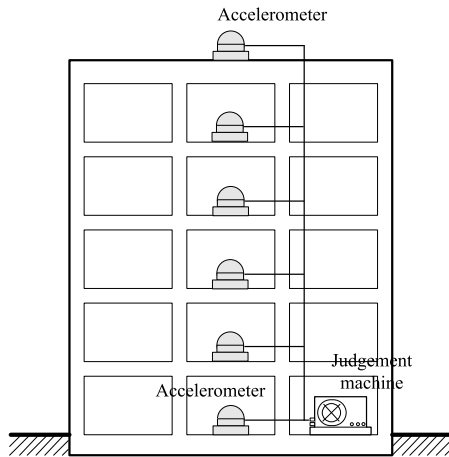
Figure 1. Configuration of the system (Kusunoki et. Al. (2008))

Besides, the same method can be applied to predict the maximum response during an aftershock by considering the mainshock and the following aftershock as one very long duration earthquake. As the input energy of the combined earthquake is consequently larger than that of the mainshock, then the maximum response may be larger than that of the mainshock. It means that the equivalent damping effect due to non-linear response considering both the main and aftershock effectively becomes smaller than that considering only the mainshock, and is shown as "Curve 3" in Figure 2. The predicted maximum response during the aftershock is the intersection of Curve 3 and the demand curve, labeled as point (D), with the assumption that the maximum aftershock is the same as the mainshock.
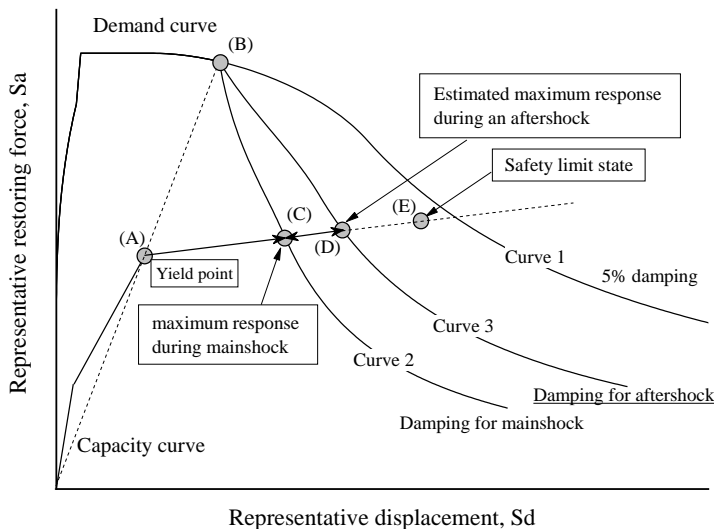
Figure 2. Outline of the evaluation (Kusunoki et. Al. (2018)

3   CAPACITY CURVE FROM THE MEASURED ACCELERATIONS

3.1   Simplification method of MDoF system to SDoF system (Kusunoki.et.al (2001), MLIT (2001), JABRP (2001), Kusunoki et. Al. (2018))

In this section, the simplification method to SDoF system, which is used in practice as the equivalent linearization method, is introduced. The capacity curve is the relationship between representative acceleration and representative displacement. The representative acceleration for s-th mode, $\left({}_s\ddot{\Delta} + \ddot{x}_0 \right)$, where ${}_s\ddot{\Delta}$ is the representative floor acceleration response relative to ground and $\ddot{x}_0$ is the ground acceleration response, is calculated following Equation (1) when the external

lateral force of $_sP_i$ and relative displacement of $_sx_i$ are obtained from a pushover analysis with the lateral force distribution shape defined as s-th mode shape.

$$\left(_s\ddot{\Delta} + \ddot{x}_0 \right) = \frac{_sQ_B}{_s\overline{M}} = \frac{\sum m_i \cdot {_sx_i}^2}{\left(\sum m_i \cdot {_sx_i} \right)^2} \cdot \sum_{i=1}^{N} {_sP_i} \tag{1}$$

where; $_sQ_B$: base shear of s-th mode, m_i mass of i-th floor, $_s\overline{M}$ equivalent mass for s-th mode (Eq. (2)).

$$_s\overline{M} = \frac{\left(\sum m_i \cdot {_sx_i} \right)^2}{\sum m_i \cdot {_sx_i}^2} \tag{2}$$

The representative displacement $_s\Delta$ is calculated from Eq.(3).

$$_s\Delta = \frac{\sum m_i \cdot {_sx_i}^2}{\sum m_i \cdot {_sx_i}} \tag{3}$$

The relationship between $_s\ddot{\Delta}$ and $_s\Delta$ is shown in Eq. (4), in which $_s\omega$ is the s-th Eigen angular frequency.

$$_s\ddot{\Delta} + \ddot{x}_0 \approx {_s\omega}^2 \cdot {_s\Delta} \tag{4}$$

When a building is inelastic, the maximum values of $\left| _s\ddot{\Delta} + \ddot{x}_0 \right|$ and $\left| _s\Delta \right|$ are the same as the response spectra of S_a and S_d with an adequate damping coefficient, and curve of the relationship between $\left| _s\ddot{\Delta} + \ddot{x}_0 \right|$ and $\left| _s\Delta \right|$ is defined as the capacity curve. The slope of the points on the capacity curve to the origin is square of the equivalent angular frequency, ω^2, in the nonlinear range. The slope of the demand curve, which is the relationship between S_a and S_d, is also square of the equivalent angular frequency. The intersection of the performance and demand curves has the same equivalent angular frequency as shown in Eq. (4).

3.2   *Capacity curve from the measured accelerations*

The calculation method for the capacity curve, which is the relationship between the representative acceleration, $_s\ddot{\Delta} + \ddot{x}_0$, and the representative displacement, $_s\Delta$, from the measured acceleration at each story is introduced in this chapter. The predominant component of the response acceleration, which is usually the first mode component (i.e., s = 1), needs to be extracted from the measured signal. The wavelet transform method (WTM) is applied to decompose the signal into several frequency bands and to extract the predominant component.

The WTM is a time-frequency analysis method to show the similarity between a signal $f_{(x)}$ and a mother wavelet. The signal of N data points f_0 is decomposed into a signal that has only a certain frequency band, g_1, and the remaining component of the signal, f_1, by Eq. (5).

$$f_0 = g_1 + f_1 \tag{5}$$

The decomposed signals g_1 and f_1 have N/2 data points. By repeating the decomposition procedure, the original signal f_0 is decomposed by Eq. (6).

$$f_0 = g_1 + g_2 + g_3 + \cdots g_n + f_n \tag{6}$$

The number of decomposition, n, is calculated by Eq. (7).

$$n = \log_2 N \tag{7}$$

The eventual remaining f_n is a single value. The decomposed components g_j are orthogonal to each other. g_j and f_j are calculated from Eq. (8) and Eq. (9), respectively.

$$g_j = \sum_k d_k^j \cdot \psi_{(2^j x - k)} \tag{8}$$

$$f_j = \sum_k c_k^j \cdot \phi_{(2^j x - k)} \tag{9}$$

where; d_k^j is the sequence to calculate g_j, c_k^j is the sequence to calculate f_j, $\psi_{(x)}$ is the mother wavelet, and $\phi_{(x)}$ is the scaling function. The B-spline with an order of 4 was selected as the mother wavelet as shown in Figure 3.

As described above, the WTM is a time-frequency analysis method using a mother wavelet as window. The width of the window in the temporal domain, $2\Delta_{\hat{f}}$, and frequency domain, $2\Delta_f$, has the uncertainty relation as stated by Eqn. (10). The time increment for g_j, $\Delta_{t,j}$, is calculated by Eqn. (11) with the time increment Δ_t of an original signal. Thus, the Nyquist frequency of g_j, $\Delta_{f,j}$, is calculated by Eq. (12) from combing Eqn. (10) and Eqn. (11). The WTM is one of the most efficient time-frequency analysis methods, since it theoretically satisfies the minimum uncertainty relation.

$$2\Delta_{\hat{f}} \cdot 2\Delta_f > 2 \tag{10}$$

$$\Delta_{t,j} = \Delta_t \times 2^j \tag{11}$$

$$\Delta_{f,j} = \frac{1}{2\Delta_t} \times 2^{j-1} \tag{12}$$

(a) Mother wavelet   (b) Scaling function
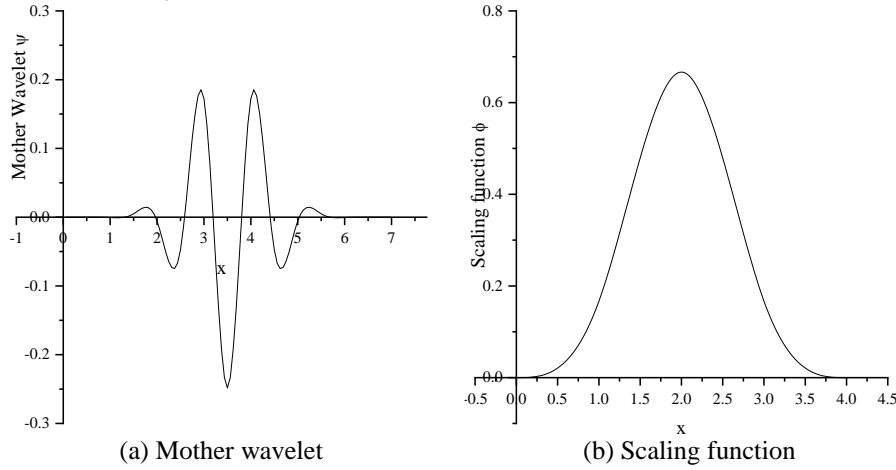
Figure 3. Mother wavelet and scaling function for the B-spline with an order of 4 [9]

The recorded absolute acceleration vector $\{_M\ddot{X}\}$ can be decomposed as shown in Eq. (13) with WTM.

$$\{_M\ddot{X}\} = \sum_{i=1}^N \{g_{\ddot{X},i}\} + \{f_{\ddot{X},N}\} \tag{13}$$

The ranks for predominant modes of vibration are thus combined to obtain the acceleration response of the predominant mode, $\{_1\ddot{X}\}$. The relative displacement to the basement is calculated as Eq. (14).

$$_1x_i = \iint \left(_1\ddot{x}_0 + _1\ddot{x}_i\right) dt^2 - \iint _1\ddot{x}_0 dt^2 \tag{14}$$

Lower rank components, which are very short period component, and higher rank components, which are very long period components, are filtered out and hence excluded from the double integral.

3.3 The capacity curve with WTM

It is already shown in section 3.1 that the representative acceleration, $_s\ddot{\Delta} + \ddot{x}_0$, and representative displacement, $_s\Delta$, can be derived as Eq. (1) and Eq.(3), respectively. Since the proposed method

in this paper is based on the first mode, Eq. (15) and Eq. (16) are obtained from Eq. (1) and Eq. (3), respectively.

$$\left({}_1\ddot{\Delta} + {}_1\ddot{x}_0 \right) = \frac{\sum m_{i\cdot}\,{}_1x_i^2}{\left(\sum m_{i\cdot}\,{}_1x_i\right)^2} \cdot \sum_{i=1}^{N} {}_1P_i \tag{15}$$

$$_1\Delta = \frac{\sum m_{i\cdot}\,{}_1x_i^2}{\sum m_{i\cdot}\,{}_1x_i} \tag{16}$$

The representative displacement can be calculated as Eq. (16) using the relative displacement calculated as Eq. (14).

The distribution shape of the external force, ${}_1P$, in Equation (15) should be proportional to the first mode vector. The contribution of the ground acceleration to the story acceleration at each story is constant as ${}_1\ddot{x}_0$. On the other hand, the distribution shape of the relative acceleration taken by the Wavelet transformation, ${}_1\ddot{x}_i$, is proportional to the first mode vector. As a result, the distribution shape of the absolute acceleration, ${}_1\ddot{x}_0 + {}_1\ddot{x}_i$, is not proportional to the first mode vector. In order to make the absolute acceleration proportional to the first mode vector, the stimulation factor of the first mode, ${}_1\beta \cdot \{{}_1u\}$, which is calculated as Eq. (17), needs to be multiplied to the ground acceleration, ${}_1\ddot{x}_0$. It means that the first mode of the unit vector of {1} is multiplied to the ground acceleration. As a result, the external force proportional to the first mode vector is calculated as Eq. (18).

$$_1\beta \cdot \{{}_1u\} = \frac{1}{{}_1\Delta}\{{}_1x\} \tag{17}$$

$$_1P_i = m_i\left({}_1\ddot{x}_i + {}_1\beta \cdot {}_1u_i \cdot {}_1\ddot{x}_0 \right) \tag{18}$$

The representative acceleration is calculated following Eq. (19), which was derived by substituting Eq. (18) to Eq. (15).

$$\left({}_1\ddot{\Delta} + {}_1\ddot{x}_0 \right) = \frac{\sum m_{i\cdot}\,{}_1x_i^2}{\left(\sum m_{i\cdot}\,{}_1x_i\right)^2} \cdot \sum_{i=1}^{N}\left(m_i \cdot {}_1\ddot{x}_i + m_i \cdot {}_1\beta \cdot {}_1u_i \cdot {}_1\ddot{x}_0\right)$$

$$= \frac{\sum m_{i\cdot}\,{}_1x_i^2}{\left(\sum m_{i\cdot}\,{}_1x_i\right)^2}\sum_{i=1}^{N} m_i \cdot {}_1\ddot{x}_i + {}_1\ddot{x}_0 \tag{19}$$

As shown in Equation (19), only the relative acceleration term of the representative acceleration needs to be divided by the equivalent mass ratio when the representative acceleration is derived from the measured accelerations.

In Equations (16) and (19), the order of the mass m_i, is the same for denominator and numerator. Therefore, the absolute value of mass is not necessarily required as long as the ratio of the mass between floors is correct. If the usage of the building is unique, the floor area ratio may be used as the mass ratio, assuming that the weight density is consistent on all floors.

4   DEMAND CURVE

The demand curve, which is compared with the capacity curve to predict the maximum response, is calculated with using the ground acceleration, $\ddot{x}_0$, measured at the basement of the building. The ground acceleration for the capacity curve, ${}_1\ddot{x}_0$, is the predominant component of the ground acceleration obtained by the WTM. Therefore, the ground accelerations for the demand curve and capacity curve are not the same. Since ${}_1\ddot{x}_0$ is taken from $\ddot{x}_0$ as the predominant component that affects the response of the building, the size of the demand for the predominant period of the building from both demand curves calculated with $\ddot{x}_0$ and ${}_1\ddot{x}_0$ are almost the same.

For the elastic demand curve, viscous damping coefficient of 5% is applied. Additionally, further damping should be considered due to the non-linearity of the building during the main shock and

aftershock as shown in Figure 2. The additional damping effects, in addition to the 5% viscous damping, for the main shock for reinforced concrete structure and steel structure are defined in Notification from Ministry of Land, Infrastructure, and Transportation #1457-6 as Eq. (20) and Eq. (21), respectively.

$$h_{eq} = 0.25(1 - 1/\sqrt{\mu}) + 0.05 \qquad (20)$$

$$h_{eq} = 0.20(1 - 1/\sqrt{\mu}) + 0.05 \qquad (21)$$

where μ is the ductility demand of the building at a global level. The demand curve is reduced with the reduction factor of F_h according to the equivalent damping ratio of h_{eq}, which is also defined in the notification as shown in Eq. (22).

$$F_h = \frac{1.5}{1+10 h_{eq}} \qquad (22)$$

For the aftershock, Eq. (20) and Eq. (21) cannot be used. Therefore, numerical study with non-linear dynamic analysis with SDoF was performed to develop new functions to evaluate the equivalent damping coefficient for the maximum aftershock, which is assumed to be of equal intensity as the same as the main shock. The functions for equivalent damping ratios are proposed as Eq. (24) for R/C structures and Eq. (25) for steel structures, respectively (Kusunoki et. Al. (2006)).

$$h_{eq} = 0.10(1 - 1/\sqrt{\mu}) + 0.05 \qquad (24)$$

$$h_{eq} = 0.06(1 - 1/\sqrt{\mu}) + 0.05 \qquad (25)$$

5   DAMAGE CLASSIFICATION

The performance curve is calculated with Eq. (16) and Eq. (19) from the measured accelerations. In most case, the measured response may not reach the safety limit state of the building. In order to evaluate the damage level of the building, the performance curve needs to be extended to the safety limit state, as shown in Figure 4. Firstly, the restoring force is assumed to be constant after the maximum response point. The inter-story drifts are extended so that the mode shape is proportional to the measured maximum response point. When one of the inter-story drift reaches its safety limit drift, which should be calculated in advance, the building is supposed to reach the safety limit state, as shown in Figure 5.
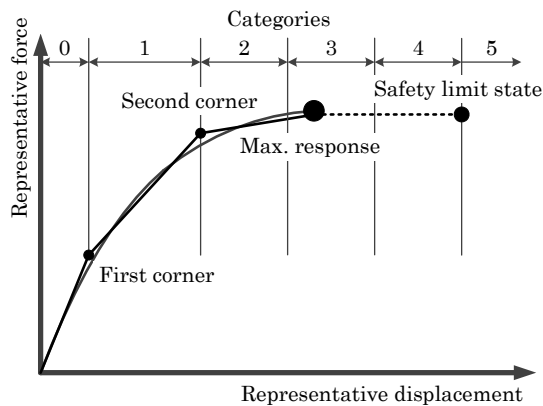
Figure 4. Capacity curve and damage classification (Kusunoki (2019))
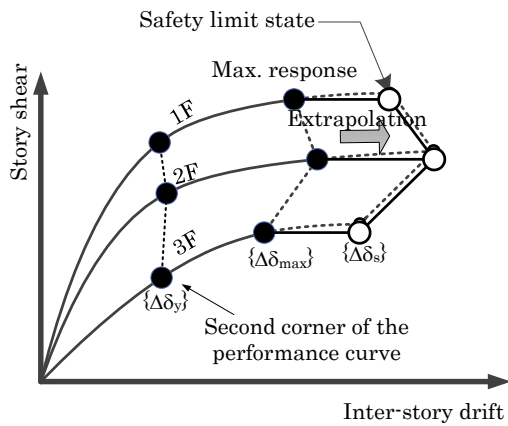
Figure 5. Maximum response points and safety limit points (Kusunoki (2019))

Damage is classified into five classes, as shown in Figure 4. At first, the measured performance curve is modeled into a tri-linear model. If it is impossible and modeled as linear, the damage is classified as "0". If the maximum point is before the second corner point in Figure 4, it is classified as "1". If the maximum response point exceeds the safety limit state, it is classified as "5". The range between the second corner to the safety limit state is evenly divided into three portions and classified as "2", "3", and "4".

In order to predict the damage class during the maximum after shock, the yield displacement needs to be defined on the performance curve to calculate the response reduction factor for the aftershock with Eq. (24) or Eq. (25). The displacement at the second corner of the tri-linear model is taken as the yield displacement.

6   EXAMPLES

6.1   Shaking table test (Yamazoe et. Al. (2018))

A 3-story two-span-one-bay R/C building with pile foundation, which was scaled 1/3, was shaken on E-Defense shaking table. The piles were fixed at the bottom of an R/C box with mechanical pins at the first inflection point. The elevation and floor plan are shown in Figure 6. Since the PC strand in the piles was not correctly scaled, the strength of piles was double of that expected. The upper structure was also designed so that the strength was double to the practical value. As a result, the base shear coefficient of the upper structure was about 1.0.
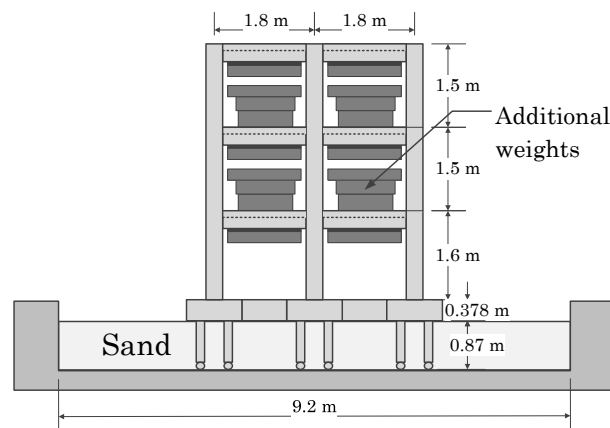
(a) Elevation

(b) Plan

Figure 6. Specimen for shaking table test (Yamazoe et. Al. (2018))

An artificial wave was applied for the input motion. The target spectrum for the wave was defined according to an expected earthquake near Tokyo, as shown in Figure 7. Since the strength became double to the practical value, 200% input motion is the same level as the code requirement for the specimen. The design spectrum defined in the code is also superimposed into the Figure. The specimen was shaken with the levels of 100%, 200%, and 300%.
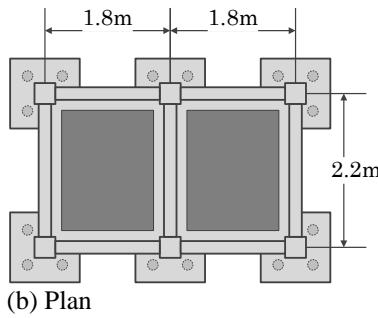
The maximum deflection angles of the pile and upper structure for input levels are listed in Table 1. The upper structure remained elastic with a maximum inter-story deflection angle of 1/570 even during 300% input motion. On the contrary, plie foundation just yielded during 100% input motion with the maximum deflection angle of 1/160, and then it reached about safety limit state during 200% input motion. Finally, pile suffered severe damage and failed in shear at the top of piles during 300% input motion, then lost the vertical load-carrying capacity.

The seismic damage classification of the specimen was conducted with the proposed method. The pile foundation was considered as a "story" and the specimen was regarded as a 4-story building. The inter-story drift angles at the safety limit state were assumed as 1/37 for pile foundation and 1/50 for the upper structure, respectively. The angle for the pile foundation of 1/37 was derived from the supplementary member test. Figure 7 shows the damage classification result for 200% input motion. The damage class was evaluated as class "3" for both directions. The predicted damage class for the maximum aftershock was evaluated as the class "5". Since the input level after 200% was increased to 300% (i.e., the applied "aftershock" was 50% greater than the mainshock), the aftershock prediction using the damping ratios from Eq. (22) and Eq. (23) cannot be proven directly. Nonetheless, the occurrence of collapse during 300% input motion does not disprove the prediction.

Table 1. Shaking table test results (Yamazoe et. Al. (2018))

Input level	PGA of table (cm/s^2)	Max. Deflection angle (structure)	Max. Deflection angle (pile)
100%	180	1/1310(1F)	1/160
200%	410	1/700 (1F)	1/33
300%	680	1/570 (2F)	1/7
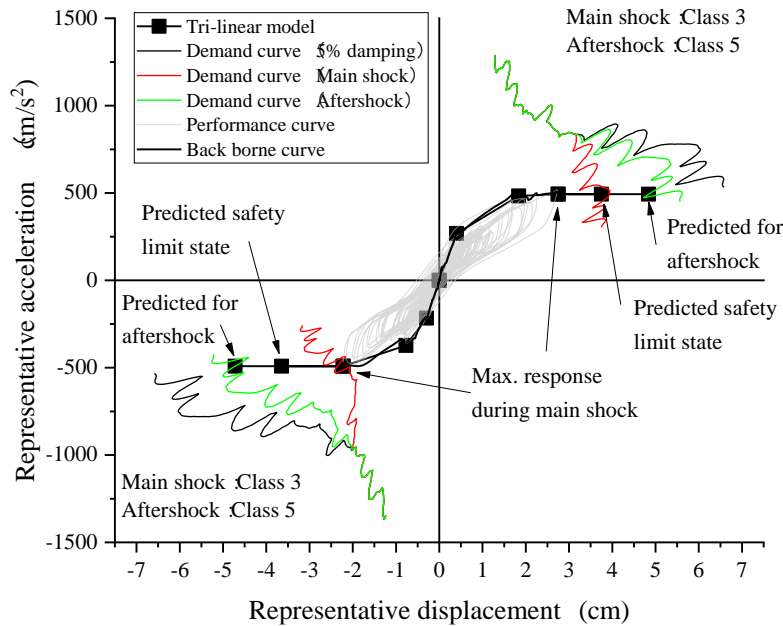
Figure 7. Damage classification result for 200% input motion (Kusunoki (2019))

7   CONCLUSIONS

A new residual seismic capacity evaluation method with recorded accelerations based on the capacity spectrum method is proposed. The validity of the method was confirmed with the monitoring data of the existing building and shaking table test. Results from the studies are as follows:

- A performance curve calculated with recorded accelerations and decomposition method using Wavelet Transform Method (WTM) was proposed.

- The developed WTM can efficiently decompose the dynamic response into its predominant response frequency bands.

- The damage classification method based on the derived performance curve and predicted response point during the aftershock is proposed.

- The proposed method validated using the actual response data and visual damage observation of an instrumented building at Yokohama University during the 2011 Tohoku Earthquake, and by a shake-table test of a 3-story building on pile foundations.

ACKNOWLEDGMENTS

REFERENCES

Building Center of Japan (BCJ), 1996.3. Report on the reconnaissance committee on the building damages due to the Hanshin-Awaji Great Earthquake Disaster, 1995 - Summarization - (in Japanese)

Freeman, S.A., 1978. Prediction of Response of Concrete Buildings to Severe Earthquake Motion, Proceedings of Douglas McHenry International Symposium on Concrete and Concrete Structures, SP-55, American Concrete Institute

Sigmund A. Freeman, 2004.4. REVIEW OF THE DEVELOPMENT OF THE CAPACITY SPECTRUM METHOD, *ISET Journal of Earthquake Technology*, No. 438, Vol. 41, No. 1, pp. 1-13

Japan Building Research Promotion Association (BRPA), 2000.7. Guidelines for performance evaluation of reinforced concrete buildings, *Gihodo*, (in Japanese)

Hiroshi KURAMOTO, Masaomi TESHIGAWARA, Norihide KOSHIIKA and Hiroshi ISODA, 2001.8. Conversion of Multi-Story Building into Equivalent SDoF System and Its Predictability for Earthquake Response, *Journal of Structural and Construct Engineering*, AIJ, Vol. 546, pp.75-85

Building Guidance Division of Hosing Bureau, Ministry of Land, Infrastructure, Transport and Tourism, 2001. Calculation examples and commentaries for the capacity spectrum method ver. 2001, *Kougaku Tosyo*

Engineering affairs division of Ministry of Construction and Japan Association for Building Research Promotion, 2000.07. Guidelines for evaluating the seismic capacity of reinforced concrete buildings, Gihodo Press

Koichi Kusunoki, Daiki Hinata, Yuuki Hattori and Akira Tasai, 2018.1. A new method for evaluating the real-time residual seismic capacity of existing structures using accelerometers, *Structures with multiple degrees of freedom, Japan Architectural Review*, Architectural Institute of Japan, Vol. 1, No. 1, pp.77-86

Koichi KUSUNOKI, Ahmed Elgamal, Masaomi Teshigawara and Joel P. Conte. 2008.10. Evaluation of structural condition using Wavelet transforms, *The 14th World Conference on Earthquake Engineering*

Koichi Kusunoki、Masaomi Teshigawara, 2006.7. Study on the substitute damping ratio for aftershocks, *Proceedings of the Japan Concrete Institute*, Vol. 28, No.2, pp.1057-1062 (in Japanese)

Kusunoki, K., Tasai, A., Teshigawara, M., 2012. Development of Building Monitoring System to Evaluate Residual Seismic Capacity after an Earthquake, *the 15th World Conference on Earthquake Engineering*

Kusunoki, K., 2019.7. Analytical Study on The Extrapolation Method for the Performance Curves of R/C Structures Derived from Recorded Accelerations, *Journal of Structural and Construction Engineering*, AIJ, Vol.84, No. 761, pp.961-971 (in Japanese)

Masatoshi Yamazoe, Koichi Kusunoki, Yuji Sako, Hajime Okano, Yo Hibino, Kuniyoshi Sugimoto, Yohsuke Kawamata, and Hisatoshi Kashiwa, 2018.7. E-Defense shaking table test on soil-pile-structure interaction system, *Journal of Structural and Construction Engineering*, AIJ, No. 749, pp.985-995 (in Japanese)

Study on seismic damage control of wall-type RC structure based on static loading test of a 1/2 scale 5-story 3D specimen

Masaomi TESHIGAWARA[1], Tsutomu OHTA[2], and Tatsuya ASAI[3]

[1] Professor, Graduate school of environmental studies, Nagoya University, Nagoya, Japan
[2] President, Horie Architectural Engineering Lab., Tokyo, Japan
[3] Assistant Professor, Graduate school of environmental studies, Nagoya University, Nagoya, Japan

ABSTRACT: Wall-type reinforced concrete (hereinafter referred to as WRC) building are relatively inexpensive among reinforced concrete structures, and can be used in a spacious space because the column and beam protrusions do not come into the room. In addition, no significant damage has been reported even in the large earthquakes, and the damage prevention performance is recognized to be high. This study conducted a horizontal force loading test of a 1/2 scale 5-story typical WRC building satisfying minimum structural requirements, and quantitatively examined and evaluated the damage to the WRC building against a large earthquake. The design horizontal strength of the specimen in the term of base shear coefficient is 0.74 in design stage. Test specimen has a base shear coefficient of about 0.8 at an inter-story deformation angle of 1/200. Based on the load-deformation relationship and the hysteresis damping constant obtained from the experiment, the response of the test specimen against a large earthquake is estimated in less than 1/400, by equivalent linearization method. Considering the response deformation angle and the experimental results, it is considered that the WRC building targeted in this paper has sufficient damage prevention performance against large earthquakes. And to ensure high damage prevention ability against large earthquakes, some structural requirements might be added to apply the strength to wall beams.

1   INTRODUCTION

Wall-type reinforced concrete (hereinafter referred to as WRC) building are relatively inexpensive among reinforced concrete structures, and can be used in a spacious space because the column and beam protrusions do not come into the room. In addition, no significant damage has been reported even in the large earthquakes, and the damage prevention performance is recognized to be high, AIJ (2015), Teshigawara et al. (2017). In the structural design, a simple calculation method called as an average shear stress method is applied, and there are following structural requirements; the wall length (wall amount) per unit floor area in each direction, the wall thickness, the bending reinforcement set at the edge in accordance with the opening height, and the minimum wall reinforcement.

The average shear stress method is conducted as follows;

1) Average shear stress acting on the wall is obtained by dividing the shear force with a shear coefficient of 0.2 by the horizontal cross-sectional area of the floor wall.

2) The shear force carried by the wall is obtained by multiplying the average shear stress by the cross-sectional area of the load bearing wall.

3) The moment at the end is obtained by setting the inflection point of each bearing wall to half the opening height of the bearing wall, and

4) The cross section of the wall beam is calculated with a stress commensurate with the moment.

Even with complex wall arrangements, there is no difficulty in modeling the building, and there is no problem with modeling the bearing wall itself.

This study conducts a horizontal force loading test of a 1/2 scale 5-story WRC building designed in the method mentioned above, and quantitatively examined and evaluated the extent of damage to the WRC building against a large earthquake.

2   OUTLINES OF EXPERIMENT

2.1   Test specimen

The test specimen used in this experiment is built so that the lower two stories of the five-story typical WRC building designed based on the WRC standard, AIJ (2015), are the same as the design, and the upper three stories are modeled for loading. Test specimen is reduced to 1/2 scale. The design policy is described 2.1.1.

2.1.1   Prototype of test specimen

Typical prototype five-story WRC building is designed so that the amount of wall and bar arrangement satisfy the minimum requirements of the WRC standard, AIJ (2015). The L-type and T-type load-bearing walls are determined so that the wall amount is about 1/3 of the total, and the wall amounts are equal in the orthogonal horizontal directions. The layout of the walls is the same on each floor. The vertical and horizontal bars of the wall are within the range that satisfies the allowable stress level design (approx. 0.5 to 0.9), and the amount of the standard shear reinforcement ratio specified by WRC standard 1). The beam reinforcement was also determined to satisfy the allowable stress design. The wall edge reinforcement is also equal to or greater than the minimum requirement of the WRC standard, AIJ (2015). However, when the orthogonal wall is attached, the reinforcement is 1-D13 added to. The slab reinforcement was D13 @ 200mm.

2.1.2   Test specimen

The above five-story building is reduced to 1 / 2-scale five-story building, in which the lower two stories (from the first-floor wall to the third-floor beam) were reduced as it is, and the upper three stories are modeled for loading. The cross-section of the 4th floor beam is determined so that the horizontal strength of the half scale 5-story building and the test specimen were almost equal. Figure 1 shows a plan view and axis diagram of the specimen. Each member is listed in Tables 1 and 2. When calculating the base shear coefficient, the weight of the specimen is assumed to be when the average shear stress of 0.45 N / mm^2 occurs in the 1st-story bearing wall in the loading direction when the story shear force coefficient of Co = 0.2, and the total weight ΣW is 0.45 A1 / 0.2 = 1881 kN (A1: Total cross-sectional area of the first floor bearing wall in the direction of force [mm^2]). The actual weight of the specimen is 1100 kN at 1 FL and above and 1006 kN at 2 FL and above. For reference, the horizontal force distribution for the 1/2 scale five-story building and the specimen is shown in Fig. 2. Using these lateral force distributions, 1344 kN (CB = 0.72) for 1/2 scale 5-story building and 1394 kN (CB = 0.74) for the specimen are calculated (the concrete strength is Fc = 21 N / mm^2, and the yield strength of the reinforcing bars is 1.1times of the nominal yield strength).

2.2   Loading method

The lateral forces are applied at the top stub and at the 2nd floor in the positive and negative direction. The lateral force distribution is determined so that the shear forces and the overturning moments in the 1st and 2nd story are approximately equal to the 1/2 scale 5-story building (lateral

force distribution is shown in Fig. 2 (a)). The ratio of the horizontal force is 1: 7.358 for the specimen. In loading schedule, the first two cycles are controlled based on shear force coefficient, $C_B = \pm 0.1, \pm 0.2$, and then the loading is controlled by the deformation angle of the lower two
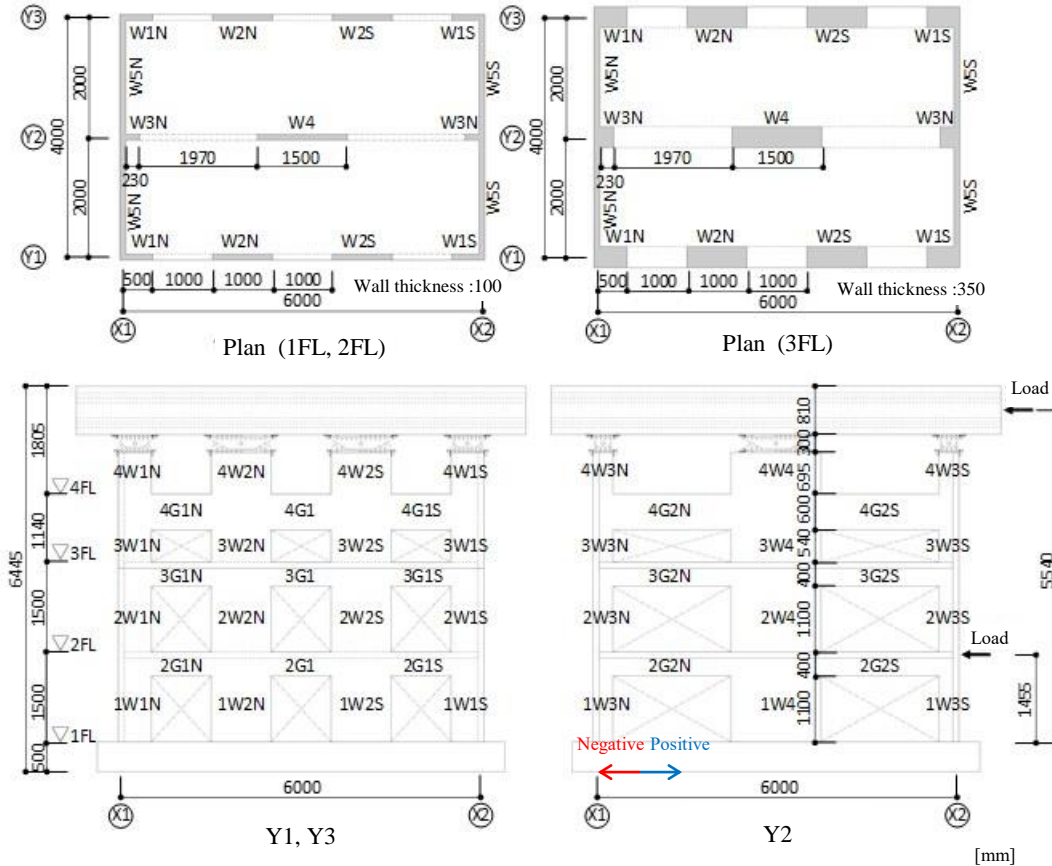
Figure 1. A plan view and axis diagram of the specimen

a) 1/2 scale 5-story building

b) Specimen
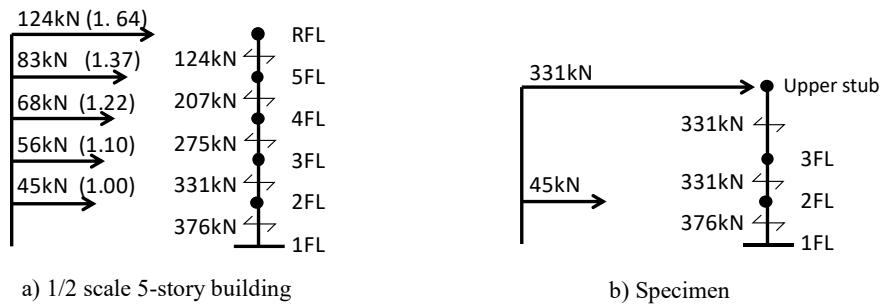
Figure 2. Lateral force distribution when base shear coefficient Co=0.2

stories, $Rc = \pm 1/2000, \pm 1/1000, \pm 1/400$ (2), $\pm 1/200$ (2), $\pm 1/133$ (2), $\pm 1/100$ (2), $+ 1/80$ (number of repetitions in parentheses) .

Table 1. List the bar arrangement of beams

Symbol	Main upper rebar	Main bottom rebar	Shear rebar
2G1,3G1	2-D13	2-D13	1-D6@75
2G2,3G2	1-D16, 1-D13	2-D16, 1-D13	1-D6@50
4G1, 4G2	4-D16	4-D16	2-D10@100

14

Table 2. List the bar arrangement of walls

Symbol	Vertical rebar	Horizontal rebar	Rebar at wall edge
1st and 2nd layer			
W1	1-D6@125	1-D6@125	1-D16 + 1-D13 (external edge), 1-D16 (inner edge)
W2	1-D6@125	1-D10@125	1-D16
W3	1-D6@125	1-D6@125	1-D16 + 1-D13 (outer edge), 1-D16 (inner edge)
W4	1-D6@125	1-D10@100	1-D16
W5	1-D6@125	1-D6@125	1-D16 + 1-D13
3rd and 4th layer			
W1～W4	2-D13@200	2-D10@100	4-D19
W5	1-D6@125	1-D6@125	D13 + D13

2.3   Material properties

Tables 3 and 4 list the material properties of the reinforcing bars and concrete used in the experiment, respectively. High-strength concrete is used above 4 FL.

Table 3. Material property of reinforcing bars

Size	material	σ_y[N/mm^2]	ε_y [μ]	E_s [kN/mm^2]
D6	SD295A	343	1871	183
D10	SD295A	351	1935	182
D13	SD295A	360	1908	189
D16	SD295A	355	1959	181

Table 4. Material property of concrete

Floor	F_c [N/mm^2]	F_t [N/mm^2]	E_c [kN/mm^2]
1 FL～2 FL	23.7	2.07	26.1
2 FL～3 FL	19.7	1.71	23.1
3 FL～4 FL	19.8	1.93	25.5
4 FL～	58.9	2.59	33.3

3.   TEST RESULTS

3.1   Load v.s. deformation

Figure. 3 to Figure. 6 show the base shear force v.s. the deformation angle Rc (control deformation angle), the yield of reinforcing bars in the lower 2 stories (no yield of reinforcing bars has been confirmed in 3 stories), the deformation mode and final fracture condition of the specimen (after Rc = +1/80 cycle). The calculated horizontal force is plotted in Fig. 3 with a chain line, and Figure. 4 shows the loading cycle by which the reinforcing bar has yielded (that is, the yield strain in Table 3). Figure. 4 shows Y2-Y3 and Figure. 6 shows Y1-Y2, so both results do not correspond, and the fracture condition in Fig. 6 is as shown in the upper left of the figure. Please note that the results are confirmed from inside.

As shown in Fig.3 and Fig.4, this specimen has bending yield at foot of the W4 at $Rc = 1/2000$ cycle, and at the W2 foot and W5 (orthogonal wall) foot at $Rc = 1/1000$ cycle. Bending yield and tensile yielding occur at the $Rc = 1/400$ cycle, bending yield at the W1 and W3 foots, and shear yielding at the inner wall at the $Rc = 1/200$ cycle. Maximum strength is 1580 kN. This value is 13% higher than the calculated value of 1394 kN. Increasing the lateral force, the concentration of deformation occurs into the 1st story (Fig. 5), so the deformation angle of the 1st story at the maximum strength ($Rc = + 1/200$) was +1/168, and the deformation angle at the 2nd story was larger than +1/245.
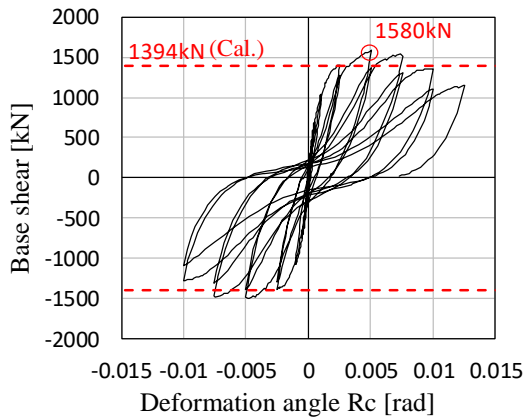

Figure 3. Base shear v.s. drift at lower 2-story Rc

Figure 5. Deformation mode at each peak
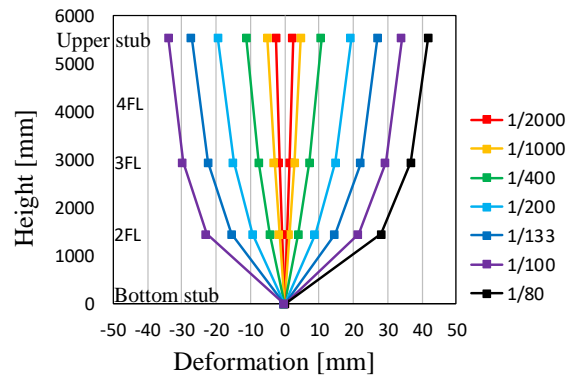
* Results of 2nd cycle are shown after Rc = 1/400
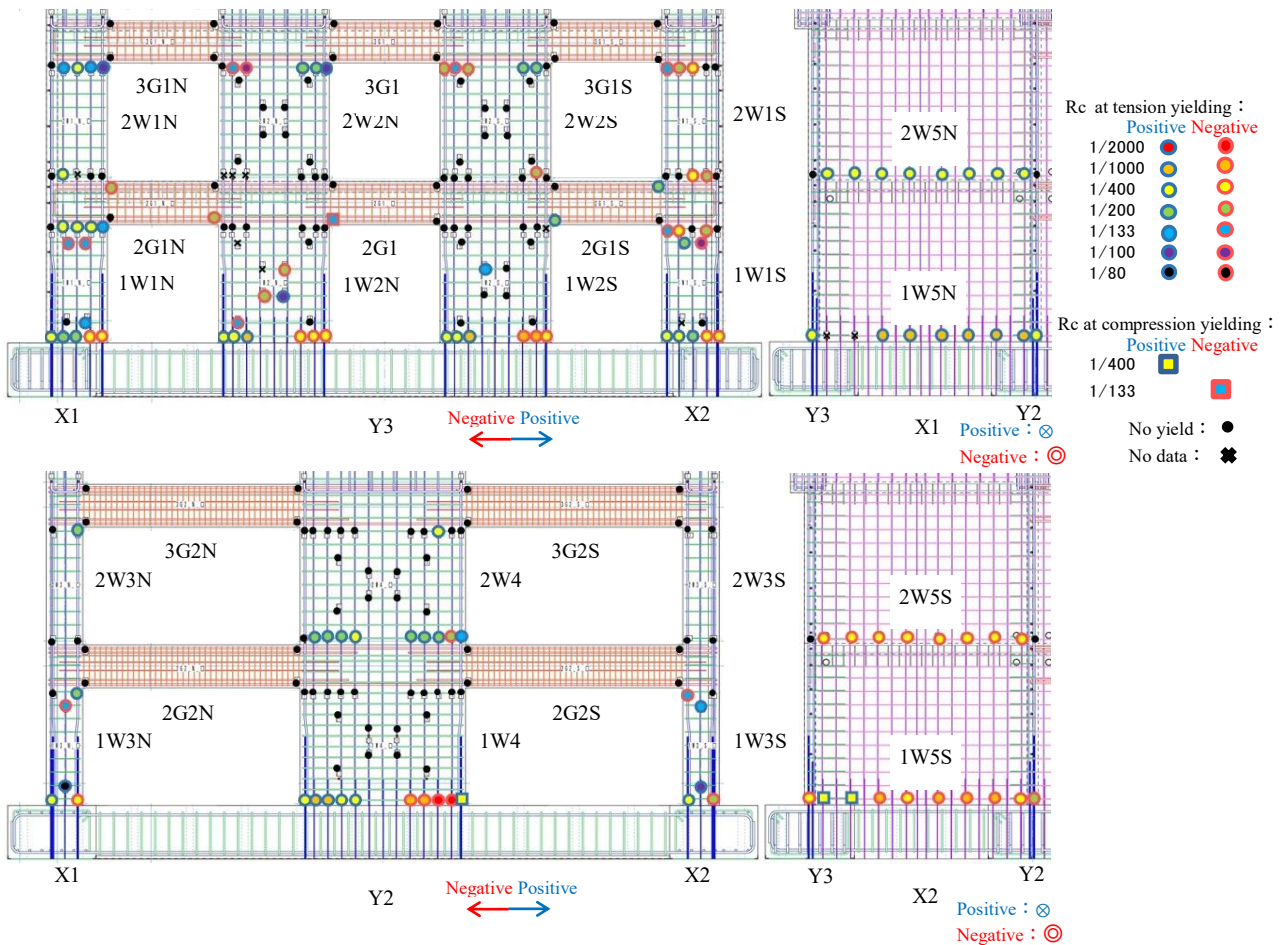
Figure 4. The yield of reinforcing bars in the lower 2 layers

16
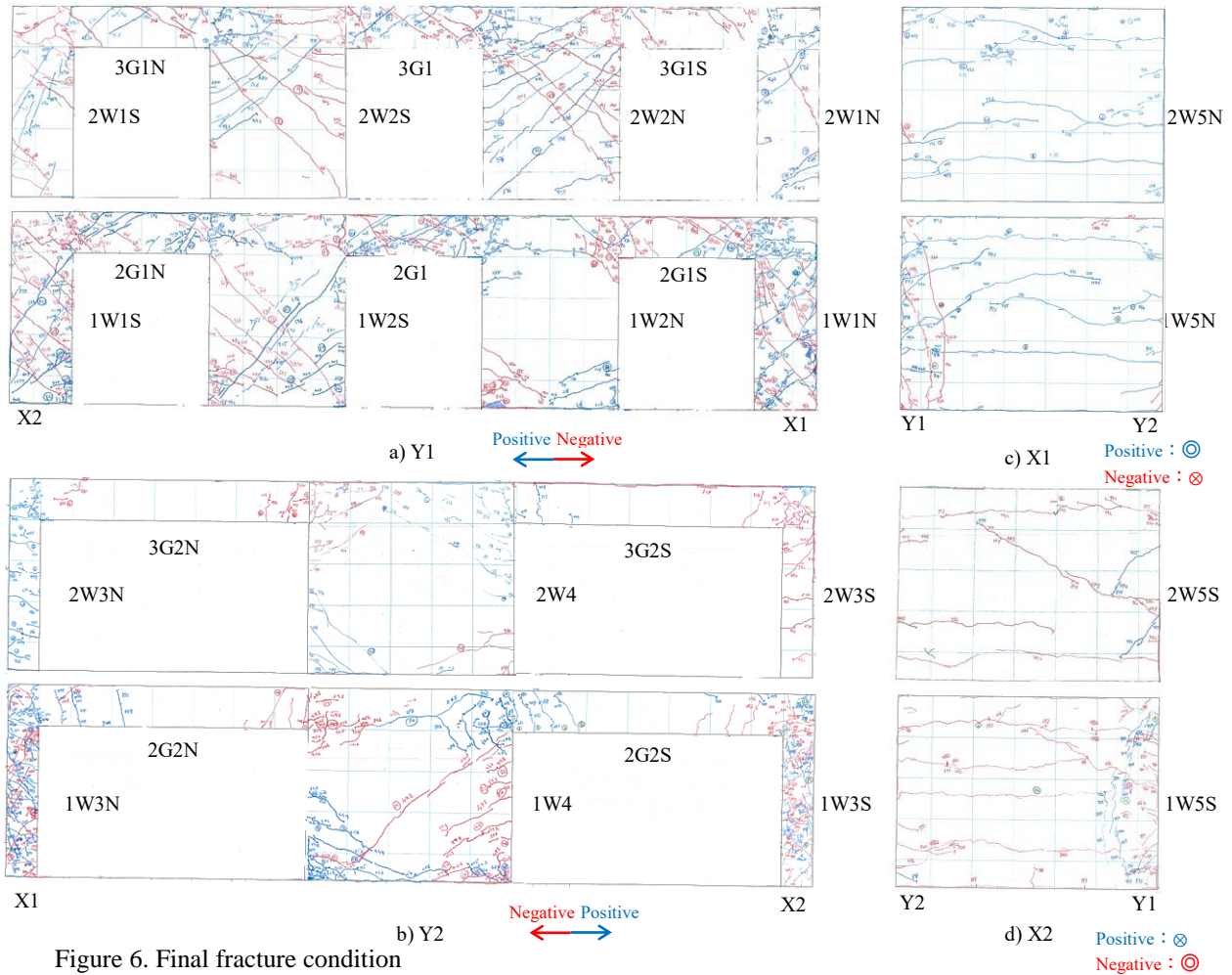
Figure 6. Final fracture condition

Figure 6 shows the cracks that occur in each member of the specimen. In this figure, 1W2N, 1W4, and 2W4 have less shear damage than other members (1W4 and 2W4 have no shear yield (Fig. 4)). This is thought to be due to the fact that the slip failure of both walls preceds the shear failure because the slip of the wall foot is observed during the experiment. In addition, although less than half of the beam main bars are observed to yield, because the bending cracks that occur at the end of the beam propagate toward into the joint with the wall. Yield may occurs inside the joint, not at the beam end where a strain gauges are affixed.

3.2   Hysteresis damping

Using the load deformation relationship obtained in this experiment, the hysteresis damping constant h_{eq} of each force cycle is obtained by the following procedure. a) First, the hysteresis energy consumption $\varDelta W$ [kNm] in one cycle is obtained as the area surrounded by the hysteresis curve. b) Next, the potential energy W [kNm] of the equivalent elastic system is obtained by equation (1). In this formula, the average values of the potential energies (W_{+p} [kNm] and W_{-p} [kNm]) for positive and negative forces are used. In addition, the maximum deformation value (δ_{+p} [m] and δ_{-p} [m]) and the maximum load value (Q_{+p} [kN] and Q_p [kN]) in the force cycle do not always occur at the same time. The h_{eq} is determined using both maximum values (h_{eq} is evaluated (smaller) on the safe side).

$$W = \left(W_{+p} + W_{-p}\right)/2 = \left(\frac{1}{2}Q_{+p}\delta_{+p} + \frac{1}{2}Q_{-p}\delta_{-p}\right)\Big/2 \quad (1)$$

c) Using the values obtained from a) and b), calculate the hysteresis decay constant heq.

$$h_{eq} = \frac{1}{4\pi} \frac{\Delta W}{W} \qquad (2)$$

Figure 7 shows the hysteresis damping constant, h_{eq}, calculated by the above procedure using the load deformation relationship of the total building. The h_{eq} is about 8% to 14% in the first cycle, and about 7% to 12% in the second cycle ($Rc = 1/400$ cycles and after).

3.3   Residual seismic capacity
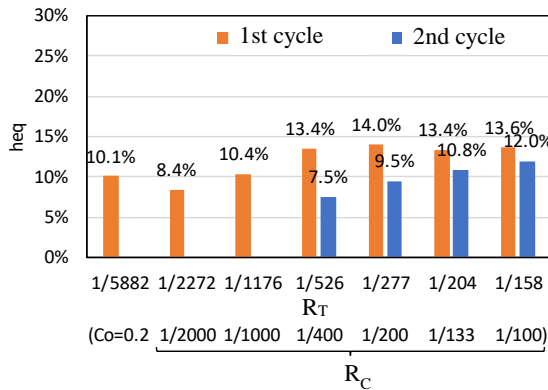
Figure 7. Hysteresis damping constant
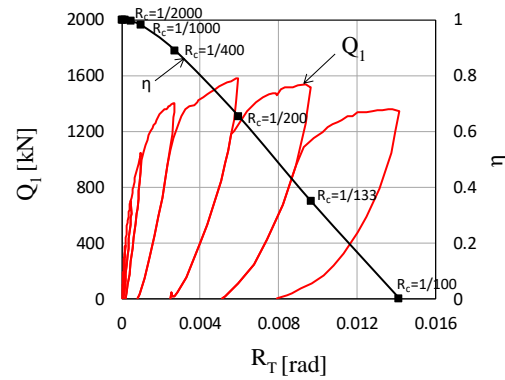
Figure 8. Q_1 vs R_T and η vs R_T

Figure 8 shows the relationship between the Q_1 v.s. R_T envelope and η v.s. R_T on the positive loading side. In order to evaluate the relationship between the deformation of the building and the residual energy absorption capacity (η), the seismic performance reduction factor η defined in reference, JBDPA (2015), is referred to. In the load deformation relationship during positive loading obtained by experiment, the total energy that can be absorbed by the building up to $Rc = 1/100$ cycles (total area surrounded by red line in Fig. 8) then, from its value, the value excluding the energy consumed by each deformation angle is defined as the residual absorbable energy, and the seismic performance reduction factor η is calculated by taking the ratio of the latter to the former. This building has a residual absorbable energy of about 83% at a deformation angle $Rc = 1/400$ and about 55% at 1/200.

4.   RESPONSE AND DAMAGE EVALUATION

Based on the above experimental results, the response of the WRC building used in this experiment against an extremely rare earthquake is predicted, and the damage situation at that time is examined.

4.1   Response evaluation method

The response is obtained by the response and limit strength calculation method, NILIM (2015), using the load deformation relationship and the hysteresis damping constant, heq, obtained in the previous chapter. The total weight of the WRC building is 1881 kN as described in Section 2.1, and the mass distribution is assumed that the mass of one story, m, is in each of the 1st story and the 2nd story, and the mass of upper three stories is concentrated at the top stub center position level (a height of 5.54 m from 1 FL) as shown in Fig.9.

a) First, the effective mass m_e [t], representative displacement x_e [m], representative height He [m] and equivalent acceleration S_a [m / s2] is obtained by equations (3) to (6), respectively.

$$m_e = \left(\sum_{i=1}^{n} m_i x_i \right)^2 \Big/ \sum_{i=1}^{n} m_i x_i^2 \qquad (3)$$

Center of upper stub
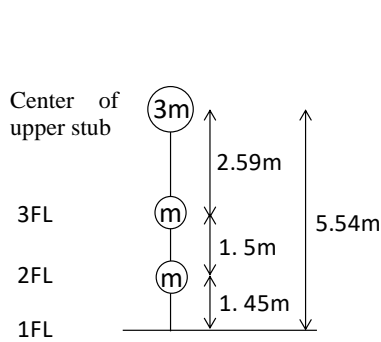
Figure 9. Assumption of mass distribution
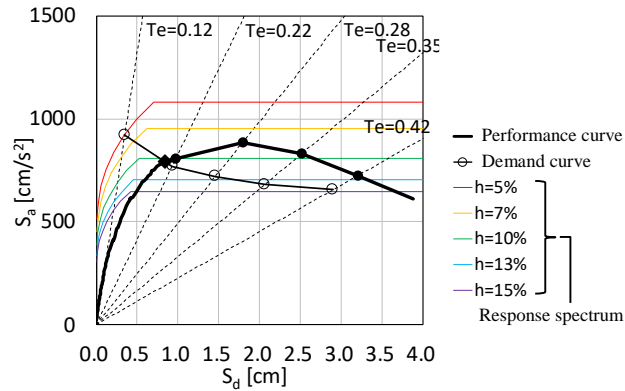
Figure 10. Estimation of earthquake response (calculation)

$$x_e = \sum_{i=1}^{n} m_i x_i^2 \Big/ \sum_{i=1}^{n} m_i x_i \qquad (4)$$

$$H_e = \sum_{i=1}^{n} m_i x_i H_i \Big/ \sum_{i=1}^{n} m_i x_i \qquad (5)$$

$$S_a = Q_1 / m_e \qquad (6)$$

Here, n is the number of mass points ($n = 3$ in this study), and m_i [t], x_i [m], and H_i [m] are the mass, displacement, and height of the mass point i (i = 1, 2, 3), respectively.

b) Obtain the response spectrum S_a, S_d for extremely rare earthquakes based on the NILIM (2015). The ground type is assumed to be the second type ground, the region coefficient $Z = 1.0$, and the hysteresis damping constant is assumed to be 5%, 7%, 10%, 13%, and 15%.

c) Equivalent damping constant h_{eq} is obtained by adding viscos damping of 5% to 0.8 times the hysteresis damping constant calculated in the previous chapter (using the result of the second cycle) (Table-5). The performance curve of the equivalent single degree of freedom system is obtained, and the intersection of the curve and the required curve is obtained as a response deformation as shown by symbol ▲ in Fig. 10.

Table 5. h_e at each Rc (Rc: Drift angle of lower 2-story)

R_c	− (Elastic)	1/400	1/200	1/133	1/100
x_e	−	0.97cm	1.79cm	2.52cm	3.20cm
h_e	5%	11.0%	12.6%	13.6%	14.6%

4.2   Response evaluation result

Figure 10 shows the result of the calculation of the limit strength by the procedure in the previous section. In the figure, the performance curve of the reduced system is represented by a thick black solid line, the response spectrum is represented by a solid line of each color corresponding to the equivalent damping constant h, and the required curve is represented by a black thin solid line. From the figure, the maximum response deformation of the reduced system for extremely rare earthquakes is calculated to be 0.84 cm. At this time, the deformation angle Rc of the lower two stories was Rc = 1/480 (1 story: 1/457, 2 stories: 1/504), which was less than 1/400.

4.3   Damage of WRC building against large earthquake

Examining the damage situation of the WRC building at the response deformation angle to the extremely rare earthquake, the specimen does not reach the maximum strength (Rc = 1/200) (Fig. 3).), Bending yielding of wall members occur, but no shear yielding occur (Fig. 4), and the seismic performance reduction factor η is about 0.8 (Fig. 8). Considering the above, it is considered that the WRC building used in this paper has sufficient damage prevention performance against a large earthquake.

5   CONCLUSIONS

The damage prevention ability of a WRC building in the event of a large earthquake is evaluated based on a static loading test of a specimen focusing on the lower two stories of a 1/2 scale 5-story typical prototype WRC building. The findings obtained are summarized below.

(1) In this specimen, the bending yield of the wall starts from the deformation angle 1/2000 cycle, the tensile yield of the orthogonal wall starts from 1/1000 cycle, and the shear yield starts from 1/200 cycle and the maximum strength is obtained.

(2) The seismic performance reduction factor calculated with the ultimate deformation as the deformation angle of 1/100 is about 0.85 at the deformation angle of 1/400 and about 0.6 at 1/200.

(3) Based on the load-deformation relationship and the hysteresis damping constant obtained by the experiment, the response of the WRC building during a large earthquake is estimated by the "Response and the ultimate strength method", and the drift angle of the lower 2-story is 1/480.

(4) At the same drift angle, the building does not reach its maximum strength, bending yielding occurs, no shear failure occurs, and the seismic performance reduction factor is about 0.8.

The WRC building is considered to have high damage prevention performance against large earthquakes. It is necessary to ensure high damage prevention ability against large earthquakes, some structural requirements might be added for example to apply strength to wall beams.

In the future, we plan to conduct further detailed analysis of the results of this experiment, including slip failure at the wall foots,

REFERENCES

Architectural Institute of Japan: Wall-type reinforced concrete design / calculation criteria / comment, 2015

Teshigawara, Masaomi et al .: Study on seismic damage control of RC wall structure, Part 1 ~ 9, Summary of Academic Lectures of Architectural Institute of Japan, Tsubaki, pp.845-862, 2017.8

Ministry of Land, Infrastructure, Transport and Tourism, National Institute for Land and Infrastructure Management: Commentary of Structural Standards for Buildings 2015 edition, 2015

Japan Building Disaster Prevention Association: Earthquake damage classification criteria and restoration technology guidelines, 2015

Development study for low-rise residential building of masonry walls using AAC blocks

K.Takashima[1], A.Tasai[2], S.Nakata[1], R.Nakamura[3], H.Iida[3], T.Hanai[3], K.Sugimoto[2], K.Kusunoki[4]

[1] Asahi-kasei Homes Co., Tokyo, Japan
[2] Yokohama National University, Yokohama, Japan
[3] Ebisu Building Laboratory Co., Tokyo, Japan
[4] Earthquake Research Institute, Tokyo, Japan

ABSTRACT: Masonry is a traditional construction method with stones and bricks, which has high durability, fire resistance, sound insulation, and its unique aesthetic so that widely used worldwide. In this study, in order to realize new AAC (Autoclaved aerated concrete) masonry system, material and shear performance of the wall was investigated. After understanding the basic compression and shear performance of masonry prism, in-plane shear test of full-scale wall was conducted. The AAC masonry was subjected to compression and shear tests, and the significant values were obtained by the concept of effective strength and rigidity considering the stress transmission path. Rigidity up to 1/1500 rad was able to be evaluated with a simple FEM analysis model that is assumed to be a continuum of AAC masonry with single material characteristics, both with and without openings.

1   INSTRUCTIONS

Masonry is a traditional construction method with stones and bricks, which has high durability, fire resistance, sound insulation, and its unique aesthetic so that widely used worldwide. Masonry construction in Japan, due to the historically unfamiliar construction method, industrialization is not thriving are not popular. However, it is reported that the concrete block structure (reinforced CB structure) reinforced with reinforcing bars has high earthquake resistance. On the other hand, in CB-built houses, etc. insulation is applied to the outside, and its beauty is lost. Autoclaved aerated concrete (AAC) can be used as a masonry material. AAC masonry is an efficient structural system because its light weight resulted from its material characteristics by its own cellular structure reduces seismic inertia forces under earthquake excitations. Moreover, AAC has some strength despite its low specific gravity, and its light weight also improves workability at its construction site and thermal insulation quality for comfortable environments. Currently, AAC panels are manufactured in Japan, but their use is limited to curtain walls and floors that do not need to bear in-plane shear. Reviewing AAC as a stonework material, there is a possibility that a house with high quake resistance and heat insulation and a unique aesthetic can be realized as shown in Figure 1.

Therefore, the purpose of this study, in order to realize AAC masonry system, was to clarify material and shear performance. After understanding the basic compression and shear performance of masonry prism, in-plane shear test of full-scale wall was conducted (Takashima et al, 2017). Finally, the in-plane shear performance of the wall was evaluated from the existing RC theory. Through this research, it is possible to provide safe, comfortable and inexpensive housing even for developing countries where long-loved buildings such as masonry have been reviewed

and there are many unreinforced masonry structures.

Figure 1. An ideal house with high quake resistance and heat insulation with AAC blocks

2 MASONRY MATERIALS AND STRUCTURAL) SYSTEM

Tow types of AAC blocks are shown in Table 2.1 and the block configurations and structural system of bearing walls are shown in Figure. 2.1.

Masonry walls were constituted by two types of AAC blocks. One had nominal dimensions of 750 x 150 x 250mm (wide w_b, height h_b and thickness t_b) and specific gravity in oven-dry of 3.7 kN/m³ (AAC(37)). The other had nominal dimensions of 500 x 200 x 250mm and specific gravity in oven-dry of 4.2 kN/m³ (AAC(42)). AAC(37) was reinforced with 3.2mm internal bars and AAC(42) was unreinforced. Both cases had grooves of wide 150mm and depth 15mm from the bottom and sides and 50mm diameter vertical holes at 250mm spacing. Vertical reinforcements of 20mm had screws at both ends and they were cast in the vertical holes of the blocks at 750mm spacing. The vertical bars were jointed to anchor bolts embedded in beams with high nuts. Horizontal re-bar of 10mm were cast in the bottom grooves of the blocks at 600mm spacing. The blocks were pasted with sealant and built. The grooves and vertical holes were fully grouted in order to achieve a good bonding behavior between the bars and blocks.

Mechanical properties of the materials presented in Table 2.2 shows mean values obtained from test results. Compression tests of the AAC referring to Japanese Industrial Standard: JIS A 5416-2007, compression tests of the grout referring to JSCE Standard Specifications for Concrete Structures: JSCE-G 521-2013 and tensile tests of the bars referring to JIS Z 2241-2011 were carried out. Test setups used were an amsler testing machine or an electromechanical universal testing machine. Maximum strength was obtained from maximum force per cross sectional area. Yield point was obtained from upper yield point of vertical and horizontal bars and 0.2% offset yield strength of internal bars. Young modulus was obtained from secant stiffness between the origin point and one-third point of the maximum stress in stress - strain curve. The strain was obtained from strain gauges on the test specimens.

Table 2.1. Types of AAC blocks

block type	internal bars	configuration (w_b x h_b x t_b)	specific gravity (oven-dty)
AAC(37)	exist	750 x 150 x 250mm	0.37 kN/m³
AAC(42)	non	500 x 200 x 250mm	0.42 kN/m³
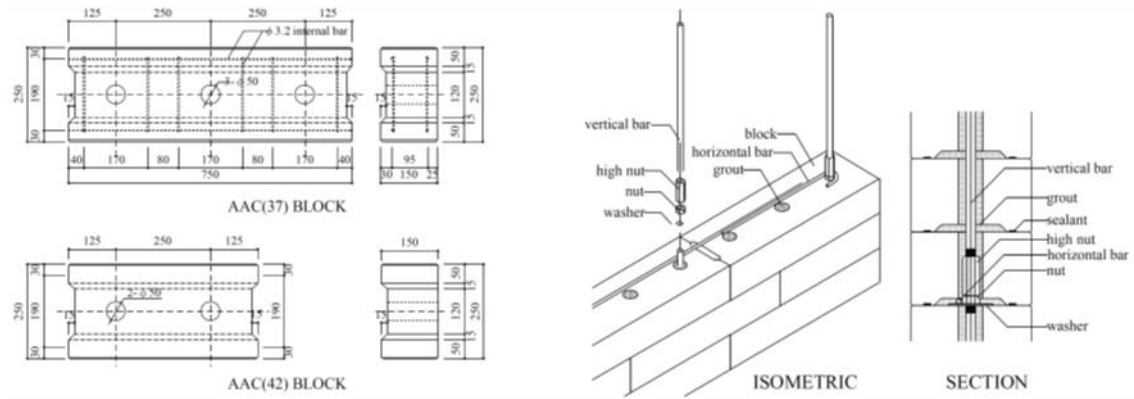
Figure 2.1. Block configurations and structural system

Table 2.2. Mechanical properties of materials

test	material	test specimen (mm)	number	yield point (N/mm²)	strength (N/mm²)	Young modulus (kN/mm²)
tensile	vertical bar	φ20 x 500	3	354	560	208
	horizontal bar	φ10 x 450	3	363	508	202
	internal bar	φ3.2 x 600	9	673	686	214
	AAC(37)	φ50 x 100	6	-	0.61	1.67
	AAC(42)		5	-	0.66	1.45
compression	AAC(37)	75 x 75 x 75	6	-	3.3	1.71
	AAC(42)	100 x 100 x 100	5	-	2.7	1.04
	grout	φ50 x 100	18	-	42.4	17.6

3 COMPRESSION AND SHEAR TESTS OF LAMINATED AAC BLOCKS

3.1 Outline of specimens and Loading

Test schemes are shown in Table 3.1, and configurations of test specimens are shown in Figure 3.1 and test setups are shown in Figure 3.2. Three specimens constituted by AAC(37) or AAC(42) were carried out each in case of compression tests and shear tests. Loading was conducted by an amsler testing machine. Force and axial deformations were measured in case of compression test and force and diagonal deformations were measured in the case of shear test.

3.2 Test results and behavior

3.2.1 Compression test

Final cracking patterns and pictures of the specimens at the end of compression test are shown in Figure 3.3. The specimens used with AAC(37) developed vertical cracks immediately before the maximum force, and those cracks proceeded towards the axial direction in post-peak. The cracks of the cut ends were observed near internal bars and corners of the bottom grooves of the blocks. The specimens used with AAC(42) developed first vertical cracks in central part of surfaces of the blocks at half of the maximum force. Thereafter the cracks of the cut ends were observed near corners of the bottom grooves immediately before the maximum force, and those cracks proceeded towards the axial direction in post-peak.

Representative compressive stress - strain curves are shown in Figure 3.4. It was found that the stress - strain curve shows a straight line right before the maximum force in specimens. The stress was obtained from the force per cross section area. As for the AAC(37) specimens, sudden drop was observed in post-peak and the deformation proceeded while the force kept about 70% of the

Table 3.1. Test schemes

test	blocks	configurations (mm)	number
compression	AAC(37)	250 x 750 x 750	3
	AAC(42)	250 x 250 x 1000	3
shear	AAC(37)	750 x 750 x 250	3
	AAC(42)	1000 x 1000 x 250	3

(a) Compression test   (b) Shear test

Figure 3.1. Test specimen

(a) Compression test   (b) Shear test
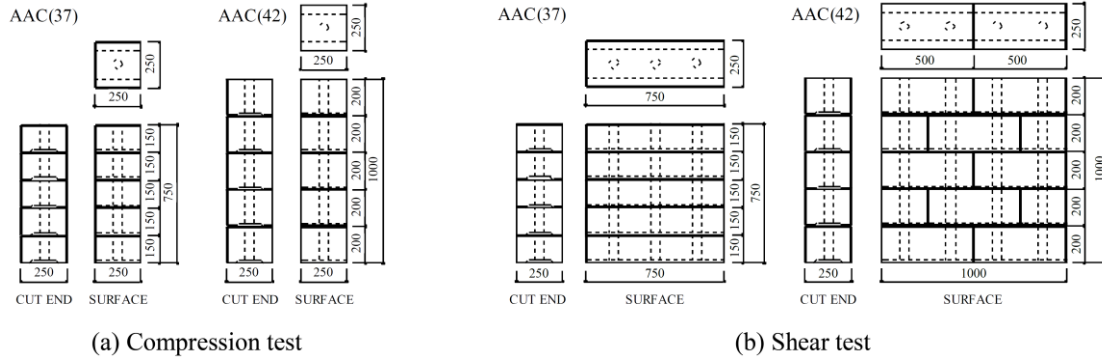
Figure 3.2. Test setup

(a) AAC(37)   (b) AAC(42)
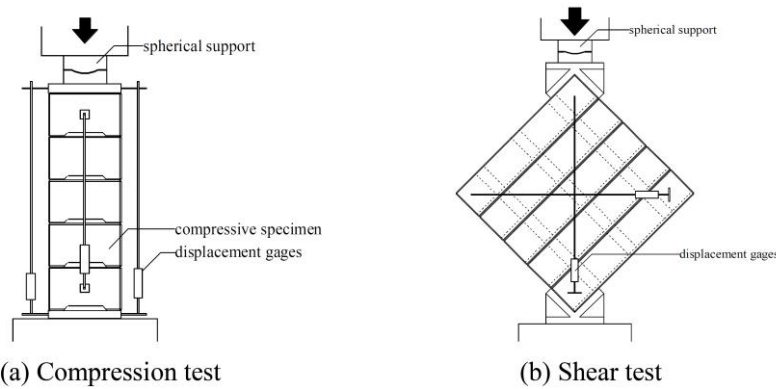
Figure 3.3. Final cracking patterns and pictures of the specimens at the end of compression test
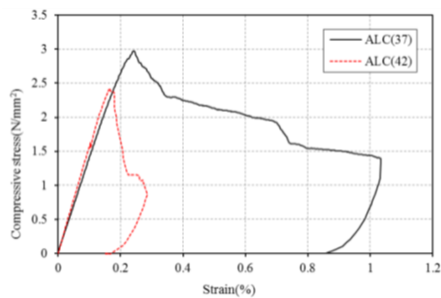
Figure 3.4. Compression stress-strain relationship

Table 3.2. Compression test results

block type	compressive strength (N/mm²)		Young modulus (N/mm²)		strain (%)	
	A	A$_e$	A	A$_e$	P$_{max}$	0.85P$_{max}$
ALC(37)	2.8	4.6	1211	2015	0.24	0.30
ALC(42)	2.4	3.9	1407	2346	0.18	0.19

maximum force. Thereafter the strain achieved 1% in half of the maximum force. As for the AAC(42) specimens, sharp post-peak drop was observed in post-peak and the strain achieved 0.2% in half of the maximum force.

Mean values of compression test results are shown in Table 3.2. The blocks were built after sealant was applied to the bottom of the blocks in order to prevent grout from leaking in joints of the walls. There was a slight space between each surfaces of the blocks and the groove and holes of the blocks were grouted. Therefore, it is considered that the stress in the walls is transferred in contact parts of the blocks and grout (effective cross section, A$_e$). Accordingly, effective compressive strength and effective Young modulus was obtained from using A$_e$ in addition to all cross section, A. The strain was obtained at the maximum force, P$_{max}$ and 85% of the maximum force, 0.85P$_{max}$.

3.2.2 Shear test

Final cracking patterns and pictures of the specimens at the end of shear tests are shown in Figure 3.5. Shear cracks developed when shear strain achieved about 0.1% in all specimens. The AAC(37) specimens developed new shear cracks. As for AAC(42), the shear cracks proceeded and widened extremely. It is considered that the internal bars avoid progress and widening of the shear cracks in Specimen with AAC(37).

Representative shear stress - shear strain curves are shown in Figure 3.6. The shear stress - shear strain curve showed a straight line right before maximum force. As for AAC(37), post-peak drop was observed in post-peak and the shear strain achieved about 2% in half of maximum force. As for AAC(42), the shrap post-peak drop was observed and the shear strain achived 0.5 % in half of maximum force. It is considered that shear reinforcing effect of the internal bars avoid sharp post-peak drop and enhance displacement capacity. The mean value of shear test results is shown in Table 3.3. As with compression test, the shear strength and shear modulus was obtained from using both A$_e$ and A.
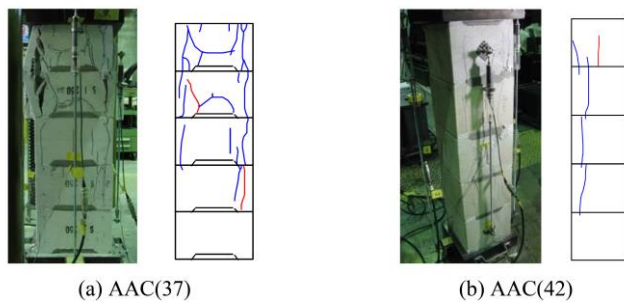

(a) AAC(37) (b) AAC(42)
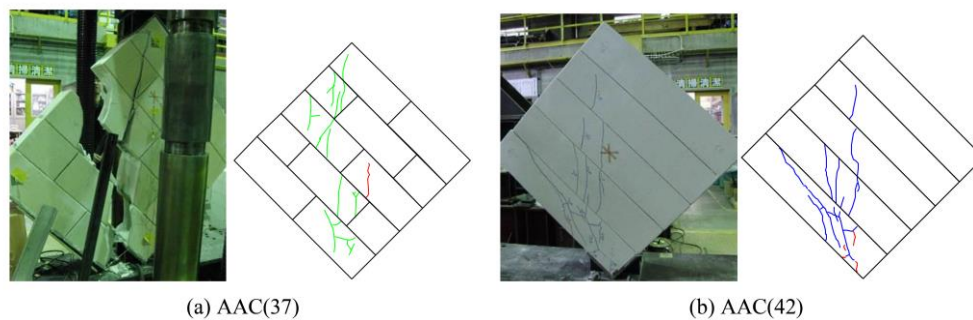
Figure 3.5. Final cracking patterns and pictures of the specimens at the end of shear test
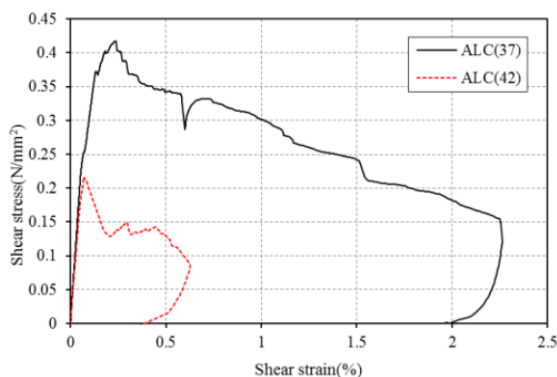
Figure 3.6. Shear stress-Shear strain relationship

Table 3.3. Shear test results

block type	shear strength (N/mm²)		shear modulus (N/mm²)		strain (%)
	A	A_e	A	A_e	P_{max}
ALC(37)	0.41	0.69	303	504	0.23
ALC(42)	0.20	0.33	265	441	0.08

4 IN-PLANE TEST OF BEARING WALL

4.1 In-plane behavior of wall with no opening for horizontal load

4.1.1 Outline of the test

In-plane tests of bearing walls were carried out on full scale masonry walls built with the two types of AAC blocks. Test schemes, test setup, configurations of test, and target story drift levels, are shown in Table 4.1, in Figure 4.1, in Figure 4.2, and in Table 4.2, respectively. Two walls with a length l of 1.5m and 4.5m were built with AAC(37) blocks and the other with a length l of 1.5m was built with AAC(42) blocks. A reinforced concrete top beam was built in each wall in order to distribute better the applied lateral force. No vertical load was applied. The vertical holes which the vertical reinforcements were cast in, were grouted and the others were not grouted. Test setup used was a cantilever system which was fixed at the base and free at the top. Lateral force was applied by a displacement-controlled horizontal hydraulic actuator.

4.1.2 Test results

Pictures of the specimens at the end of tests are shown in Figure 4.3, and force - deformation curves are shown in Figure 4.4. The force was obtained from the force per wall length. Integrated behavior was observed in all specimens. It is assumed that each AAC masonry blocks was sufficiently bonded with grout. The 1.5m wall with AAC(37) developed flexural cracks at 1/941 rad (0.10% drift) and shear cracks at 1/192 rad (0.51% drift). A vertical bar which was applied tension achieved yield strength at 1/186 rad (0.53% drift), then maximum force of 44.7 kN/m was obtained at 1/51 rad (1.96% drift). Force kept 80% of the maximum force in post-peak and the wall failed in shear failure mode at 1/26 rad (3.84% drift).

The 4.5m wall with AAC(37) developed flexural cracks at 1/1454 rad (0.07% drift) and shear cracks at 1/736 rad (0.13% drift). A vertical bar which was applied tension achieved yield strength at 1/352 rad (0.28% drift), then the maximum force of 67.3 kN/m was obtained at 1/251 rad (0.40% drift). Force kept 90% of maximum force in post peak and a horizontal re-bar fractured in shear failure mode at 1/22 rad (4.55% drift). It is noteworthy fact that stiffness per wall length

of 4.5m wall was 4 times as large as that of 1.5m wall in the first flexural cracks.

The 1.5m wall with AAC(42) developed flexural cracks at 1/488 rad (0.21% drift) and shear cracks at 1/293 rad (0.34% drift). A vertical bar when applied tension, achieved yield strength at 1/163 rad (0.61% drift), then the maximum force of 37.7 kN/m was obtained at 1/131 rad (0.76% drift). Force deteriorated in post peak and the wall failed in shear failure mode at 1/34 rad (2.94% drift). It is considered that the internal reinforcements avoid post-peak drop and enhance displacement capacity as observed in the shear tests.

Table 4.1. Test schemes

block type	internal bars	length (m)	height (m)	thickness (m)	vertical reinforcement	horizontal re-bar
AAC(37)	exist	1.5	3	0.25	φ20	φ10
AAC(37)		4.5				
AAC(42)	non	1.5				

Figure 4.1. Test setup

(a) AAC(37) *l*=1.5m   (b) AAC(37) *l*=4.5m   (c) AAC(42) *l*=1.5m
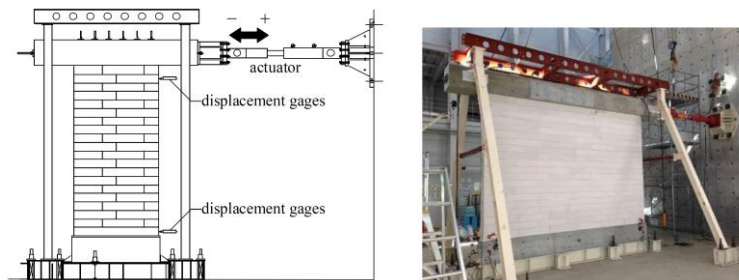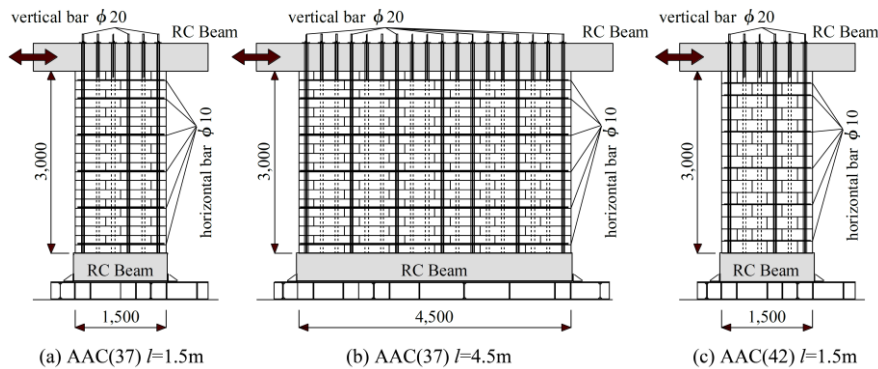
Figure 4.1. Test specimens

Table 4.2. Target story drift level (rad.)

l (m)	Target story drift level (rad)
1.5	±1/2000, ±1/1000, ±1/500, ±1/300, ±1/150, ±1/100, ±1/300, ±1/50, Monotonic force(+)
4.5	±1/4000, ±1/2000, ±1/1500, ±1/1000, ±1/750, ±1/500, ±1/250, ±1/150, Monotonic force(+)

(a) AAC(37) *l*=1.5m   (b) AAC(37) *l*=4.5m   (c) AAC(42) *l*=1.5m
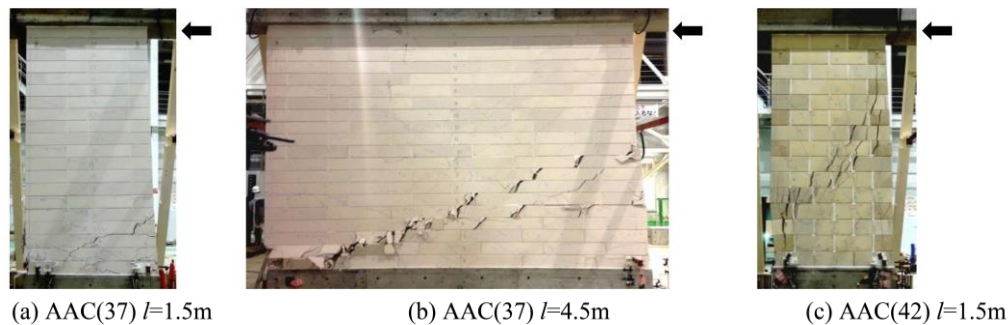
Figure 4.3. Pictures of the specimen at the end of test under positive direction loading

(a) AAC(37) l=1.5m   (b) AAC(37) l=4.5m   (c) AAC(42) l=1.5m
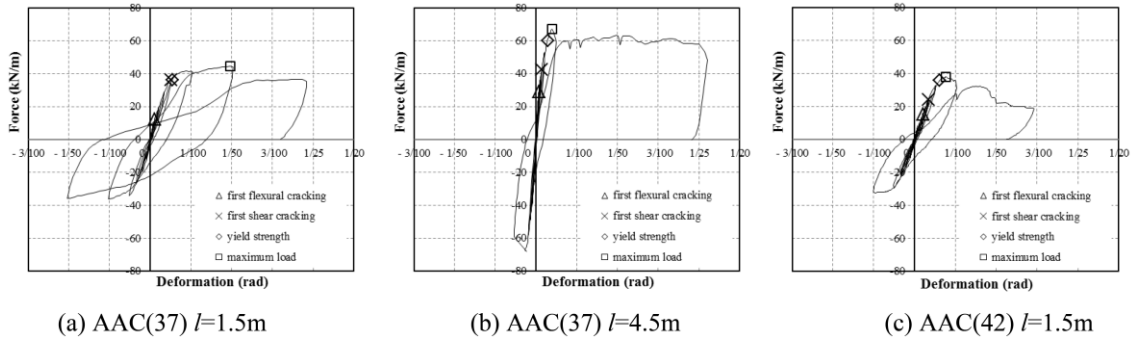
Figure 4.4. Force-deformation relationship

(a) Cantilever beam   (b) Equivalent stress block in ultimate moment

	AAC(37)	AAC(42)
k1	0.74	0.66
k2	0.37	0.33
k3	0.85	0.85
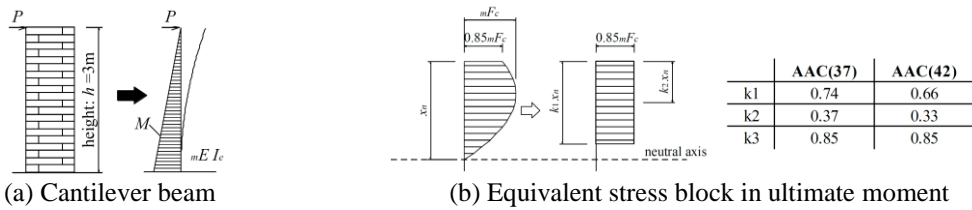
Figure 4.5. Assumption for calculation

(a) AAC(37) l=1.5m   (b) AAC(37) l=4.5m   (c) AAC(42) l=1.5m
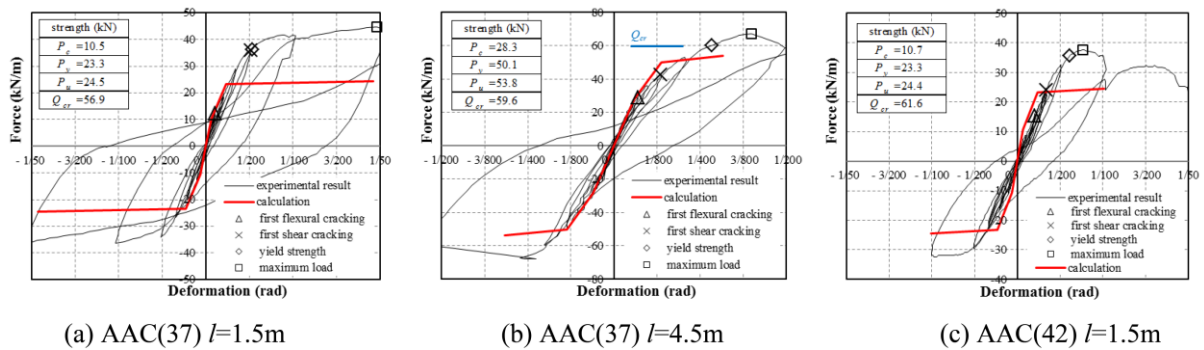
Figure 4.6. Comparison between experimental results and calculation

4.1.3   Simulation of the force – deformation relationship

The test results of bearing wall were evaluated by following hypothesis and calculation model. The bearing wall was calculated as a cantilever beam which has an effective cross section, A_e according to Navier's hypothesis in Figure 4.5(a). The AAC and grout were considered as a homogeneous material which has effective compressive strength, Young modulus, and shear modulus, obtained from compression and shear tests. Tensile strength of the material was provided by tensile strength of AAC. Compressive stress of the material was directly proportional to strain of the material until yield moment. In ultimate moment of flexural failure mode, an equivalent compressive stress block which has the same area as that of actual stress and 85% of effective compressive strength replaced actual compressive stress in Figure 4.5(b). The value of k_1 was obtained from the compression tests. The vertical reinforcement was considered as elastic perfectly plastic model which has yield point and Young modulus obtained from the experimental tests.

Comparison between the experimental results and the calculation was shown in Figure 4.6. Deformation of the calculation was given by sum of the flexural deformation and shear deformation. As for AAC(37) walls, the flexural cracking strength and deformation obtained from the experimental results were in good agreement with one of calculation, however the shear cracking strength lower than those calculated value. The stiffness of experimental results after flexural cracking agreed with them of calculation. As for AAC(42) wall, the flexural cracking strength of

experimental result showed good agreement with one of calculation, however the flexural cracking deformation and shear cracking strength did not. The yield strength and ultimate strength of AAC(37) and AAC(42) walls obtained from experimental results were higher than that of calculation. The deformation of peak force was approximately agree with that of calculation.

4.2   In-plane behavior of wall with openings for horizontal load

Experiments and FEM analyzes of AAC masonry walls with openings were conducted and methods for evaluating proof stress and rigidity were studied. Figure 4.7 shows the shape of the specimen. Three specimens with different opening shapes were used, and the materials used were in accordance with AAC(37) in Table 2.2. The loading method was repeated loading using positive and negative alternating loads using a hydraulic jack attached to one side of the RC stub installed on the top of the test specimen.

Figure 4.8 shows the load deformation relationship. The 1 / 1500rad circle in the Figure indicates the allowable deformation angle (short-term allowable deformation angle) for level 1 earthquake motion. There is no residual cracking up to ± 1 / 1000rad in all specimens, and the maximum displacement showed a ductile behavior of about 1/50 rad. Specimen A37_w45-W1_15 cracked at the corner of the opening at 1 / 2000rad and then extended. In specimen Specimen A37_w45-W2_15, cracks occurred at the corners of the opening and the wall legs at 1 / 2000rad. Specimen A37_w45-W3_15 cracked at 1 / 1500rad.

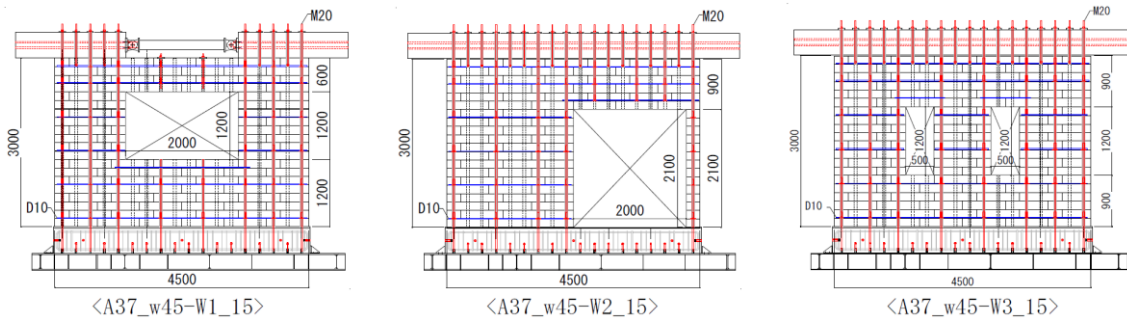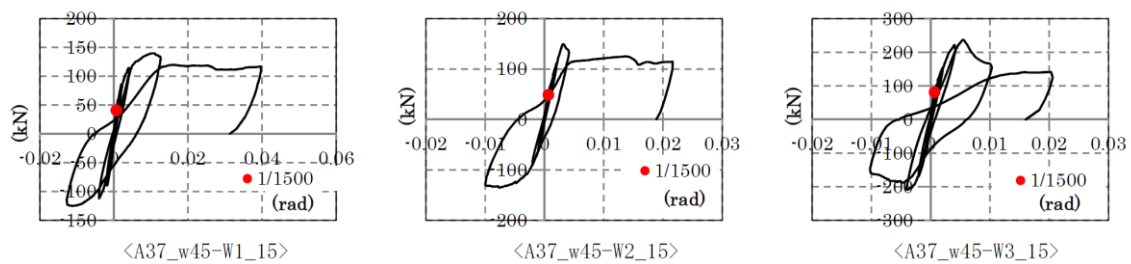Figure 4.7 Outline of specimens

Figure 4.8 Force-deformation relationship

(a) Wall strength in each length   (b) Reduction factor to aperture ratio
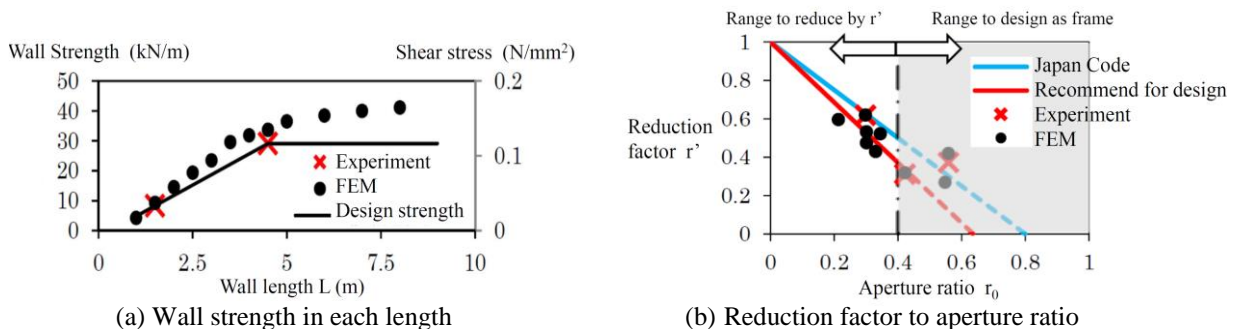
Figure 4.9. Investigation reduction factor of wall with opening

Although this construction method is a masonry construction of AAC blocks, it has been confirmed by experiments that it can move as a unit up to 1 / 1500rad. Therefore, the analysis is performed assuming that the continuum of the AAC masonry having the single material characteristics. FEM analysis was performed on the non-opened walls described in the previous section, and the open wall. The load and rigidity at 1/1500 rad almost agreed with the experimental values. In other words, it was confirmed that the elastic performance can be estimated by FEM analysis using a simple model. Based on this, the same analysis was carried out for other wall lengths, and an attempt was made to interpolate yield strength and rigidity. Figure 4.9.(a) shows the analysis results and experimental results. As the wall length increased, the load per unit wall length increased, but when the wall length exceeded a certain level, the tendency to converge was confirmed. The design strength as shown by the solid line in the Figure is set on the safety side.

As with the non-opening walls, FEM analysis was performed on the walls with openings that differed from the experiments, and the reduction factor of wall stiffness due to openings in the Building Standards Act Notification in Japan. The analysis result showed that the reduction was slightly larger than the notification formula when the aperture ratio r_0 was 0.4 or less (Figure 4.9.(b)). For example, by using r′ in Equation (1), the average rigidity of the wall with openings can be estimated.

$$r' = 1 - 1.57\sqrt{h_{op} \cdot l_{op}/(h \cdot l)} \qquad (1)$$

Where, $h_{op} \cdot l_{op}$, $h \cdot l$: found area of opening and bearing wall, respectively

5   CONCLUSIONS

(1) The AAC masonry was subjected to compression and shear tests, and the significant values were obtained by the concept of effective strength and rigidity considering the stress transmission path. Internal rebar was effective of suppressing the force deterioration after the maximum resistance, and damage such as cracks, when compression and shear forces are applied to the block.

(2) The rigidity per unit length of the wall was larger as the wall length was longer. The test specimen with reinforcing bars inside the masonry did not cause a sudden decrease in yield strength even after the maximum load, and had the ability to deform while maintaining about 80% of the maximum load until deformation of 1/30 rad. Also, the shorter the wall length, the greater the rate of bending deformation.

(3) In the experiment of the wall with an opening, cracks occurred at the corner of the opening at 1/2000 rad, but there was no residual crack up to 1/1000 rad, and after that it showed stable behavior up to 1/50 rad. Rigidity up to 1/1500 rad was able to be evaluated with a simple FEM analysis model that is assumed to be a continuum of AAC masonry with single material characteristics, both with and without openings.

REFERENCES

K.Takashima, S.Nakata, R.Nakamura, H.Iida, T.Hanai, A.Tasai, 2017, Experimental study on masonry walls using AAC blocks, 16WCEE, N⁰705.

K.Takashima, S.Nakata, R.Nakamura, H.Iida, T.Hanai, A.Tasai, K.Kusunoki et al, 2015, Experimental study on material properties and in-plane shear behavior of masonry walls using ALC blocks, (Part 1)-(Part 5), AIJ Summaries of technical papers of annual meeting, CD-ROM.

R.Nakamura, K.Takashima, A.Tasai, K.Sugimoto et al, 2016, Experimental study on material properties and in-plane shear behavior of masonry walls using ALC blocks, (Part 7), AIJ Summaries of technical papers of annual meeting, CD-ROM.

2nd International Workshop on Advanced Materials and
Innovative Systems in Structural Engineering:
Novel Researches

ISTANBUL
fib IWAMISSE
Turkey 2019

Repair of severely damaged columns with innovative techniques and High Performance Concrete

Camillo Nuti[1], Davide Lavorato[2], Gabriele Fiorentino[3], Alessandro Vittorio Bergami[4], Bruno Briseghella[5]

[1] Full Professor, Department of Architecture, Roma Tre University, Rome, Italy
[2] Associate Professor, Department of Architecture, Roma Tre University, Rome, Italy
[3] Research Associate, Department of Architecture, Roma Tre University, Rome, Italy
[4] Assistant Professor, Department of Architecture, Roma Tre University, Rome, Italy
[5] Full Professor and Dean, College of Civil Engineering, Fuzhou University, Fuzhou, China

ABSTRACT: This work aims at describing some innovative retrofitting interventions made on Chinese Reinforced Concrete (RC) bridge piers which were damaged due to string earthquakes. These interventions can guarantee proper energy dissipation due to the formation of plastic hinges as well as a larger shear strength in line with capacity design criteria. In this work are discussed some improvements made to repair and retrofitting techniques applied during previous experimental campaigns in Italy and China on bridges designed without appropriate seismic details. The improvements in these techniques are: a) A novel type of concrete jacket which uses Ultra High Performance Concrete (UHPC), using fibers to replace the damaged areas and improving the shear strength of the pier; b) the introduction of new shaped rebar parts to substitute the damaged rebar parts; c) Novel systems to realize the connections between the new rebar parts and the undamaged original rebars. Plastic dissipation is assured by the new rebar parts. The rebar connections are realized by strong steel couplers and welding chords to simplify the connection at the construction site. Different fiber contents (1,2, 3%) were considered for the UHPC used in the concrete jacket. According to the formulation CNR-DT 204/2006 it is confirmed that the concrete jacket with fibers provides the necessary shear strength. Some RC pier specimen (scale 1:6) were repaired and retrofitted by means of the proposed interventions with and without new stirrups in the repaired zone and external wrapping (CFRP or steel). Cyclic tests have been carried out on these scaled specimens at Fuzhou University SIBERC lab (China) to evaluate the effectiveness of the proposed technique. In particular, the experimental tests on the pier specimen repaired by using the UHPC jacket with fiber without new stirrups and external wrapping confirm that the concrete jacket assures the necessary shear strength increment.

1 INTRODUCTION

The time necessary to re-open a bridge damaged after a strong earthquake, is a key point for the selection of the proper repair and retrofitting interventions on the bridge. In fact, bridges are usually considered as strategic structures and their quick opening for the emergency response is priority. Different solutions were presented in literature to execute rapid repair interventions on Reinforced Concrete (RC) columns or piers (Sun et al. 2011, He et al. 2013, Cheng et al. 2003). In this paper is presented a new rapid repair solution, which improves the repair and retrofitting interventions proposed and tested successfully by means of PSD (pseudo-dynamic) tests on seismic damaged Italian bridges piers at the Department of Architecture of University of Roma Tre lab (Lavorato et al. 2015a) or by cyclic tests on Chinese piers at SIBERC lab (Sustainable

and Innovative Bridges Engineering Research Center of the Fujian Province University) at University of Fuzhou (Lavorato et al. 2015b). The damaged parts of the RC pier are repaired and retrofitted (plastic hinge, Fig. 2) by means of: the substitution of damaged rebar parts using new shaped rebar parts, the construction of a concrete jacket without modifying the pier dimension (Fig. 2b) to restore the damaged concrete and new stirrups in the repaired damaged zone and/or an external C-FRP wrapping to increase the pier shear strength and ductility. The substitution of the damaged stirrups was limited to the use of a minimum stirrups content to simplify the new concrete casting. The effectiveness of the shaped rebar was tested successfully on pier specimen (scale 1:6) by cyclic test at Fuzhou University lab (Lavorato et al. 2015b). In this paper, some new technique improvements are presented about the rebar substitution, the concrete restoration and the shear and ductility improvements to simplify the interventions reducing time and cost. In particular, the shaped rebar connection with the original rebar was realized by means of strong steel coupler using symmetric side welding connections. This system is simple to perform in situ on vertical longitudinal rebar in modest space (removed concrete) and it guarantees a rebar connection along the same axis avoiding local bending action on the connection. Another improvement regards the use of a fiber concrete jacket to restore the damaged concrete without modifying the pier dimension. This concrete was designed to guarantee also the shear strength improvement without using transversal steel reinforcement and external C-FRP wrapping to obtain time and cost saving. In fact, different research studies demonstrated how concrete with fibers can give an important contribution to the ductility and shear strength capacity of RC beam and columns (Le Huang et al. 2015, Foster and Attard 2001, Mansur et al. 1986). In particular, Ultra-High Performance Concrete (UHPC) with steel fibers were designed properly at Fuzhou University Lab considering different fiber content (1 %, 2 % and 3%) and tested by compression and flexural tests. Some pier specimen in scale 1:6 were repaired with and without new steel stirrups and external wrapping (CFRP or Steel) in plastic hinge only using fiber concrete to evaluate the feasibility and the effectiveness of the interventions. The use of steel tissue was considered as alternative to the C-FRP wrapping to increase shear strength and ductility of the pier specimen with external wrapping. The shear strength due to the UHPC concrete jacket was evaluated using the model by CNR-DT 204/2006 using the concrete experimental test results.

2   RC BRIDGE CASE STUDY

An irregular RC bridge (Fig. 1) was designed according the Chinese codes (JTG D60-2004, JTG/T B02-01-2008, JTG D62-2004). The transversal pier reinforcement reproduced the one of some existing bridges with insufficient shear reinforcement to consider the problem of the shear and ductility retrofitting during the repair operations (a problem for many existing RC bridges). The RC bridge geometries are shown in Fig. 1 whereas the design details for the steel reinforcement of the bridge piers are described in Lavorato et al. (2015b). The center pier of this bridge, the most stressed pier during seismic action application, was severely damaged at the pier base in plastic hinge and damage consisted in: concrete spalling and crushing, transversal stirrups rupture, longitudinal rebar buckling and ruptures and evident shear cracking.
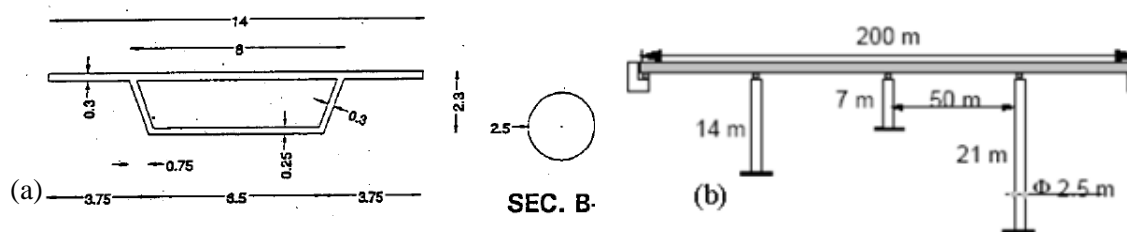

Figure 1. Chinese irregular RC bridge geometries: a) deck and pier sections b) irregular pier configuration.

3   RAPID REPAIR AND RETROFITTING INTERVENTION ON RC BRIDGE PIERS

A rapid repair and retrofitting solution was applied on the most stressed and damaged RC bridge pier in plastic hinge only (Lavorato et al. 2015a). This technique consisted of: damaged concrete and rebar parts removal along the entire pier surface in plastic hinge (Fig. 2a), substitution of the damaged rebar parts by new rebar parts, damaged concrete restoration by self-compacting concrete (Fig. 2b) and shear strength and ductility improvements by the application of an external C-FRP wrapping (Fig. 2c).
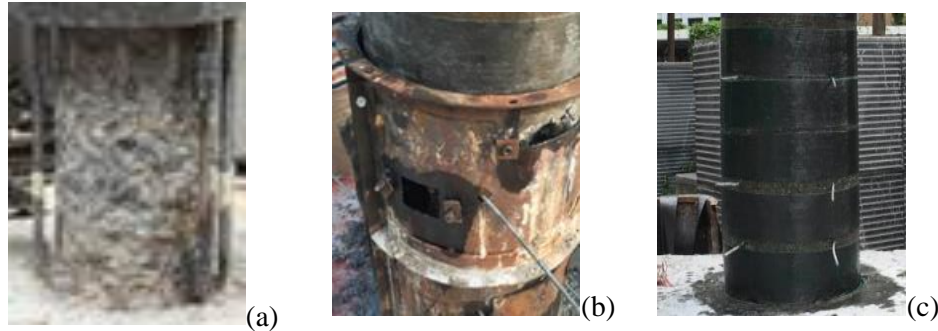
Figure 2. Rapid repair and seismic retrofitting solution for damaged RC pier (Lavorato et al. 2015a,b): a) damaged concrete and rebar parts removal; b) concrete restoration; c) seismic retrofitting by C-FRP wrapping.

The previous research campaign on Italian and Eurocode EC8 bridges assures the feasibility and the effectiveness of the interventions to restore the pier strength. However, high local plastic strains were observed in some rebar welding connections between the original undamaged rebar and the new rebar parts. For that reason, a new research campaign in collaboration with the Fuzhou University tested with success shaped rebar systems to replace the damaged rebar parts. The shape of this new rebar permitted a proper plastic distribution along the new rebar parts only and it was tested successfully on Chinese repaired pier specimen (scale 1:6) by cyclic tests at Fuzhou University. In this paper new improvements of rebar substitution and concrete restoration are presented to simplify the intervention. In particular, the connection in situ between new and original rebar parts during the rebar substitution is analyzed and strong welding connection systems by steel coupler and two symmetric strong side welding chords were designed to connect the new shaped rebar parts with the original undamaged rebar parts in the pier. This connection system is simple to perform in situ on vertical longitudinal rebar in modest space (removed concrete). The new and original rebar parts are connected along the same longitudinal axis avoiding local rotation and plastic deformation as observed in Lavorato et al. 2015a.

A concrete jacket (CJ) realized by means of an UHFRC (Ultra-High Fiber Reinforced Concrete) can restore the removed concrete cover and the external parts of the core and increases the insufficient original shear strength and ductility without using new stirrups and/or external wrapping reducing time and cost of the interventions. The pier geometries are not modified as the CJ substitutes the removed concrete parts only and the pier appearance does not change after the repair. The UHFRC was designed to have: great pass-ability during the casting in the very modest space with steel reinforcement (as a fresh Self compacting concrete), the development of the maximum compressive strength after a few days for a rapid opening of the bridge, the necessary shear strength by steel fibers contribution to reduce as possible as the steel stirrups and external wrapping and great durability as the cover dimension are not changed. In particular, three different UHFRC mix designs were considered (Table 1). Each mix design includes: a super-plasticizer, silica fume and fine sand to guarantee high mobility and pass ability similar to the ones of a self-compacting concrete (SCC). In this way, the casting results simple, rapid and uniform also in modest space (cover and external part of pier core).

Table 1. Mix designs of the UHFRC developed at Fuzhou University lab to restore the damaged concrete parts of the Chinese pier specimen in scale 1:6.

Steel Fiber content	water/ cement (W/B)	Cement (C)	Silica fume/ cement (SF/C)	Sand/ cement (S/C)	Superplasticizer/ cement (Su/C)
1 %					
2 %	0.26	1	0.3	1.20	0.025
3 %					

Steel fibers were added to the UHFRC mix design to increase the durability and guarantee the necessary shear strength of the CJ without steel stirrups and external C-FRP wrapping. These fibers have an ultimate tensile strength of 2000 MPa and modulus of Elasticity of 200 GPa. The mechanical performance of the UHFRC depends on the aspect ratio and the volume fraction of the fibers. The selected fibers are straight and smooth with length $l_f = 13$ mm and equivalent diameter $d_f = 0.20$ mm. Different percentage of fibers (V_f) were considered 1 %, 2 % and 3 % (volume of steel fibers to the volume of concrete) to evaluate the corresponding shear strength contribution and the fresh state properties to permit the casting of the concrete in modest space. UHFRC specimen were built at Fuzhou University lab to execute compression and flexion tests. In particular, the compression tests were executed on three UHFRC cube specimen (100 x 100 x 100 mm) for each fiber percentage after 6 days to evaluate the cylindrical compression strength (f_{cm6}) developed by the specimen in short time (Table 2). The mean value of the cylindrical compressive strength after 28 (f_{cm28}) days was also calculated according to Fib model code 2010 (Table 2). The comparison between cylindrical compressive strength after 6 or 28 days shows that almost the maximum strength value was exhibited after 6 days. This result confirms that the UHFRC is a good material for a rapid concrete restoration. Finally, flexion tests were carried out on three prismatic specimen for each steel fiber percentage (100 x 100 x 400 mm prismatic specimen bended under four flexion points) with a notch size of 30 mm obtaining an equivalent flexural strength (f_{eq2}) corresponding to crack opening of 1.8 mm in agreement with the CNR-DT 204/2006 (Table 2). The characteristic value of the ultimate tensile residual strength (f_{Ftuk}) was also obtained according to CNR-DT 204/2006.

Table 2. UHFRC mechanical properties: percentage of fibers in concrete (V_f), cylindrical compression strength after 6 days (f_{cm6}) and after 28 days (f_{cm28}); equivalent flexural strength (f_{eq2}), ultimate tensile residual strength (f_{Ftuk}). All value in MPa

V_f	f_{cm6}	f_{cm28}	f_{eq2}	f_{Ftuk}
1 %	84	99	12.3	4.1
2 %	91	108	15.1	5.0
3 %	97	114	16.5	5.5

4   REPAIRED SCALED 1:6 PIER SPECIMEN
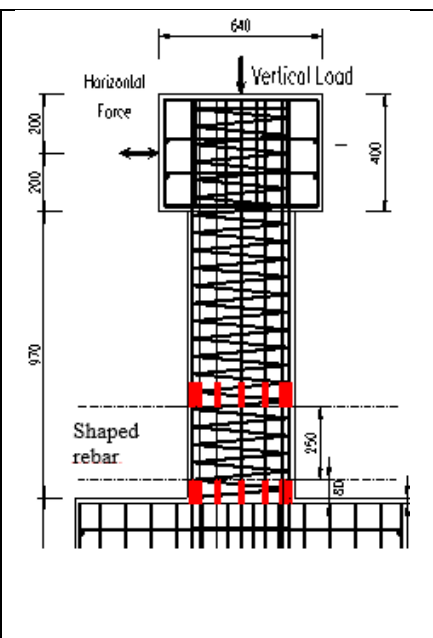
The most stressed pier of the Chinese irregular RC bridge in Fig. 1 during the seismic action application is the center one (Lavorato et al. 2015b) and the main damage of the bridge focuses on this pier. For that reason, some 1:6 scaled pier specimen representative of this pier, were designed. Their geometries and reinforcement details were obtained using scale factors which

guarantee similitude criteria between pier model and pier prototype in terms of global quantities (flexural and shear strength and confinement effect; Lavorato et al. 2015a, 2015b). The perfect geometrical scaling of materials is not necessary allowing the use of ordinary concrete mixing and commercial steel rebars simplifying the construction of the pier specimen and the tests on concrete and steel rebars specimen. Nine RC pier specimen in scale 1:6 were damaged after some cyclic tests and then were repaired with different types of repair and retrofitting interventions in plastic hinge zone only (Table 3). These pier specimen had diameter equal to 420 mm and height 1170 mm (Table 3), longitudinal reinforcement composed by 14 rebars with diameter of 18 mm and transversal reinforcement out of the plastic hinge with space of 60 mm and diameter of 4 mm. The repaired specimen have different reinforcement configuration in plastic hinge zone. In particular, there are pier specimen with and without stirrups and external wrapping. The repaired specimen have insufficient shear strength and the ductility and different retrofitting solution were evaluated.

Table 3. Repair and retrofitting details for Chinese pier specimen (scaled 1:6): type of concrete jacket (CJ), lenght of the new shaped rebar (Ls), diameter of the new shaped rebar (ΦSR), diameter of the sirrups (Φs), spacing of the stirrups (s), number of the external C-FRP wrapping layers (ne). [mm]

Label	CJ	Ls	ΦSR	Φs	s	ne
1	SCC	250		4	60	1
2	SCC	125		4	60	1
3	SCC	250		4	60	1
4	HFRC-I	250		4	60	1
5	HFRC-I	250	15	-	-	-
6	UHFRC	250		4	60	1
7	UHFRC	250		-	-	-
8	UHFRC	250		-	-	-
9	SCC	250	18	4	60	-

Note: concrete jacket (CJ) types: self compacting concrete (SCC); High performance fiber reinforced concrete developed at Roma Tre Lab (HFRC-I), Ultra High performance fiber reinforced concrete developed at Fuzhou University (UHFRC).

The pier specimen (5, 7 and 8) without stirrups and external confinement will be tested to evaluate the shear strength contribution of the fiber concrete jacket CJ only. Different concrete mix designs were developed to restore the specimen damaged concrete: an UHFRC with steel fiber developed and tested at Fuzhou University (it was described above) and a High Fiber Reinforced Concrete (HFRC-I) developed at Roma Tre University Lab (Italy). The HFRC-I was realized using 2 or 3 % of polymeric fibers (by ISTRICE) and a commercial repair mortar (commercial name Geolite MAGMA by Kerakoll) very fluid at fresh state with optimum compressive strength after 6 days. The HFRC-I will be not described here in details.

The pier specimen with stirrups and external confinement (1, 2, 3, 4, 6 and 9) have been tested to compare their responses with the ones of the specimen without stirrups and external confinement. An external C-FRP wrapping with one layer only (ne=1) was selected for this first part of the research campaign. The external wrapping provides ductility and shear strength enhancements. The C-FRP mechanical properties are: thickness of 0.167mm, elastic modulus 242GPa and maximum deformation of 0.005 in accordance with CNR DT 200/2013 Italian guideline. External

steel sheet wrapping (by Kerakoll) will be used as alternative to the C-FRP wrapping during the second part of the ongoing research campaign to increase the shear strength and the ductility. This reinforcement combines excellent mechanical and installation properties with high durability thanks to galvanization of the individual wires and is extremely easy to handle and shape. The steel sheets represent an interesting alternative with respect to C-FRP sheet. In fact, they can be anchored and fastened on concrete elements by simple metal plates without taking particular precautions about sheet-anchorage system interactions as in case of C-FRP sheet. Furthermore, steel can be tensioned to add active confinement actions.

The new rebar parts, which were used for longitudinal damaged rebar substitution for each specimen, had the same length (Ls) and diameter reduction (Φ_{SR}) of the shaped part (Lavorato et al. 2015b) except for the control specimen 9.

5 SHEAR STRENGTH OF REPAIRED PIER SPECIMEN WITHOUT STEEL STIRRUPS AND EXTERNAL C-FRP WRAPPING

The shear strength improvement was guaranteed by a fiber reinforced concrete jacket in case of repaired specimen 5, 7 and 8 (Table 3). The design shear action is the maximum experimental one (Ve equal to about 198 kN, Fig. 3) measured on the retrofitted and repaired pier specimen P26 and P36 during the previous cyclic tests at Fuzhou University Lab (Lavorato et al. 2015b). These two pier specimen were very similar and the shear strength improvement provided by stirrups and external C-FRP wrapping was calculated according capacity design rules.
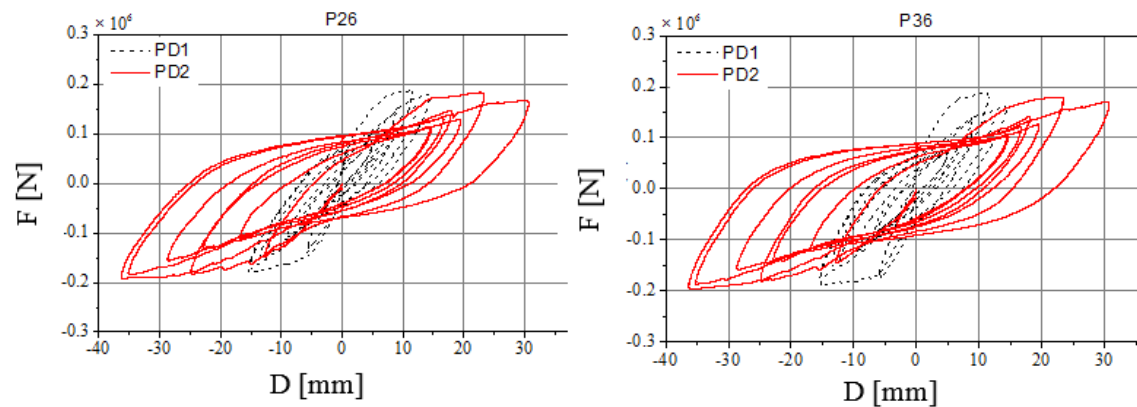
Figure 3. Force (F) VS displacement (D) histories recorded during the cyclic tests on Chinese repaired and retrofitted rc pier specimen P23 and P36 with shaped rebar, stirrups and C-FRP wrapping (scale 1:6). Displacements history obtained by PSD tests (Lavorato 2015a, b) using Tolmezzo (PD1, dot black line) or Tolmezzo scaled to double (PD2, red line) accelerograms.

The shear strength of the repaired specimen by fiber CJ was calculated as the sum of two contributions: the shear strength of the CJ ($V_{Rd,UHFRC}$) and the one of the original pier specimen core ($V_{Rd,OC}$) contributions. The CJ shear strength contribution ($V_{Rd,UHFRC}$) was calculated according to CNR-204/2006 formulation (equ.1) substituting the shear area A_{HS} to b_{wd}. The shear area of the CJ (A_{HS}) was calculated according to Priestley et al. (1994) assuming the crown thickness equal to 100 mm (the removed concrete thickness).

$$V_{Rd,UHFRC}=\left[\frac{0.18}{\gamma_c}\cdot k\cdot(100\,\rho_1\cdot(1+7.5\cdot\frac{f_{Ftuk}}{f_{ctk}})\cdot f_{ck})^{1/3}+0.15\sigma_{cp}\right]\cdot b_w\cdot d$$

(1)

In equation 1, γ_c is the partial safety factor for the concrete without fibers, ρ_l is the reinforcement ratio for longitudinal reinforcement, f_{ck} is the cylindrical characteristic compression strength of the concrete, k is a factor that takes into account the size effect, σ_p is the average stress acting on the concrete cross section, f_{ctk} is the characteristic tensile strength of the concrete matrix and f_{Ftuk}

is the characteristic value of the ultimate residual tensile strength. The concrete matrix tensile and compression strengths were obtained by the experimental tests on concrete specimen with different fiber contents (1 %, 2 % or 3 %) performed at Fuzhou University.

The shear strength contribution of the original specimen concrete core ($V_{Rd,OC}$) was calculated according the equ. 2 proposed by Sezen and Moehle (2004) for older columns having less transverse reinforcement:

$$V_{Rd,OC} = \frac{0.5\sqrt{f'_c}}{a/d} \sqrt{1 + \frac{P}{0.5\sqrt{f'_c}A_g}} \, 0.8 A_g \qquad (2)$$

where P is the axial load, A_g the gross section area, f'$_c$ the compressive strength of the concrete and a/d is the rc element aspect ratio. The values of $V_{Rd,UHFRC}$, $V_{Rd,OC}$ and $V_{Rd,tot}$ for different fiber contents (1 %, 2 % or 3 %) are shown in Table 4. The comparison among the total shear strength ($V_{Rd,tot}$) and the design shear action (V_e) shown that a CJ built by means of a UHFRC with a fiber content of 2 % is sufficient to improve the original shear strength without using stirrups and CFRP jacket. The pier specimen 7 and 8 repaired with a UHFRC fiber concrete jacked using 2% of fiber will be tested at Fuzhou University lab to check experimentally by cyclic tests these numerical results.

Table 4. Retrofitted and repaired pier specimen by fiber concrete jacket (C$_J$): fiber content (V$_f$), shear strength of the C$_J$ (V$_{Rd}$, UHFRC), shear strength of the original pier concrete core (V$_{Rd}$, OC), total shear strength of the repaired specimen (V$_{Rd}$,tot). Concrete jacket (C$_J$) section scheme.

V_f	$V_{Rd.UHFRC}$ [kN]	$V_{Rd,OC}$ [kN]	$V_{Rd,tot}$ [kN]
1 %	137.1		186.9
2 %	149.3	49.8	199.1
3 %	156.1		205.9
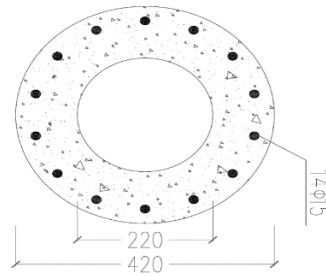
6   CONCLUSIONS

This paper presents a rapid repair and retrofitting technique applied on damaged RC bridge pier with insufficient shear strength. The proposed intervention was applied on the damaged concrete and steel reinforcement parts of some RC bridge pier specimen (scale 1:6) in plastic hinge only where the damage was great. The substitution of the damaged rebar parts consisted in the use of new shaped rebar parts connected with the original undamaged ones by steel coupler system. These shaped rebars guarantee the distribution of the plastic deformation along the rebar in plastic hinge only and their effectiveness was tested experimentally during a previous research study. The connection system among the new rebar parts and the original ones was realized using strong steel coupler elements and two symmetric side welding chords. This connection is an upgrade of the rebar substitution intervention that results simple to realize in situ on vertical longitudinal rebars in modest space. It guarantees that the connected rebars have the same rebar axis avoiding local rotation of the connection and so local bending actions. In this way, the large local plastic demand observed in some connection during the previous tests on repaired pier can be avoided. Another intervention upgrade is about the damaged concrete restoration by using concrete jacket (CJ) built with Ultra-High Performance Concrete (UHPC) with steel fibers. These CJ can guarantee the necessary shear strength without using steel stirrups and external wrapping (C-FRP or steel). A UHPC was designed and tested by compression and flexion tests on concrete specimen

considering different percentage of steel fibers (1 %, 2 % and 3 %). The concrete jacket (CJ) built with this material to restore the damaged concrete parts guarantees that:

- The bridge pier can be repaired in short time as this UHPC exhibits almost the maximum compression strength after 6 days.
- An improvement of the pier durability without modifying the original cover dimension as the fiber restrains the concrete crack opening.
- The improvement of the pier shear strength by means of the shear strength contribution of the concrete jacket with fibers also without stirrups and external wrapping. In this way, time and cost of the repair intervention are reduced.

The shear strength of the CJ ($V_{Rd.UHFRC}$) was calculated by CNR-DT 204/2006 equations relative to fiber concrete elements without stirrups and compared with the experimental maximum shear action (V_e) measured during the previous cyclic tests performed on repaired and retrofitted pier specimen at Fuzhou University lab. This numerical comparison shows that a CJ built with UHFRC using 2 % or 3% of steel fibers can provide the necessary shear strength to sustain the shear action considering also the contribution of the original core ($V_{Rd,OC}$). Finally, the feasibility of the proposed repair intervention was proved building some RC pier specimen in scale 1:6 with and without steel stirrups and external wrapping. Cyclic test on these specimen will be performed at Fuzhou University to evaluate the effectiveness of the proposed intervention.

ACKNOWLEDGEMENTS

REFERENCES

Cheng CT, Yang JC, Yeh YK, Chen SE. (2003) Seismic performance of repaired hollow-bridge piers. Construction and Building Materials, Elsevier Science Ltd.

Cheng L., Karbhari VM. (2006) New bridge systems using FRP composites and concrete: a state-of-the-art review. Progress in Structural Engineering and Materials. John Wiley & Sons, Ltd.

CNR DT 200/2013 Guide for the Design and Construction of Externally Bonded FRP Systems for Strengthening Existing Structures; Italian NATIONAL RESEARCH COUNCIL (CNR).

CNR-DT 204/2006 Guide for the Design and Construction of Fiber-Reinforced Concrete Structures; Italian NATIONAL RESEARCH COUNCIL (CNR).

Foster S. and Attard M. (2001) Strength and Ductility of Fiber-Reinforced High-Strength Concrete Columns. J. Struct. Eng. (ASCE)

He R, Sneed LH, Belarbi A. (2013) Rapid Repair of Severely Damaged RC Columns with Different Damage Conditions: An Experimental Study International Journal of Concrete Structures and Materials.

JTG D60-2004 Chinese code. General code for design of highway bridges and culverts

JTG D62-2004 Chinese code. Code for design of highway reinforced concrete and prestressed concrete bridge and culverts.

JTG/T B02-01-2008 Chinese code. Guidelines for seismic design of highway bridges

Lavorato D., Nuti C. (2015a). Pseudo-dynamic tests on rc bridges repaired and retrofitted after seismic damage. Engineering Structures - Journal - Elsevier.

Lavorato D., Nuti C., Briseghella B., Santini S., Xue J. (2015b) A repair and retrofitting intervention to improve plastic dissipation and shear strength of Chinese rc bridges. IABSE Conference Geneva, Switzerland.

Le Huang, Lihua Xu, Yin Chi, Haoran Xu (2015) Experimental investigation on the seismic performance of steel–polypropylene hybrid fiber reinforced concrete columns. Construction and Building Materials.

Mansur M., Ong K., and Paramasivam P. (1986) Shear Strength of Fibrous Concrete Beams without Stirrups. J. Struct. Eng (ASCE).

Priestley MJN., Seible F., Xiao Y., Verma R. (1994) Steel jacket retrofitting of reinforced concrete bridge columns for enhanced shear strength. Part 2: test results and comparison with theory. ACI Materials Journal.

Sezen, H. and Moehle, J.P. (2004), "Shear strength model for lightly reinforced concrete columns," J. Struct. Eng.

Sun Z., Wang D., Du X., SI B. (2011) Rapid repair of severely earthquake-damaged bridge piers with flexural-shear failure mode Earthquake Engineering and Engineering Vibration.

Xue J., Lavorato D., Bergami A.V., Nuti C., Briseghella B., Marano G.C., Ji T., Vanzi I., Tarantino A.M.,

Santini S. (2018) Severely Damaged Reinforced Concrete Circular Columns Repaired by Turned Steel Rebar and High-Performance Concrete Jacketing with Steel or Polymer Fibers. Appl. Sci. 2018, 8, 1671; doi: 10.3390/app8091671

2nd International Workshop on Advanced Materials and
Innovative Systems in Structural Engineering:
Novel Researches

ISTANBUL
fib IWAMISSE
Turkey
2019

Missing Links:
Solutions to Add Reinforcement in Existing Concrete

Jakob Kunz[1]

[1] Hilti Corp., Schaan, Liechtenstein

ABSTRACT: With the increasing importance of rehabilitation and strengthening of existing structures it has become a frequent task of designers to connect reinforcement into existing concrete. This paper shows the application range of the so-called post installed reinforcement where holes are drilled into the concrete and reinforcement is installed into the holes by means of appropriate adhesives. Unlike cast-in reinforcement, post-installed bars cannot be anchored with hooks or bends. Therefore, specific investigations into the anchorage of post-installed reinforcement are required. Three typical applications will be addressed:

- For extensions of existing concrete structures, continuity is created between new and existing concrete. According to current codes and approvals, bars set with qualified adhesives can be designed identically to cast-in bars. But the dimensions of the existing structures can require anchorage lengths that are lower than the dimensions of the concrete. Moreover, serviceability aspects are not covered by the approvals.

- If the bending behavior of existing concrete slabs is not adequate, a solution is to add a new concrete layer to the existing slab to increase bending strength and / or to reduce deflections. Slip in the interface between the two layers needs to be avoided by interface shear reinforcement which again needs to be installed into drilled holes in the existing concrete slab.

- It regularly occurs that the shear strength of existing concrete slabs or beams is not sufficient because there is too little or no shear reinforcement. If post-installed bars are used as transverse reinforcement, the anchorage of their straight end must be taken into account.

1   POST-INSTALLED TENSILE REINFORCEMENT

Post-installed reinforcement is reinforcement that is installed into hardened concrete members by drilling holes and installing the bars with adhesive mortars. Fig. 1 shows some typical applications like the connections of floors to walls or of columns to slabs. In many cases they are an adequate means to replace cast in bars that have been placed in the wrong position. They allow for load transfer between existing concrete members and new sections that are attached subsequently. One main challenge is that the bars need to be installed correctly. While the installation length of bonded anchors, typically threaded rods, is about 4 to 20 times the nominal diameter, anchorage and splice lengths in reinforced concrete are usually significantly longer. Therefore, professional equipment for the installation of post-installed reinforcement is required. The topic of this section, however, is to highlight the issues to be considered in the design of post-installed reinforcement anchorages or splices.

1.1   Splitting failure mode

Splitting of concrete is a relevant failure mode when designing required anchorage lengths of cast-in or post-installed reinforcement with small concrete cover.

Figure 1. Typical applications of post-installed reinforcement connections

For cast-in reinforcing bars, the splitting failure mode becomes decisive at clear concrete covers c lower than 3 to 4ø. In contrast, high-bond injection mortars typically used as glue for post-installed reinforcing bars ("rebars") can provide superior bond strength values up to about 2 times (product dependent) the bond strength of cast-in reinforcement. Therefore, higher loads may be activated over much shorter embedments than in cast-in situations. According to Randl & Kunz (2013), special attention must be paid to the splitting failure mode which may be observed at edge distances larger than c = 3ø.

With respect to the lack of knowledge in the field of post-installed reinforcement, a comprehensive testing program was conducted, investigating in detail the bond-splitting failure mode of post-installed rebars in comparison to cast-in reinforcement. The applicability of the MC2010 approach also for post-installed reinforcement and the range of validity is analyzed.

1.1.1   Experimental campaign

A large number of pull-out tests from concrete substrates with cast-in and post-installed reinforcing bars was performed with different geometrical configurations and test setups. The two used setups were A) the confined pull-out test setup recommended for post-installed anchorage & reinforcement according to EOTA (2017) (Fig. 2; used for most tests) and B) the pull-out setup acc. to RILEM (1983) developed for judging the bond strength of cast-in reinforcing bars.
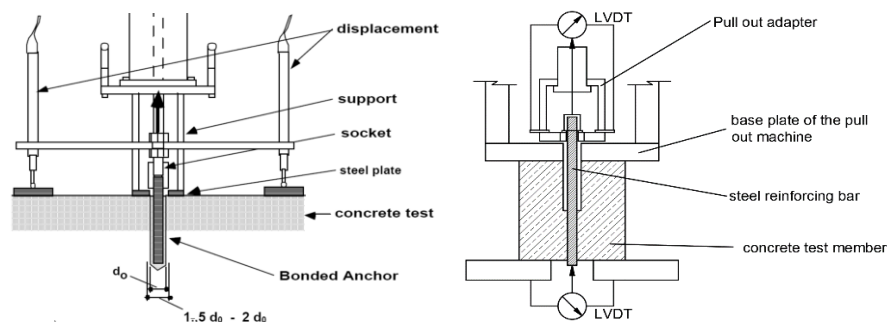
Figure 2. Confined pull-out test (setup A) acc. EOTA (2013) and Pull-out test (setup B) acc. RILEM (1983).

Apart from different geometric configurations (edge / corner / narrow member), the following parameters were systematically investigated: edge distance c, concrete strength f_c, anchorage length l_b, rebar diameter ø and top vs. bottom as well as cast-in versus post-installed situation.

1.1.2   Evaluation of test results

For the evaluation, only test results were considered where concrete splitting was the primary failure mode. Based on the format of the MC2010 approach as explained in fib (2013) and Cairns

(2015) for cast-in reinforcement, the following best-fit expression (rounded exponents) has been derived for post-installed reinforcing bars after performing nonlinear multiple regression analyses with all test results:

$$\tau_{bu,sp} = 28 \cdot \left(\frac{f_{cm}}{25}\right)^{0,3} \cdot \left(\frac{l_b}{\phi}\right)^{-0,55} \cdot \left(\frac{25}{\phi}\right)^{0,2} \cdot \left(\frac{c_{min}}{\phi}\right)^{0,2} \cdot \left(\frac{c_{max}}{c_{min}}\right)^{0,1}$$

(1)

Fig. 3 displays the trend of the calibrated test results with post-installed rebars (bottom side situation) over the concrete cover, and Fig. 4 shows the correlation between measured and estimated (calculated acc. equation (1)) splitting bond strength. The upper limit in equation (1) is given by the lower of the two values of the product-dependent bond strength and the steel tensile strength.
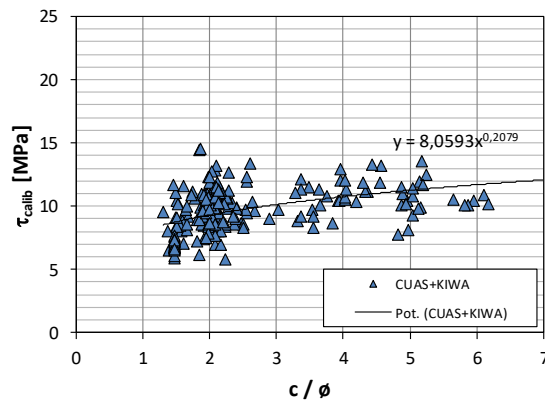
Figure 3. Effect of concrete cover for post-installed rebars (calibrated ø25, $f_{c.cube}$=25 MPa, l_b=10ø).
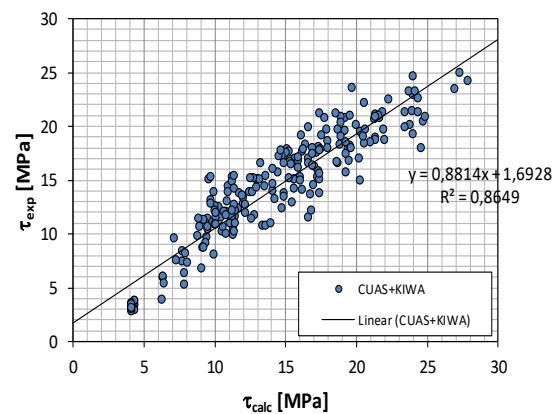
Figure 4 Calculated versus experimental results for post-installed rebars.

While the format of equation (1) is valid for all types of reinforcement anchorages, the factor 28 and the exponents shown here are valid for the tested adhesive, they will have to be adapted to specific test results obtained for other adhesives and configurations.

1.2   Crack width at serviceability limit state

The basic idea of the European Technical Approvals for reinforcement connections assumes that achieving the bond strength of cast-in reinforcing bars proves that post-installed bars will show a behavior at least as favorable as that that of cast-in bars, c.f. EOTA (2018). However, this only refers to the ultimate limit state while serviceability aspects have not been considered in this context so far. Randl and Kunz (2014) investigated into the crack opening at the interface between existing and attached concrete parts where post-installed reinforcement was used to create continuity:

A test specimens was conceived according to frequently occurring practical application, but with shorter splice lengths than those prescribed by Eurocode 2: the connection of a cantilever added to a simply supported concrete slab by overlap splices

The test specimens were subjected to increasing loads according to fig. 5 while the crack openings at the surface were continuously measured. Parallel to the tests, the theoretical crack openings were calculated. The serviceability steel stress was assumed to be σ_s=0.5·f_{yk}=275N/mm^2. The calculation procedure was as follows:

a) Calculation of the slip on the new concrete side where the bars are cast-in according to the relationships for single cracks by the provisions of Eurocode 2 and MC 2010, respectively.
b) Calculation of the slip on the post-installed side from the data gathered in pullout tests.
c) Addition of the two values and projection to the concrete surface.
d) Comparison with the crack widths measured at the concrete surface.
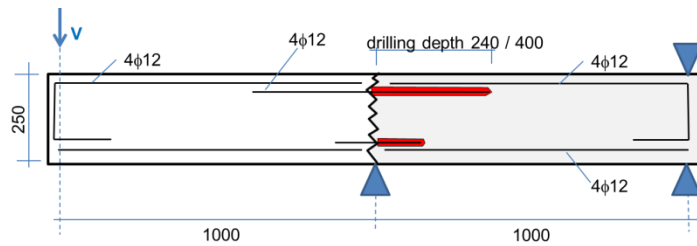
Figure 5. Specimen for crack opening tests: slab cantilever

The results are listed in Table 1. Good accordance of calculated and measured values is observed.

Table 1. Observed and calculated crack widths at serviceability load level

Test	Adhesive	Setting depth	Observed crack width*	Average	Calculated slip cast-in bar	Slip post-installed bar	Calc.crack width at concrete surface **	Max of calc. width ; twice the slip of cast-in bars
		[mm]	[mm]	[mm]	[mm]	[mm]	[mm]	[mm]
2.1	A	240	0.32	0.39		0.16	0.35	0.35
2.2	A	240	0.45					
2.3	A	400	0.31					
2.4	A	400	0.35	0.34		0.17	0.36	0.36
2.5	A	400	0.35		0.11			
2.6	B	400	0.23	0.24		0.08	0.25	0.29
2.7	B	400	0.25					
3.1	A	400	0.30	0.28		0.17	0.36	0.36
3.2	A	400	0.25					
3.3	B	400	0.28	0.28		0.08	0.25	0.29

* Average of values measured visually along the cracks at several locations at serviceability load ($\sigma_s \cong 275$ N/mm²)
** The values are calculated at the axis of the reinforcement and then extrapolated to the surface

2 INTERFACE SHEAR REINFORCEMENT

The repair or the strengthening of concrete structures by concrete overlays has become a special branch of the construction industry. A monolithic behavior of the resultant structure should be ensured. Different attempts have been made to achieve this goal, mainly by a special treatment of the existing concrete surface. However, experiences made by such methods often result in delamination processes, which can occur right away or also after some time. To remedy this problem anchors have been used; they serve as connection elements between the two layers to transfer the forces away from the critical interface zone.

Figure 6. Reinforcement and strengthening of a) concrete bridge b) building slab

2.1 Problem description

To prevent the problem of delamination in the interface of new
and old concrete, different kinds of connectors are used: Bent
rebars, rebars with forged heads or threaded rods with plates and
nuts, concrete screws or special connectors, see section 2.3. The
anchors are fixed in the old construction like adhesive anchors
and in the new concrete it is cast in.

For rehabilitation of bridges and parking decks, there is a need
to adjust the heads of the connectors relating to the surface of the
new concrete because of the irregular old surface after removing
asphalt and the carbonized concrete layer.

Figure 7. Bridge rehabilitation
with threaded rod and plate

2.2 Load bearing behavior of the connection

The phenomena defining the strength of
reinforced interfaces between existing
and new concrete are a) dowel action, b)
pullout tension resulting in friction and c)
cohesion as shown in figure 8. Specific
shear tests (fig. 9) were carried out in the
laboratories of Hilti Corporate Research
to investigate the interrelationships of
various degrees of roughness and
transferable shear stresses with various
amounts of transverse reinforcement. The

Figure 8. Shear transfer in cracked concrete interface

test results confirm the strong influence of roughness on shear resistance and shear stiffness. The
three components of cohesion, friction and dowel action can be isolated and determined
quantitatively. They make different contributions to the overall resistance depending on surface
roughness and amount of reinforcement. Figure 10 shows the load-displacement curve from a
shear test with water blasted (high roughness) interface. At a very small horizontal displacement,
peak load is attained. With increasing displacement, the resistance first drops strongly because
surface interlock is overcome. Finally, the resistance increases again due to increasing dowel
action and friction. However, cracks may appear in the interface due to shrinkage and temperature
differences. Once a crack appears, it stops at the location of the connector. The stiffer the pre-
peak behavior of the interface, the smaller the appearing cracks will be. Moreover, to obtain a
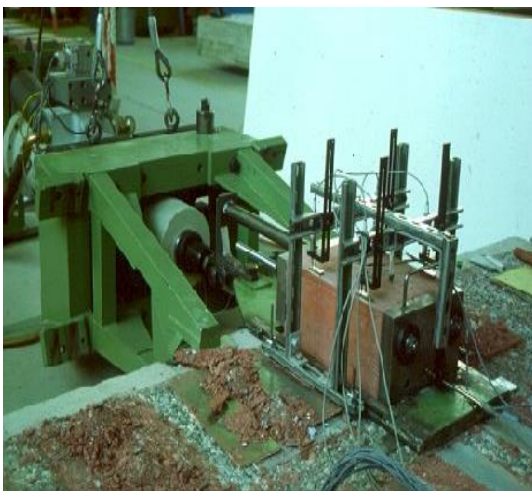
Figure. 9: Shear test at Hilti Corporate Research
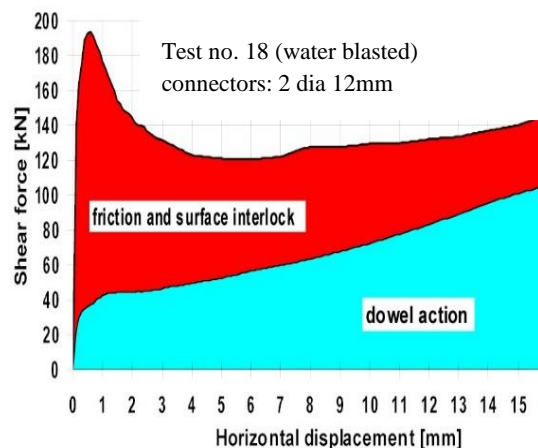
Figure. 10: Load displacement curve for
shear test with rough interface

reliable post-peak behavior of the connection, the resistance drop after peak load should be as small as possible. Therefore, an optimized connector would be characterized by a pre-peak curve as stiff as possible and a decrease after peak load as small as possible.

2.3 Optimization of the Connector by Numerical Simulation

Numerical simulation was used to obtain a connector shape that fulfills the requirements stated at the end of section 2.3. New shapes were compared to the traditional threaded rod with an anchor plate at the top as in fig. 7. Good results were obtained with the shape shown in fig. 11.
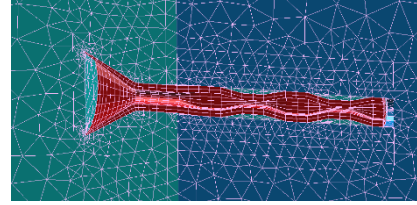
Figure. 11: Optimized geometry: HCC-connector

In the simulation of the interaction between the rod, the mortar and the surrounding concrete had to be considered. The very simple assumption, based on the relatively small load introduced, was to stick the nodes and to assume an elastic layer (E=1500 N/mm^2) to simulate the adhesive mortar.

The load-displacement curve obtained in this simulation corresponds to the one obtained in the corresponding test with great precision. The main goal was to shift the expected load-displacement curve to obtain a less pronounced drop of resistance after peak load for a given surface treatment (interface old-new concrete). Increasing the stiffness of the connector and improving the load introduction both in the old and in the new concrete sides, the goal could be reached.
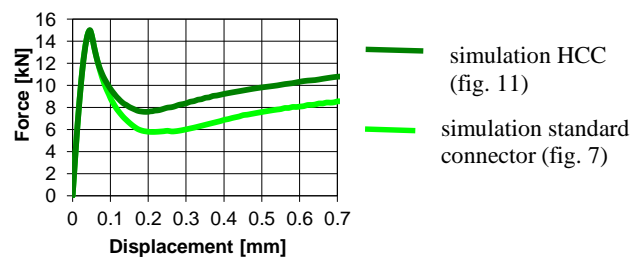
Fig. 12: Improvement by optimized connector

2.4 Design of Interface Connection

Based on the model and tests of section 2.2, a design formula was developed at the Institute of Concrete Structures at the University of Innsbruck by Randl (1997) and was, after some additional research and with minor modifications adopted in the fib Model Code 2010, fib (2013):

$$\tau_{Rdi} = c_r f_{ck}^{\frac{1}{3}} + \mu \cdot \sigma_n + \kappa_1 \rho \cdot f_{yd}(\mu \cdot sin\alpha + cos\alpha) + \kappa_2\rho\sqrt{f_{yd} \cdot f_{cd}} \leq \beta_c v \cdot f_{cd} \qquad (2)$$

where τ_{Rdi} is the design resistance of the interface, c_r represents the cohesion, f_{yd}, ρ and μ result in the friction and the term with $\sqrt{f_{yd} \cdot f_{cd}}$ represents the dowel action. The upper limit is given by crushing of the concrete compressive struts. κ_1 and κ_2 are empirical parameters depending on the interface roughness. fib (2013) specifically mentions that with post-installed connectors the "failure modes known for bonded anchors need to be considered", but the model code does not specifically mention how this consideration is can be carried out. The European Organization for Technical approvals has detailed the design approach for post installed interface shear connectors in the Technical Report TR 066, see EOTA (2019). The MC2010 formula (2) is modified to:

$$\tau_{Rdi} = c_r f_{ck}^{\frac{1}{3}} + \mu \cdot \sigma_n + \kappa_1 \cdot \alpha_{\kappa1} \cdot \rho \cdot \sigma_s \cdot \mu + \kappa_2 \cdot \alpha_{\kappa2} \cdot \rho \cdot \sqrt{\frac{f_{yk}}{\gamma_s} \cdot \frac{f_{ck}}{\gamma_c}} \leq \beta_c v \frac{0.85 f_{ck}}{\gamma_c} \qquad (3)$$

In the term for friction $sin\alpha$ and $cos\alpha$ disappear because post installed connectors are always installed perpendicular to the concrete surface and f_{yd} is replaced by the steel stress σ_s which is the maximum tensile stress that can be developed in the connector under the condition that pullout or concrete breakout must be avoided. The terms $\alpha_{\kappa1}$ and $\alpha_{\kappa2}$ represent the properties of a specific connector and are given in the respective European Technical approvals.

To ensure an adequate behavior in the serviceability limit state, the following design principles should be respected: For normal cases, where water blasting is used, the stiffness can be determined at the strengthened cross-section assuming full composite action. Where sand-blasted or smooth interfaces are used, a reduction of the stiffness must be expected.

2.5   Handling Advantage of New Solution

Figure 11. Bridge rehabilitation with optimized Connector HCC

With a systematic investigation of working steps and boundary conditions on site together with continuos improvements, it was possible to develop the new composite connector for concrete overlays also for improved handling. The advantage of the HCC connector is the easy and reliable setting procedure. It is divided in two steps: the setting of the connector into the base material (as a mechanical anchor) and afterwards the filling of the mortar. The drill hole is filled by inserting mortar into the hollow central part of the connector. Then it comes out from the bottom and flows to the surface of the base material. The whole setting time in concrete-concrete applications has shown a reduction of about 50% in comparison to the traditional methods. This brings a big step of innovation and the advantage for the user is evident.

3   POST-INSTALLED TRANSVERSE REINFORCEMENT

Several tragic incidents have shown that a certain part of the existing building stock does not provide adequate safety against punching shear failure. This type of failure is particularly dangerous because of its brittleness. As there is no pre-warning to punching shear, collapses due to this mode of failure often result in fatalities. Two examples are shown in figure 12: The piper's row car park deck in Wolverhampton (GB) failed due to insufficient maintenance; the parking garage in Gretzenbach (CH) did not resist the exceptional load case fire.

Fig. 12. Accidents due to punching shear: Wolverhampton (l), Gretzenbach (r)

Many such accidents could be avoided, if the concrete slabs were strengthened properly. There is a nmber of reasons for this: planning errors, execution errors, load increase during the lifetime of the structures and modification of the building codes due to increased knowledge on the topic.

3.1 System description

Special anchors in combination with an adhesive mortar are used to install punching shear reinforcement into already hardened concrete, see Figure 13. Inclined holes are hammer drilled from the bottom into the concrete slab under an angle of 45° and in the direction towards the column. The length of the drilled holes should be at least such that they reach the lowest level of the

Figure 13. Post-installed transverse reinforcement

upper (tensile) reinforcement, but preferably, the holes should end only at the level between the tensile reinforcements in the two directions. Adhesive mortar is injected into the drilled holes and the special strengthening anchors Hilti HZA-P are set into the mortar filled holes. The special anchors consist of a reinforcement bar of diameter 16mm or 20mm in the upper part (see Fig. 14). The lower part is a smooth shaft with a thread at the end. For the design, the strength of the reinforcement bar is decisive since the smooth shaft and thread are made of a steel of higher strength than that of the reinforcement bar.

After curing of the adhesive mortar, the lower anchor head is installed. It consists of an injection washer, a spherical washer to eliminate bending of the bar and a nut. To ensure a slip free anchorage, the annular gaps and the interface between washer and concrete surface are injected with adhesive mortar through the injection washer. The anchor head is installed in an enlarged part of the drilled hole. The embedded anchorage has the advantage that it can be covered with a fire protection mortar and is not visible after the installation.
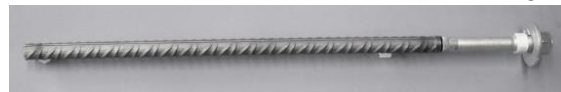
Figure 14: Strengthening anchor Hilti HZA-P

3.2 Shear tests

The efficiency of strengthening concrete slabs against shear with post-installed shear reinforcement was checked in a series of tests by Kunz et al. (2013), see figures 15. The specimens were shear-reinforced with the post-installed bonded reinforcement in the region indicated in figure 16. In the other regions, sufficient transverse reinforcement (consisting of ordinary stirrups) was provided to avoid shear failures outside the investigated area. The strengthening bars were installed in two arrangement types: a) all anchor heads at the bottom of the beam and b) all anchor heads on the tension side of the beam. In the latter case (b) the bonded area is always in the tensile zone of the beam (figure 16). Measurements during the tests included the load, the vertical deformation of the beam, the strains in the strengthening bars and the opening of the shear crack.
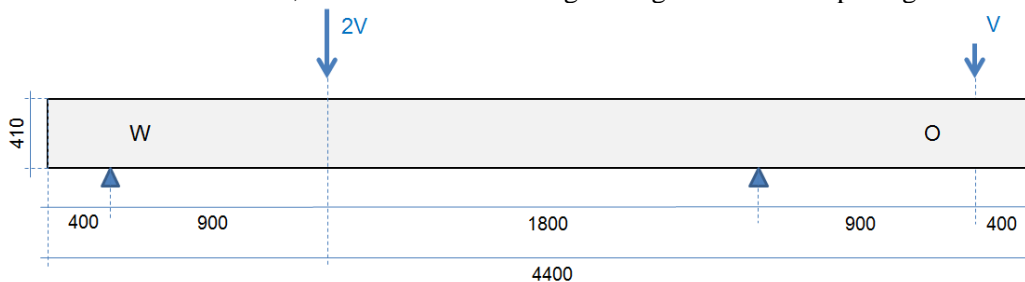
Figure 15. Dimensions of the test specimens
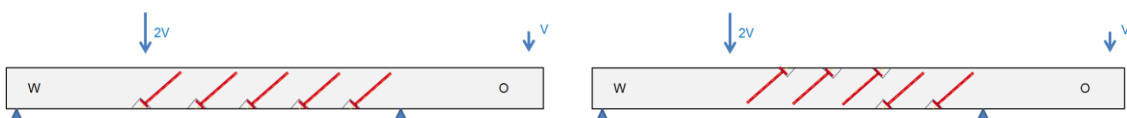
Figure 16. Arrangements a, b of shear reinforcement
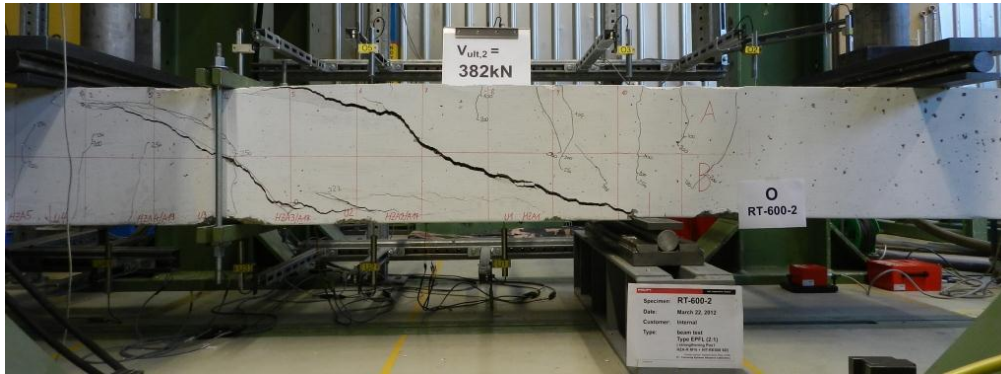
Figure 17. Specimen RT 600-2 at second failure; first crack was braced after full opening

Table 2. Summary of the shear test results

test	Width [mm]	Concrete strength f_{ccm} [MPa]	Shear reinforcement arrangement	Failure load F_{ult} [kN]	$F'_{ult}=$ $F_{ult}*(f_{ccm}/34)^{1/2}$ [kN]
		Test specimen description		Failure load	
RT 600-0	600	34.0	-	246	246
RT 600-1	600	42.4	a	345	309
RT 600-2	600	41.3	a	327	297
*2nd crack**				382	347
RT 600-3	600	42.1	b	398	358
*2nd crack**				394	354

{*} shear crack occurring after bracing the specimen over the first crack (Fig. 4)

In the tests the post-installed shear reinforcement led to increases in shear capacity between 21%
and 45% compared to a specimen without shear reinforcement RT600-0.

3.3   *Punching shear tests*

The efficiency of strengthening concrete slabs against punching shear with post-installed shear
reinforcement was checked by a series of tests by Fernandez Ruiz et al. (2010). Slabs of 3 x 3 x
0.25 m with varying amounts of tensile and shear reinforcement were subjected to monotonically
increasing punching shear load, see figure 18. Measurements during the tests were the load, the
vertical deformation of the slab, the strains in the central tensile reinforcement bar, the strains on
the concrete on the compression side and, where applicable, the longitudinal strain of a part of the

Figure 18. Punching shear test setup
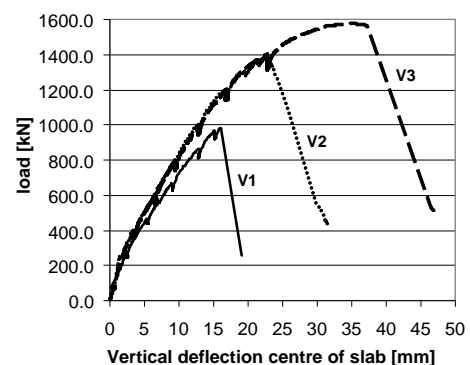
Figure 19. Load-displacement curves

reinforcement anchors. The load was applied from bottom to top by a hydraulic cylinder on which
the steel plate was positioned. The slab was held down on eight points of a circular section
(diameter 3120mm) on its outer limit. The load from two points was taken up by a steel beam

which in turn transferred it to one of four pre-stressing steel bars which were themselves anchored in the strong floor.

Figure 19 shows the piston (column) load versus the vertical deflection of the slab centre for tests V1 to V3. One can see a significant increase in the rotation capacity for slabs with post-installed punching shear reinforcement (slabs V2 and V3).

3.4   Design of post-installed transverse reinforcement

The test described in the sections above were scientifically evaluated by Muttoni and Fernandez (2013) & (2016). The reports provide detailed design methods based on the fib Model Code 2010, fib (2013) for strengthening against both shear and punching shear deficiencies.

4   CONCLUSIONS

Since post-installed reinforcement cannot be anchored with hooks or bends, it was often required to prove the anchorage capacity by additional investigations.

For post-installed connections of bending reinforcement, anchorage lengths shorter than those prescribed by the codes for cast-in bars are required. It was demonstrated that the splitting bond strength of bars bonded-in with adhesives can be significantly higher than that of cast-in bars. A material specific model was derived from extensive testing.

In concrete overlays and when floors or slabs are strengthened against (punching) shear, the transverse reinforcement cannot be anchored around the tensile reinforcement as this is foreseen by structural concrete codes. In order to increase bonding length and effectiveness, installation at 45° is recommended. Several investigations have demonstrated that, despite this drawback, post-installed elements can effectively work as transverse reinforcement. Design concepts have been derived from several test series.

The proposed design concepts are all based on fib MC 2010 and the one for concrete overlays has been implemented into a European approval system. Software as well as appropriate installation material are available for safe and effective projects from design to completion.

REFERENCES

fib, 2013. Model Code for Concrete Structures 2010. Berlin: Verlag Ernst & Sohn, 2013.

Cairns, J., 2015. Bond and anchorage of embedded steel reinforcement in fib Model Code 2010, *Structural Concrete 16/1 (2015): 45-55. DOI: 10.1002/suco.201400043*

EOTA, 2017. EAD 330499-01-0601: Bonded fasteners for use in concrete, Brussels, 2017.

EOTA, 2018. EAD 330087-00-0601: Systems for post-installed rebar connections with mortar, Brussels, 2018

EOTA, 2019, TR 066 Design and requirements for construction works of post-installed shear connection for two concrete layers. Brussels, 2019.

Muttoni, A, Fernandez Ruiz, M, 2013. Design Method for Post-Installed Shear Reinforcement with Hilti Tension Anchors HZA. *MFIC ingénieurs conseils SA, Ecublens, 4 April 2013*.

Muttoni, A, Fernandez Ruiz, M, 2016. Design of Hilti Tension Anchors HZA as Post-Installed Punching Shear – Design according to Model Code 2010 provisions. *MFIC ingénieurs conseils SA, Ecublens, 4 April 2013*.

Fernandez Ruiz, M., Muttoni, A., Kunz, J, 2010. Strengthening of Flat Slabs Against Punching Shear Using Post-Installed Shear Reinforcement. *ACI Structural Journal, V. 107, No. 4, July–August 2010*.

Kunz, J., Fernandez-Ruiz, M., Muttoni, A., 2013. Enhanced safety with post-installed shear reinforcement. fib-Symposium "*Engineering a Concrete Future", Tel Aviv, 22 to 24 April 2013*.

Randl, N., 1997. Untersuchungen zur Krafteübertragung zwischen Alt- und Neubeton bei unterschiedlicher Fugenrauhigkeit. University of Innsbruck, Austria, 1997 (PhD thesis in German).

Randl, N., Kunz, J., 2014. Post-installed reinforcement connections at ultimate and serviceability limit states, *Structural Concrete 15/4 (2014): 563-574*.

Randl, N., Kunz, J., 2018. Bond splitting behavior of post-installed and cast-in reinforcing bars in: *fib Congress 2018, 07-11 Oct 2018, Melbourne, pp. 466-467*.

RILEM, 1983. Recommendation RC6: Bond test for reinforcement steel – 2. Pull-out test.

Spieth, H.A., 2002. Tragverhalten und Bemessung von eingemörtelten Bewehrungsstäben. Doctoral Thesis, University of Stuttgart, Germany.

2nd International Workshop on Advanced Materials and
Innovative Systems in Structural Engineering:
Novel Researches

ISTANBUL
fib IWAMISSE
Turkey   2019

Prediction of Torsional Response of Multi-story Shear Wall Buildings and Its Verification

Yo Hibino[1], Chiaki Yonehara[2], and Shunsuke Inoue[3]

[1] Hiroshima University, Hiroshima, Japan
[2] Shimizu Corporation, Tokyo, Japan
[3] Hiroshima University, Hiroshima, Japan

ABSTRACT: Irregularity of location of the multi-story shear walls may cause torsional irregularity in building. Considering higher stiffness of multi-story shear walls, the torsional irregularity due to multi-story shear walls would be significant and cannot be neglected. In this study, the authors evaluate torsional response of steel reinforced concrete building due to stiffness irregularity due to multi-story shear walls. The torsional response is discussed by a plane model with springs which represents lateral stiffness of multi-story shear walls and is compared with observations. The following conclusions are drawn: 1) The torsional rotation angle of steel reinforced concrete building caused by lateral stiffness irregularity due to multi-story shear walls can be predicted by proposed plane model considering lateral stiffness and rocking stiffness of multi-story shear walls. 2) Predicted torsional rotation angle almost agrees with observed torsional rotation angle. 3) Torsional rotation angle of reinforced concrete wall building under shaking table test with large earthquakes increases with increasing of seismic force due to inelastic response of multi-story shear walls. The torsional rotation angle under large earthquake can be predicted by proposed plane model considering inelastic behavior.

1   INTRODUCTION

Commonly, since torsional response due to lateral stiffness irregularity in building can exert excessive stress on vertical structural elements, which may lead to significant damage, torsional irregularity has been investigated. The torsional irregularity is specified in most seismic codes, typically, which requires an increase of strength for vertical structural elements on the weak direction of building. Recently, torsional irregularity on multi-story building are studied with analytical approaches. Tabatabaei et al. (2011) proposed a simple nonlinear static procedure for evaluating the inelastic torsional response of multi-story buildings. Özmen et al. (2014) investigated relationship floor rotation of multi-story building and story numbers and proposed torsional irregularity definition.

On the other hand, in case that shear walls are placed at every story from ground to top, the shear walls, which is called multi-story shear walls (cantilever shear walls), behaves mostly in a flexural manner and exhibit rocking behavior due to their higher overturning moment at the base of the wall. Thus, the lateral stiffness of multi-story shear walls can be assumed by lateral flexural stiffness of the wall and the stiffness irregularity due to the wall may cause torsional irregularity. For example, total height of multi-story shear walls in building stands on slope ground may be not equal to each other, then the lateral flexural stiffness of the multi-story shear walls has irregularity. However, in torsional provisions and previous researches, those consideration are not given. Furthermore, as with columns, the multi-story shear wall is important structural elements

to upgrade seismic performance of buildings and has a great influence on the response of building during earthquake. Generally, in case of inelastic range, the stiffness irregularity is prone to make larger torsional irregularity than that in case of elastic range. Therefore, it is necessary to investigate the stiffness irregularity due to multi-story shear walls considering characteristics of dynamic response of buildings, and the lateral stiffness irregularity due to multi-story shear walls cannot be neglected.

The objective of this paper is to evaluate torsional response of buildings having multi-story shear walls with proposed plane model and discuss the validity of the prediction of torsional rotation angle of building comparing with observations in both elastic and inelastic ranges.

2   PREDICTION OF BUILDING RESPONSE

2.1   *Detail of target building*

An eight-story steel reinforced concrete building is selected to investigate torsional response due to stiffness irregularity due to multi-story shear walls. Building properties are shown in Table 1. The building has four multi-story shear walls in the transverse direction. The building is constructed on 1981 and retrofitted on 2010. The seismic retrofitting was applied to 1st to 5th stories. Designed concrete strength of the building are 21 MPa and 24 MPa; however, the actual concrete strength is from 26 MPa to 29 MPa which are taken by cylinder test. As shown in Table 1, 11 accelerometers are installed in the building which can measure accelerations in three directions with sampling rate of 100Hz. Floor plan of 8th floor and 1st basement floor, elevation and layout of piles are shown in Figure 1. The four multi-story shear walls are placed in X1, X5, X6 and X9 axes. The wall thickness was increased by seismic retrofitting from 200mm to 550mm and 325mm at the 1st and from 2nd to 4th story, respectively. The accelerometers are located near the multi-story shear walls to measure response of the walls including the rocking behavior.

Table 1. Properties of building

Location		Hiroshima, Japan
Structure		Steel reinforced concrete structure
Number of stories		8 stories with penthouse and a basement story
Built year		1981 (Retrofitted on 2010)
Building height		34.2 m
Area of building		997 m^2
Total floor area		8619 m^2
Foundation		Cast-in-place concrete pile (600ϕ – 7m and 11m)
Concrete strength	Design	21 MPa (1st basement to 2nd basement floors) 24 MPa (3rd to 9th floors)
	Cylinder test (2010)	29 MPa (1st Basement) 26 MPa (3rd to 5th floor) 21 MPa (6th to 9th floor)
Accelerometers		2 (1st floor) 2 (4th floor) 2 (6th floor) 5 (8th floor)
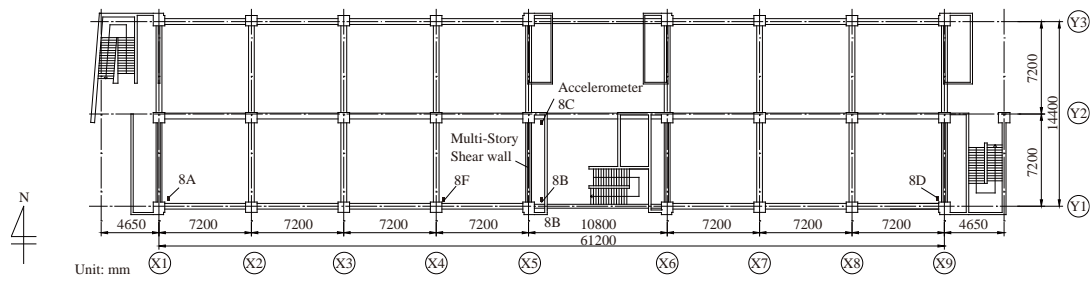
(a) Floor plan of 8th floor
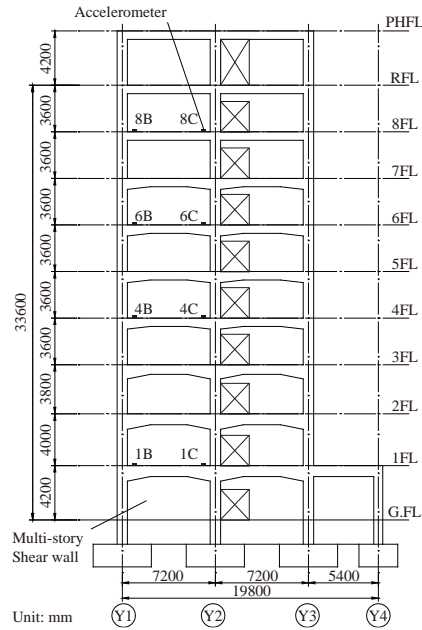
(b) Elevation of X5 axis
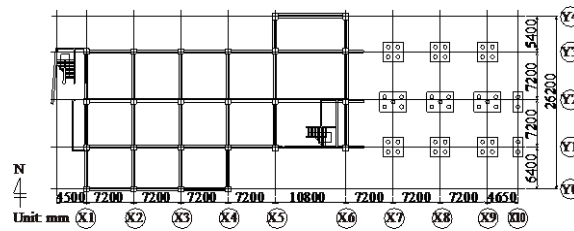
(c) Floor plan of 1st basement floor
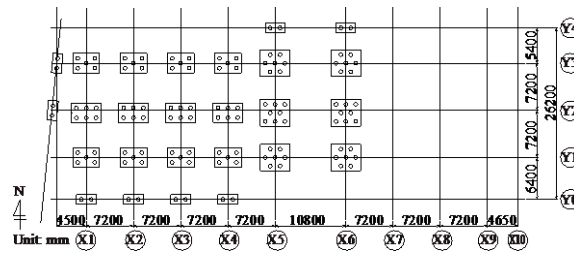
(d) Layout of piles

Figure 1. Floor plan and layout of piles.

2.2 Recorded earthquakes

This building has experienced 47 earthquakes in three years. However, the magnitude of recorded acceleration and response of the building were small. Since Japanese Meteorological Agency (JMA) seismic intensity of most of the earthquakes were lower than 4.0, the authors select eight earthquakes for this study which have relatively larger seismic intensity as shown in Table 2.

Table 2. Properties of chosen eight larger earthquakes.

ID	Date	Epicenter location	Depth (m)	M_w	JMA seismic intensity
E1	2015/7/13 02:52	Oita	58	5.7	3.9
E2	2016/4/16 01:25	Kumamoto	12	7.3	3.3
E3	2016/8/15 13:37	Iyo-Nada	71	4.3	2.0
E4	2016/10/21 14:07	Tottori	11	6.6	4.2
E5	2016/10/21 14:54	Tottori	9	5.0	2.5
E6	2018/04/09 01:32	Tottori	12	6.1	3.8
E7	2018/04/09 02:04	Tottori	10	4.2	2.4
E8	2018/06/27 17:00	Hiroshima	10	4.9	2.8

2.3   Torsional response

As shown in Figure 1(c), 1st basement floor is placed in the area between X1 and X6 axes, which result in that the height of multi-story shear walls of the X1, X4 and X5 axes are different from that of the X9 axis. The difference of the height of the walls makes lateral stiffness irregularity. Figure 2 shows displacement time history in the NS direction estimated by accelerometers 8A, 8B and 8D (See Figure 1(a) and (b)) under earthquake E4. It is seen that maximum displacement of 8A is larger than that of 8D. This indicates torsional rotation occurs. Since distinct stiffness difference is not observed among columns placed orderly, it is assumed that the torsional rotation is may be due to stiffness irregularity of the multi-story shear walls.
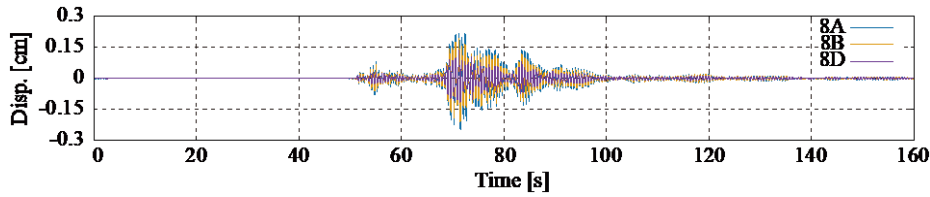
Figure 2. Displacement time history.

2.4   Plane model considering lateral stiffness of multi-story shear walls

Since lateral stiffness of multi-story shear walls is relatively higher than other vertical structural elements, the authors assumed that the dynamic response of the building with multi-story shear walls can be predicted by considering the lateral stiffness of multi-story shear walls only. To consider torsional response of building simply, a simple plane model which has springs, as shown in Figure 3, is assumed. For the analysis using the plane model, following assumptions are made: 1) seismic force is applied only in the Y direction and sway displacement u occurs at the center of gravity in the Y direction only; 2) torsional rotation angle θ occurs with respect to the center of gravity; 3) there are six springs with fixed end, supporting the plane model, which represent lateral stiffness of multi-story shear walls and that of frames in the Y and X directions, respectively: 4) lateral stiffness of columns are not considered. Considering shear force and moment equilibriums, Equations 1 to 4 can be expressed.
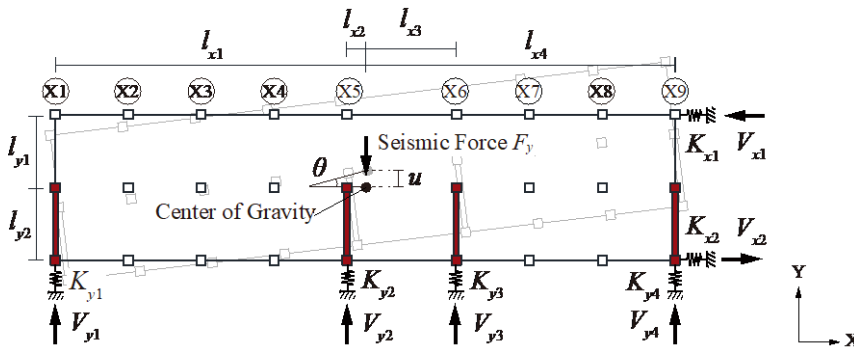
Figure 3. Plane model of 8th floor.

$$V_{xi} = K_{xi} \cdot l_{yi} \cdot \theta \tag{1}$$

$$V_{yi} = K_{yi} \cdot (u + l_{xi} \cdot \theta) \tag{2}$$

$$F_y = \sum V_{yi} \tag{3}$$

$$\sum l_{yi} V_{xi} = \sum l_{xi} V_{yi} \tag{4}$$

where l_{xi} and l_{yi} are distance from center of the gravity to ith axis, K_{xi} is lateral stiffness of frame in X axis, K_{yi} is lateral stiffness of multi-story shear wall in Y axis.

Since the response of the building in the X direction can be assumed as a vibration with single-degree-of-freedom, the spring constant K_{xi} is assumed by following.

$$K_{xi} = \left(\frac{2\pi}{T}\right)^2 \cdot \sum m_i \tag{5}$$

where T is fundamental period, m_i is mass of ith story.

The fundamental period T of 0.54 s in the X direction is taken from average value of transfer function of Fourier spectra obtained by accelerometers 1C and 8C under recorded 47 earthquakes. The spring constant K_{yi} is assumed by lateral flexural stiffness of multi-story shear wall K_w, and axial stiffness K_{vi} of the pile located beneath the wall as seen in Figure 1(c) and (d), which are derived from following equations.

$$K_w = \frac{3EI_w}{H^3} \tag{6}$$

$$K_{yi} = \frac{1}{\frac{1}{K_w} + \frac{1}{\Sigma K_{vi}}} \tag{7}$$

where E is average Young's modules of concrete, I_w is average sectional moment of inertia of multi-story shear walls, H is height of multi-story shear wall from the bottom of the wall to the top. (H is 30m for the wall in X1, X5 and X6 axis; and 25.8m for the wall in X9 axis.)

The axial stiffness of the piles ΣK_{vi} is shown in Table 3. The axial stiffness K_{vi} is assumed by formulas specified by Japan Road Association (2017) as expressed below. In calculation of the axial stiffness, numbers of piles beneath the multi-story shear walls as shown in Table 3 is considered.

$$K_{vi} = a\frac{A_p \cdot E_p}{L_p} \tag{8}$$

$$a = 0.031\left(\frac{L_p}{D_p}\right) - 0.15 \tag{9}$$

where A_p is cross-sectional are of pile, E_p is Young's modulus of pile, L_p is length of pile, and D_p is diameter of pile.

Table 3. Calculated axial stiffness of piles.

Axis	X1 – X4	X5 – X6	X7 – X9
K_{vi} [$\times 10^6$ kN/m]	0.21	2.14	2.69
Numbers of piles	11	15	9
ΣK_{vi} [$\times 10^6$ kN/m]	2.35	2.31	2.42

To verify the axial stiffness, observed axial stiffness is compared. The acting axial stiffness K_{v0} in a pile is calculated by following.

$$K_{v0} = \frac{2M_{OT}}{B^2\theta_r} \tag{10}$$

where M_{OT} is overturning moment of building about above grade beam underneath the wall, B is transverse length of building (=14.4m), θ_r is rocking angle of the wall.

Figure 4 shows relationship between axial stiffness and rocking angle of the wall. The observed axial stiffness K_{v0} is obtained by accelerometers in X5 axes. The dashed line represents predicted axial stiffness from total of ΣK_{vi} in all the axes where the walls are placed, which is 1.12×10^7 kN/m. The average observed axial stiffness of the pile K_{v0} for eight acceleration records results in 1.38×10^7 kN/m. The predicted axial stiffness almost agrees with observed axial stiffness. Then, the spring constants are calculated as shown in Table 4. The spring constant in the X axis are not the same and stiffness irregularity is found.
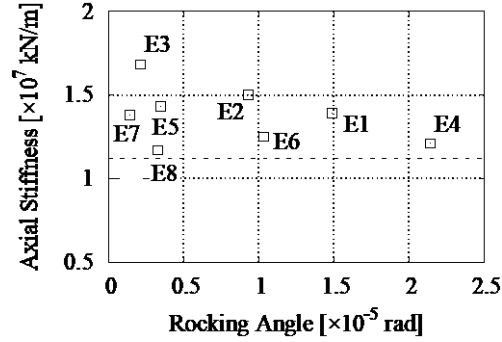
Figure 4. Comparison of axial stiffness.

Table 4. Calculated spring constants.

	Y1, Y2	X1	X5	X6	X9
K_w [kN/m]	-	0.07	0.07	0.07	0.11
K_v [kN/m]	-	2.35	3.21	3.21	2.42
K_{xi}, K_{yi} [kN/m]	1.42	0.07	0.07	0.07	0.10

2.5 Torsional response due to stiffness irregularity of multi-story shear walls

By using the plane model presented, torsional response of the building is investigated. The torsional rotation angle of building obtained by displacement of two accelerometers is expressed by Equations 11 and 12. The x and y represent displacement assumed by acceleration in the X and Y directions, respectively. The subscript of the symbols corresponds to the name of accelerometers (See Figure 1).

$$\theta_x = \frac{|x_{8A} - x_{8D}|}{L_x} \tag{11}$$

$$\theta_y = \frac{|y_{8B} - y_{8C}|}{L_y} \tag{12}$$

where L_x and L_y is distance between the accelerometers: 61.2m; and 7.2m, respectively.

The seismic force F_y can be evaluated by following.

$$F_y = \ddot{y}_{8C} \cdot \Sigma m_i \tag{13}$$

where $\ddot{y}_{8C}$ is maximum acceleration in the Y direction measured by the accelerometer 8C which is located almost at the center of the gravity of the building.

The torsional rotation angle and seismic force obtained by eight earthquakes is shown in Table 5. The relationship between torsional rotation angles and seismic shear force is shown in Figure 5(a). In Figure 5(a), it is observed that both torsional rotation angle θ_x and θ_y are almost proportional to seismic forces. Figure 5(b) shows relationship between inverted effective torsional stiffness θ/F_y and maximum acceleration of earthquakes. The solid line represents calculated θ/F_y

which is equal to 1.69×10^{-8} rad/kN. Although there is dispersion in lower magnitude of acceleration, the plotted inverted effective torsional stiffness θ/F_y is almost constant for any earthquakes. This verifies that torsional rotation angle can be evaluated by the plane model considering the lateral flexural stiffness and rocking behavior of multi-story shear walls.

Table 5. Torsional rotation angles and seismic force.

Earthquake	θ_x [$\times 10^{-6}$ rad]	θ_y [$\times 10^{-6}$ rad]	F_y [kN]
E1	21.8	18.4	1713
E2	12.6	1.03	979
E3	1.96	1.76	281
E4	27.4	22.2	2353
E5	4.93	4.21	494
E6	17.3	16.1	1381
E7	1.78	1.71	210
E8	4.17	3.47	369
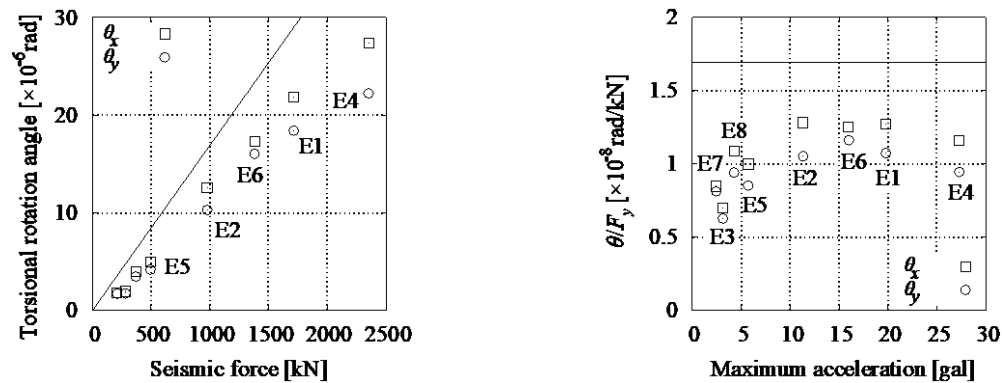
(a) Rotation angle vs seismic force relationship   (b) θ/F_y vs maximum acceleration relationship

Figure 5. Relationship between torsional rotation angle and seismic force, and θ/F_y and maximum acceleration.

3 EVALUATION OF TORSIONAL RESPONSE UNDER LARGE EARTHQUAKE

3.1 Geometry of building and input ground motions

It is verified that the torsional response due to stiffness irregularity of multi-story shear walls can be predicted by presented plane model; however, the verification is considered only in elastic range. To evaluate torsional response of building under large earthquake, dynamic response of six-story reinforced concrete wall building under shaking table test (2014) is discussed. Figure 6 shows floor plans of first story and above 2nd story, and elevation of the building. As seen in the figure, shear walls are placed in X1, X3 and X4 axes, while multi-story shear walls are placed above 2nd story in X2 and X3 axes. Although the shear walls are not single cantilever walls from the 1st to top story, it is assumed that shear force can be transferred in the slab at the 2nd floor between shear walls in X1 and X2, similarly in X3 and X4. Hence, in this study, two of single multi-story shear walls in X2 and X3 axes are assumed.

In the shaking table test, scaled 11 ground motions based on JMA Kobe and JR Takatori records were applied as shown in Table 6. The scaling factor for ground motions is increased up to 140%

for JMA Kobe ground motion. The damage observed in the test for each input ground motions is drawn in Table 6.

(a) Floor plan of 1st story   (b) Floor plan of above 2nd story   (c) Elevation of X3 axis
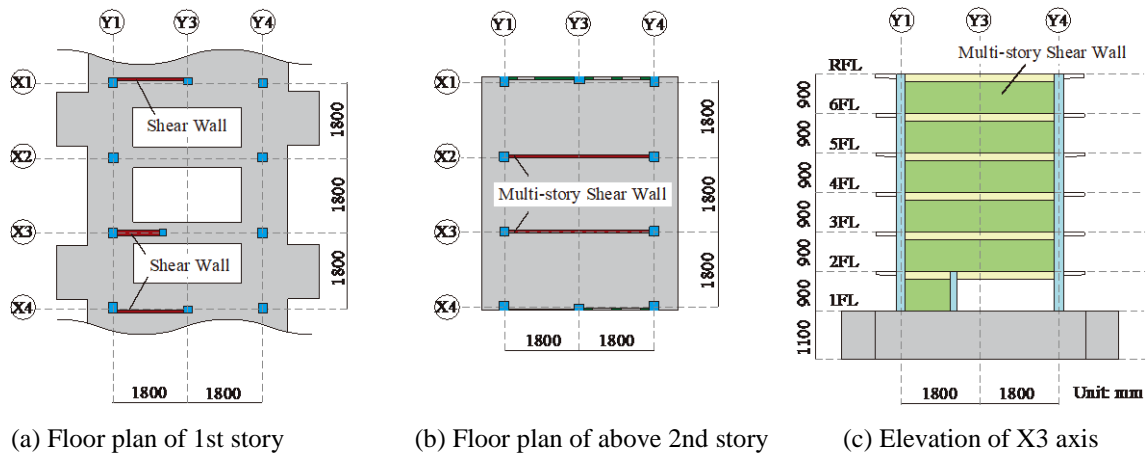
Figure 6. Floor plan of 1st story and above 2nd story, and elevation.

Table 6. Properties of input ground motions.

No.	Ground Motion	ϕ [%]	Q_B [kN] (C_b)	R_{max} [rad]	T [s]	Damage
1		10	140 (0.08)	1/12857	0.10	
2		40	769 (0.42)	1/2500	0.10	Cracking
3		55	1212 (0.66)	1/882	0.12	Yielding of main bars in column
4		70	1342 (0.73)	1/629	0.12	Yielding of shear wall
5	JMA Kobe	55	1029 (0.56)	1/736	0.14	
6		70	1342 (0.73)	1/526	0.13	
7		100	1975 (1.08)	1/148	0.17	Evidence of shear failure appeared.
8		120	2160 (1.18)	1/36	0.23	Compression failure in column
9		140	1747 (0.95)	1/13	0.36	
10		140	1161 (0.63)	1/11	0.34	
11	JR Takatori	120	1506 (0.82)	1/6	0.25	Collapse

where ϕ is scaling factor of ground motion, Q_b is base shear force, C_b is base shear coefficient, R_{max} is maximum drift at the first story, and T is fundamental period.

3.2   Evaluation of torsional rotation angle with plane model

A plane model for 6th floor of the wall building shown in Figure 7(a) is assumed. The springs are placed in Y1, Y2, X2 and X3 axes which represent lateral stiffness of the multi-story shear walls and frames. The spring constant in Y direction K_{yi} is modeled as tri-linear hysteresis shown in Figure 7(b). The story drift angle at cracking δ_c is assumed as 1/1500; reduction factor of secant stiffness at yielding point to elastic stiffness α is assumed as 0.3; and story drift angle at the yielding δ_y is assumed as 1/100 considering damage of the building. Cracking shear force and yielding force are calculated based on Japanese Building Code. Thus, the spring constant decreases according to this hysteresis. Similarly, the spring constant K_{xi} in the Y1 and Y2 axes are obtained by equivalent lateral stiffness assumed by Equation 5 with each fundamental period under elastic and inelastic conditions. The parameters in terms of spring constant are shown in

Table 7. Note that rocking effect is not considered since the basement is fixed to the shaking table. Accelerometers are placed in the corner of the floor and near to the walls as shown in Figure 7(a).

In elastic range, the spring constant for K_{xi} is assumed by fundamental period T of 0.1 s which is in 2nd case (#2). Solving Equations 1 to 4, inverted effective torsional stiffness θ/F_y results in 2.44×10^{-6} rad/kN in elastic range. In inelastic range, similarly, torsional rotation angle is calculated with degraded spring constant. In inelastic range, the spring constant for K_{xi} is assumed by fundamental period T of 0.17 s when an evidence of shear failure of the wall was observed. Inverted effective torsional stiffness θ/F_y results in 8.25×10^{-6} rad/kN in inelastic range.

Figure 8 shows relationship between torsional rotation angle and seismic force. The dashed and solid line represent the relationship in elastic and inelastic range, respectively. The torsional rotation angle is assumed by displacement predicted by accelerometers. It is assumed that the stiffness degradation occurs simultaneously for both spring and the folding point of the solid line is assumed by seismic forces corresponds to story drift angle when cracking and yielding occurred. The inelastic torsional rotation angle increases when the spring constant is decreased. The test result agrees with the dashed line before the 3rd case (#3); however, the torsional rotation angle increases drastically after 4th case (#4). On the contrary, the solid line corresponds to torsional rotational angle for 7th (#7) and 8th (#8) cases. It is verified that even torsional rotation angle in inelastic range increases after cracking, the torsional rotation angle can be evaluated by the plane model considering stiffness degradation for spring constant.

(a) Plane model of 6th floor   (b) Hysteresis of spring constant
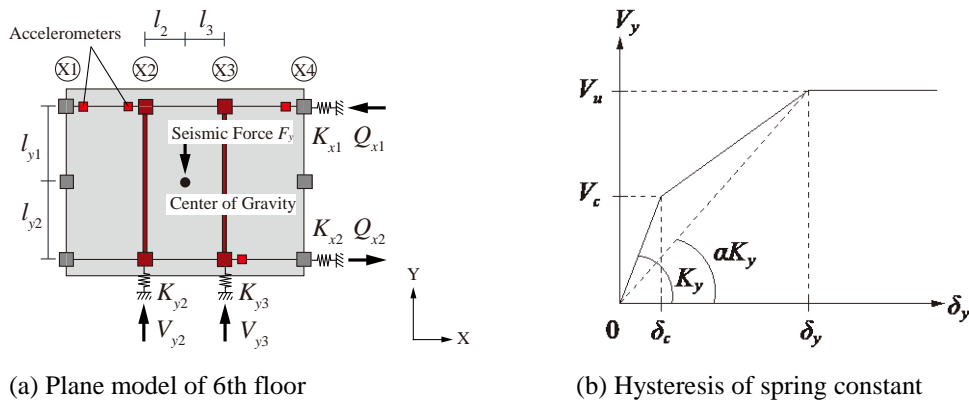
Figure 7. Plane model of 6th floor and hysteresis of spring constant.

Table 7. Parameters of hysteresis.

	K_x	K_{y2}	K_{y3}
Elastic stiffness [kN/m]	12.6	0.22	0.23
Reduction factor α	-	0.3	0.3
Yielding stiffness [kN/m]	4.36	0.07	0.07
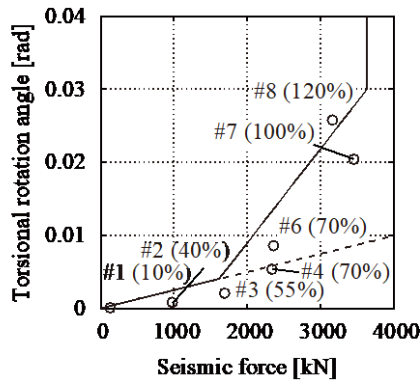
Figure 8. Relationship between torsional rotation angle and seismic force.

4 CONCLUDING REMARKS

In this paper, the authors investigate torsional response of building due to irregularity of lateral stiffness of multi-story shear walls using a plane model with springs. From the calculation using the plane model and observations, following conclusions are drawn.

1. Torsional rotation angle of steel reinforced concrete building due to irregularity of lateral stiffness due to multi-story shear walls can be assumed by a plane model which is supported by springs represents lateral flexural stiffness and rocking stiffness of multi-story shear walls.

2. It is found that predicted torsional rotation angle increases with increasing of seismic force. The predicted torsional rotation angle almost agrees with observation.

3. Torsional rotation angle of reinforced concrete wall building under shaking table test assumed by a plane model increases drastically after cracking of the shear walls due to inelastic response of multi-story shear walls. The torsional rotation angle agrees with test results in both elastic and inelastic ranges.

REFERENCES

Japan Road Association, 2014, *Specifications for Highway bridges. Part 4 Substructures*, 586.

National Research Institute for Earth Science and Disaster Resilience (NIED), 2017, Shaking Table Test of 6 Story Wall Frame Building, *ASEBI*, https://www.edgrid.jp/datas. (In Japanese, Assessed 25 Jan. 2018)

Özmen, G., Girgin, K. & Durgun, Y., 2014, Torsional Irregularity in Multi-story Structures, *International Journal of Advanced Structural Engineering*, 6: 121-131. https://doi.org/10.1007/s40091-014-0070-5

Tabatabaei, R. and Saffari, H., 2011, Evaluation of the Torsional Response of Multistory Buildings Using Equivalent Static Eccentricity, *Journal of Structural Engineering*, 137(8): 862-868. https://doi.org/10.1061/(ASCE)ST.1943-541X.0000324.

2nd International Workshop on Advanced Materials and
Innovative Systems in Structural Engineering:
Novel Researches

ISTANBUL
fib IWAMISSE
Turkey 2019

Anagennisi project - Innovative reuse of all end-of-life tyre components in concrete: Main technological achievements

Kypros Pilakoutas[1], Panos Papastergiou[2], Hang Hu[3], Abdulaziz Alsaif[4], Shan-Shan Huang[5], Maurizio Guadagnini[5], Iman Hajirasouliha[5], Samar Raffoul[6], Harris Angelakopoulos[7], Dan Bompa[8], Ahmed Elghazouli[9]

[1] Professor, Dept of Civil and Structural Engineering, University of Sheffield, UK

[2] Research Associate, Dept of Civil and Structural Engineering, University of Sheffield, UK

[3] Senior Supervisor, Dept of Engineering, Chengdu Communication Investment Corporation, China

[4] Assistant Professor, Dept of Civil and Environmental Engineering, King Saud University, Saudi Arabia

[5] Senior Lecturer, Dept of Civil and Structural Engineering, University of Sheffield, UK

[6] Research Associate, Oxford Brookes University, Oxford, UK

[7] Managing Director, Twincon Ltd, Sheffield, UK

[8] Research Associate, Dept of Civil and Environmental Engineering, Imperial College London, UK

[9] Professor, Dept of Civil and Environmental Engineering, Imperial College London, London, UK

ABSTRACT: All end-of-life tyre constituents (rubber, steel wire and textile reinforcement) are high quality materials and Anagennisi project, described in the paper, aimed to recycle and use them as reinforcement in structural concrete applications. Rubber particles were used to substitute mineral aggregates in concrete and develop Rubberised Concrete (RuC), which when confined with Aramid/Carbon FRP (CRuC), it led to compressive strengths of up to 90 MPa and, more significantly, axial deformations of up to 6%. The seismic performance of RC medium/large scale piers improved the energy dissipation up to 50% and increased ductility up to 25% - (compared to unconfined RuC). Recycled Tyre Steel Fibres (RTSF) were found to be able to partially replace manufactured steel fibres and to increase the flexural strength of concrete. The best flexural performance was found from hybrid mixes, indicating that mixes containing both RTSF and manufactured fibres (MSF) can show better flexural performance than MSF-only mixes at the same fibre dosage. Steel Fibre Reinforced Rubberised Concrete (SFRRuC) can offer a concrete pavement system that has similar flexibility to flexible pavements, flexural strength similar to rigid concrete pavements and good durability properties and freeze&thaw resistance. When subjected to elevated temperatures, Recycled Tyre Polymer Fibre (RTPF) reinforced concrete showed remarkable resistance to spalling, confirming the potential of these fibres for fire-induced concrete spalling mitigation.

1   INTRODUCTION

An estimated one billion tyres are produced annually and a similar number runs out their service life. End-of-life tyre (ELT) arisings for EU countries (incl. Turkey) were found to be amlost 3 million tonnes per year. Analysis of the destination for EU arisings shows that 5% still ends in landfill. The introduction of EC legislation has clearly resulted in a major reduction in the proportion of tyres going to landfill (from 62% in 1992). However, 49% of post-consumer tyres are currently incinerated for energy recovery and only 46% have material recovered through

various recycling processes (ETRMA, 2015). The tyre is made of multiple layers of vulcanised rubber, structurally reinforced with corded steel wire or polymer textiles. The EU-funded collaborative project Anagennisi project targeted at finding high value uses in structural applications for the main constituent materials of end-of-life tyres (Pilakoutas et al., 2015). Rather than using highly engineered materials as cheap fillers or fuel, Anagennisi aimed to use the rubber, steel and polymer fibres for their intrinsic physical properties in high value concrete applications and novel structural solutions. After appropriate sorting and cleaning processes, classified rubber particles, Recycled Tyre Steel Fibres (RTSF) and Recycled Tyre Polymer Fibres (RTPF) can be obtained and used in concrete construction.

In general, all three main constituents can be extracted from tyres through mechanical means (shredding and granulating). This method is used by the majority of tyre recyclers in Europe. In the mechanical tyre decomposition, steel is removed by magnets and free textile by vacuum. For rubber, the majority of applications use recycled rubber (bonded with polymers) to produce carpet underlay and other flooring materials such as rubber tiles, sidewalks, playgrounds, sport surfaces. It can also be moulded for various types of bumpers, curbs, pallets and railway sleepers.

Rubber can also be used in rubber modified asphalt and as aggregate in rubberised concrete or polymer concrete. The use of high volume fractions of rubber aggregate (up to 60% by volume), however, can lead to concrete with lower stiffness and significantly reduced compressive strength. To regain the compressive strength and make this concrete suitable for structural applications, its lateral dilation is controlled through externally applied confinement using fibre reinforced polymers (FRP – Aramid or Carbon). This confined rubberised concrete (CRuC) can be used as bearings for bridges or in areas where high energy dissipation is required (earthquake resistant buildings).

The steel cord used as tyre reinforcement is a very high strength cord of fine wires (0.1- 0.4mm). When extracted from tyres the same cord is either discarded or at best re-melted. Although knowledge on how to avoid balling whilst maintaining efficiency is what led to a first breakthrough, developing industrial processes to sort and classify the wire is still challenging. RTSF can partially replace manufactured steel fibres to increase the flexural strength of concrete – saving on virgin materials and reducing energy input requirements by 97%. RTSF fibres are shorter and much thinner than manufactured steel fibres, helping to control cracks at the micro and meso level.

High quality and strength textile fibres, such as aramid, rayon, nylon and polyester cords, are used to provide reinforcing strength in tyres. During the shredding process, the cords break down and expand into greyish fibre agglomerates (fluff). Until recently, most textile reinforcement ends up in landfill or is used as fuel for incineration. Currently, there are some products using this material for insulation purposes, carpet blends and underlays. The polymer textile reinforcement in tyres is of equal high quality and durability and can replace manufactured polymer fibres to control shrinkage and mitigate concrete spalling under extreme temperatures (fire) (Figueiredo et al., 2017).

The sections below will briefly present the main technological achievements made through the Anagennisi project and highlight the main experimental observations on the use of all ELT constituents as reinforcement in various structural applications.

2 MAIN TECHNOLOGICAL ACHIEVEMENTS OF ANAGENNISI PROJECT

2.1 *Compressive behaviour of FRP-Confined Rubberised Concrete (CRuC):*

Extensive laboratory studies were conducted to investigate the monotonic and cyclic compressive behaviour of FRP-confined RuC investigating: a) type of FRP confining material (Carbon or Aramid), b) confinement pressure (number of FRP layers) (Raffoul et al., 2017) and c) type of

loading (monotonic or cyclic) (Raffoul et al., 2019). Information on the concrete mix design, physical properties of rubber and sieve analysis can be found in (Raffoul et al., 2016).

Table and Table present the results from AFRP and CFRP CRuC cylinders subjected to monotonic and cyclic loading, respectively (mix 60FR60CR: 60% fine and 60% coarse aggregate replacement with rubber particles by volume). These tables also include the 28-day confined compressive strength (f_{cc}), axial (ε_{ccu}) and lateral (ε_{cclu}) strains at f_{cc}. The ratio f_{cc}/f_c, which represents the increment of CRuC cylinders' compressive strength with respect to RuC, is also included. For the cylinders subjected to cyclic loading, these values were calculated based on the envelope of their response in terms of stress-strain.

Table 1. Results from AFRP and CFRP CRuC cylinders subjected to monotonic loading.

Notation	FRP	Number of layers	f_c or f_{cc} (MPa)	ε_{ccu} ($\mu\varepsilon$)	ε_{cclu} ($\mu\varepsilon$)	f_{cc}/f_c
Plain		0	8.2	-	-	-
2LA-1-M	Aramid	2	39.9	37790	14220	4.86
2LA-2-M			44.6	46030	19270	5.44
3LA-1-M		3	73.5	49749	16229	8.97
3LA-2-M			66.2	55067	13958	8.07
4LA-1-M		4	101.3	73062	17947	12.36
4LA-2-M			90.7	55551	14164	11.07
Plain		0	6.8	-	-	-
2LC-1-M	Carbon	2	33.6	26417	7382	4.94
2LC-2-M			29.8	17329	6223	4.39
3LC-1-M		3	46.4	25621	7505	6.82
3LC-2-M			51.2	26272	9052	7.53
4LA-1-M		4	63.6	40737	8497	9.35
4LA-2-M			61.6	32410	7604	9.06

Table 2. Results from AFRP and CFRP CRuC cylinders subjected to cyclic loading.

Notation	FRP	Number of layers	f_c or f_{cc} (MPa)	ε_{ccu} ($\mu\varepsilon$)	ε_{cclu} ($\mu\varepsilon$)	f_{cc}/f_c
Plain		0	8.2	-	-	-
2LA-1-C	Aramid	2	39.5	41585	15087	4.82
3LA-3-C		3	69.6	56127	16154	8.49
4LA-3-C		4	90.3	55788	16395	11.01
Plain		0	6.8	-	-	-
2LC-2-C	Carbon	2	36.0	28321	8960	5.29
3LC-2-C		3	49.6	36956	10899	7.30
4LC-3-C		4	66.1	42647	10201	9.72

For plain RuC, the results show that the compressive RuC strength and axial strain capacity decreased, as the rubber content increased, regardless of the replacement type. The lateral strain capacity increased considerably, with increasing rubber content. For mix 60FR60CR, the compressive strength reduced by 88%, whereas the axial strain reduced by 35% and the lateral strain increased by 303% with respect to the plain mix.

For CRuC, the results confirm that the lateral confinement with FRP jackets was effective and mitigated the detrimental effects of rubber on concrete performance. RuC cylinders wrapped with 4 layers of AFRP achieved stress and strain capacities of around 90 MPa and 6% respectively, despite the high rubber content (60% total aggregate replacement). The envelope of the cyclic behaviour followed a similar path as the monotonic behaviour (Figure). The monotonic results for AFRP CRuC specimens are given in Figure 4 (section 2.2).
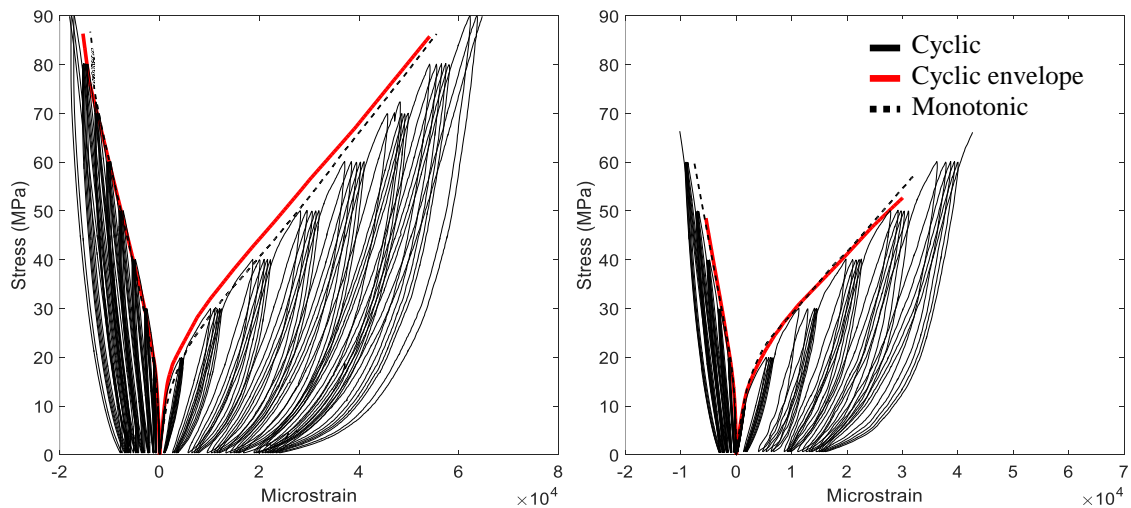
Figure 1. Cyclic and monotonic stress-strain behaviour of CRuC cylinders wrapped with 4 layers of AFRP (left) and CFRP (right).

2.2 Predicting the compressive behaviour of RuC and CRuC

Based on the experimental results, reliable and practical-to-use constitutive models were developed for the behaviour of RuC and CRuC. Figure shows the uniaxial constitutive model for plain RuC (Bompa et al., 2017). In the initial stage, degradation and post-crushing of concrete is observed. The material is defined up to stress ratios below the elastic limit $\sigma/f_{cr} \leq 0.3$. The second stage is defined by a second degree polynomial function, which is bounded by the elastic strain limit $\varepsilon_{cr1,el}$ and the crushing strain $\varepsilon_{cr1,1}$. The post-crushing stage is dependent on the post-peak crushing energy ($g_{c,2}$), represented by a triangular distribution. The uniaxial tension behaviour of rubberised concrete (Figure) can be predicted using a bi-linear behaviour.
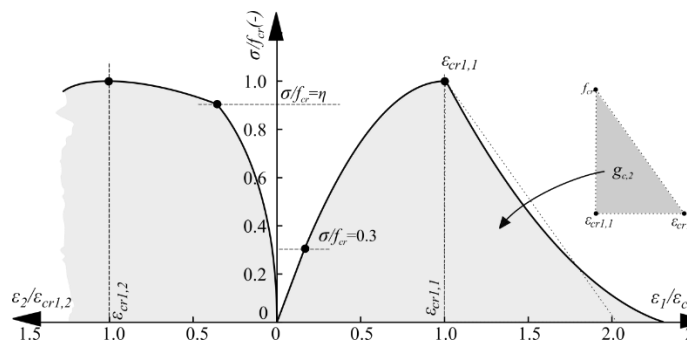
Figure 2. Uniaxial constitutive model for plain RuC.
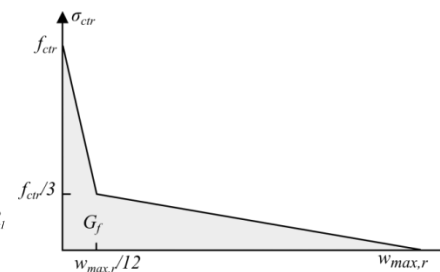
Figure 3. Assumed stress-strain diagram in tension.

The model to predict the full stress-strain behaviour of FRP-confined RuC (more details in (Raffoul et al., 2019) was based on the confinement model proposed by Mander et al. (1988) for steel-confined concrete using an iterative procedure by increasing the confinement ratio. The active confinement model assumes that a constant confinement pressure (active-confinement) is applied externally to the concrete core, while the axial stress increases, leading to stress-strain curves at the various volumetric confinement ratios. Figure shows the predicted curves using the proposed model as well as the experimental stress-strain curves for 2, 3 and 4 layers of AFRP confinement. The maximum deviation in the ultimate stress and axial strain predictions, compared to experimental results, was found to be less than 6% and 9%, respectively.
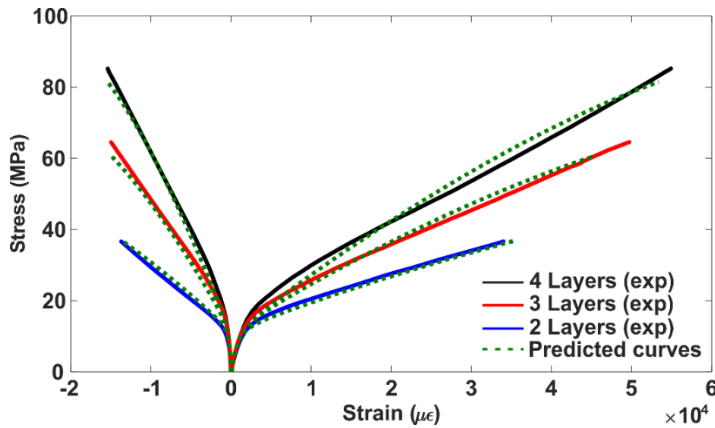
Figure 4. Model predictions and experimental results for 2, 3 and 4 layers AFRP CRuC specimens.

2.3 *Medium and large-scale tests using RuC and AFRP CRuC with conventional steel reinforcement*

This study also investigated the behaviour of 12 medium and large scale circular columns. Reinforcement was provided with conventional steel rebars and stirrups. The rubber replacement of the mineral aggregates ranged from 0% up to 60% (by volume) and the columns were tested under lateral reverse cyclic deformations with or without pre-applied axial load (Figure 5a). From the medium-scale specimens (Figure), one was made of conventional reinforced concrete (RC), one of steel reinforced rubberised concrete (RRuC – Figure 6b) and one was an externally FRP-confined rubberised reinforced concrete member (CRRuC – Figure 6c). From the 9 large-scale members 5 were RRuC and the remaining 4 CRRuC (Figure). The columns were scaled down according to the limitations imposed by the testing setup and equipment (Figure 5a) and they were designed to replicate typical circular bridge piers with a moment span of 20m. The medium scale members had a diameter of 250 mm and a cantilever length of 1000 mm, whilst the large scale columns had a diameter of 350 mm and a cantilever length of 1350 mm. The bottom part of the columns was cast using either conventional concrete, RuC, or AFRP CRRuC. Table 3 summarises the main characteristics of the 12 tested specimens (Elghazouli et al., 2018).

Table 3 Main characteristics of tested specimens.

Name	D (mm)	L (mm)	f_c (MPa)	l_{rub} (mm)	n_l (-)	l_{conf} (mm)	N (kN)	V_y (kN)	V_{max} (kN)	δ_y (mm)	δ_u (mm)
D250-R00-F0-N1	250	1000	70.2	0	-	-	200	54.0	57.3	10.8	41.5
D250-R60-F0-N1	250	1000	6.6	450	-	-	20	29.8	38.5	10.8	63.4
D250-R60-F3-N1	250	1000	55.6	450	3	500	200	39.9	43.4	10.8	59.8
D350-R45-F0-N0	350	1350	9.2	450	-	-	0	63.9	80.1	12.4	96.6
D350-R45-F0-N1	350	1350	9.2	450	-	-	140	70.4	84.9	14.6	96.0
D350-R45-F2-N0	350	1350	55.4	450	2	500	0	63.7	84.4	12.4	107
D350-R45-F2-N2	350	1350	55.4	450	2	450	800	82.6	94.4	12.0	76.4
D350-R60-F0-N0	350	1350	8.0	470	-	-	0	60.3	74.0	12.7	96.9
D350-R60-F0-N1	350	1350	8.0	470	-	-	140	66.5	77.0	15.1	102
D350-R60-F0-N2	350	1350	45.8	470	-	-	280	67.5	79.2	15.8	72.9
D350-R60-F3-N0	350	1350	8.0	470	3	600	0	55.0	78.1	12.2	103
D350-R60-F3-N2	350	1350	45.8	470	3	600	800	57.9	78.1	12.0	72.5

Notations: D – diameter, L – cantilever length, f_c – concrete strength, l_{rub} – rubberised concrete length, n_l – number of confinement layers, l_{conf} – confinement length, N – level o axial preload, V_y – yielding lateral load, V_{max} – maximum lateral force, δ_y – yield deformation at flexural yielding, δ_u – lateral deformation at ultimate load
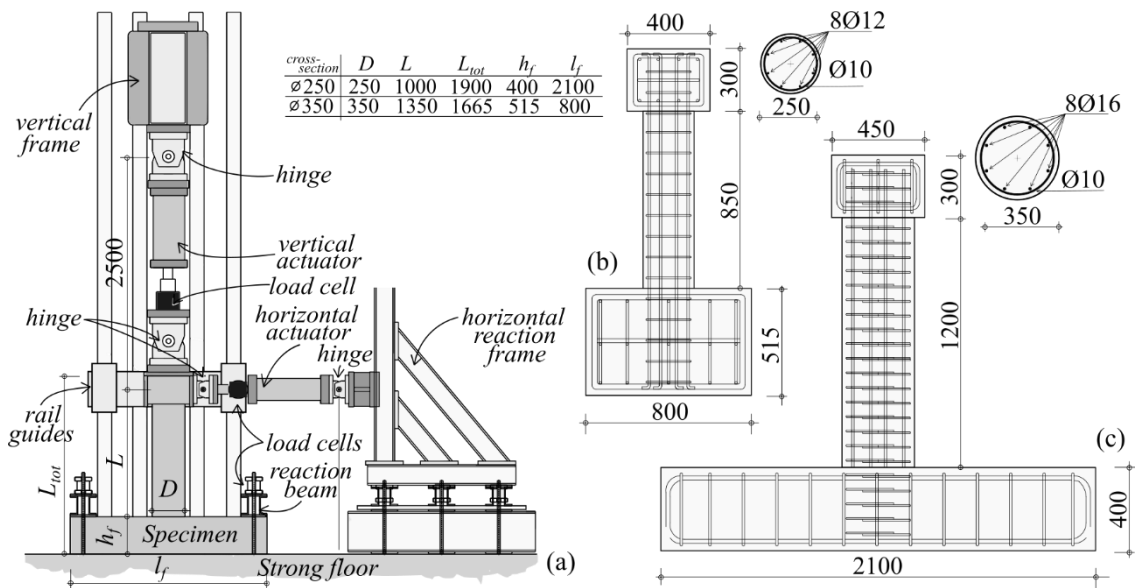
Figure 5. a) Testing arrangement; Specimen geometry and reinforcement setup: b) Medium scale columns, c) Large scale columns.
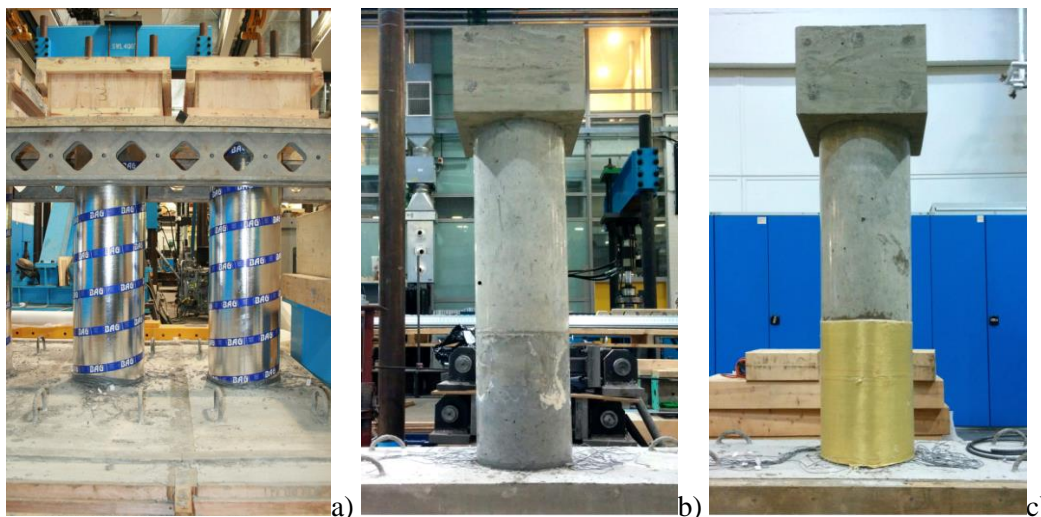
Figure 6. Large-scale specimens a) Formwork, b) RuC column c) AFRP CRuC column

The columns were tested in displacement control: first, the axial loads were applied and locked as stated in Table 1 (pre-applied axial loads). Then, reversed deformation cycles were applied using a sine wave form at 0.25, 0.5, 0.75, 1.0, 2.0, 4.0, 6.0 δ_y increasing up to failure, where δ_y is an estimated lateral yield displacement from non-linear finite element analysis.

The results indicated that AFRP CRRuC was effective at enhancing the energy dissipation (up to 169% and up to 44%) and deformation capacity (up to 33% and up 35%) of the columns in comparison to specimens cast with RRuC or conventional RC columns, respectively. The tests also showed that the yielding of the longitudinal reinforcement controlled the behaviour of the columns. Figure a and Figure a show the lateral load vs lateral displacement curves of unconfined and AFRP confined (3 layers) RuC mixes (both 60% rubber replacement), respectively, whilst Figure b and Figure b illustrate their corresponding modes of failure.

Figure 7. a) Lateral load-deformation response, b) Damage level at large lateral deformations.
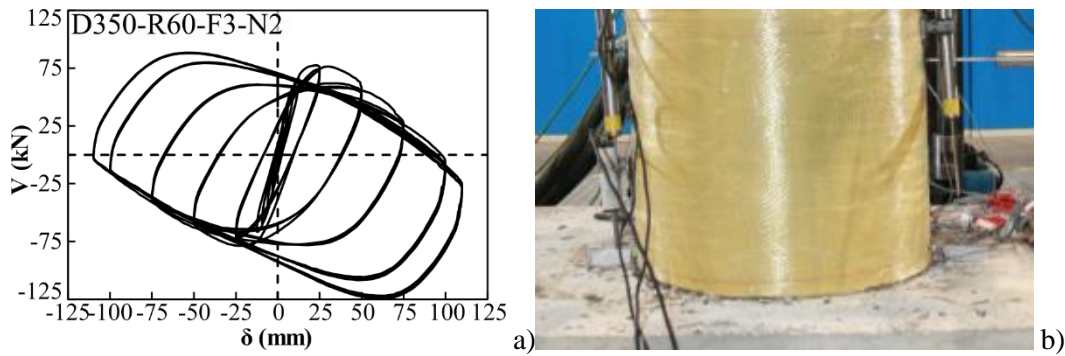
Figure 8 a) Lateral load – deformation response, b) column after testing.

2.4   Flexural performance of SFRC prisms using manufactured steel fibres and sorted RTSF

This study investigated the flexural behaviour of Steel Fibre Reinforced Concrete (SFRC) using prisms reinforced with undulated manufactured and/or re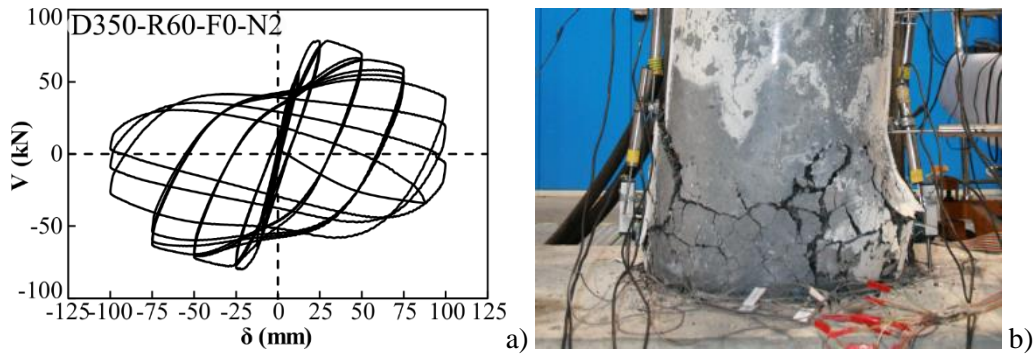cycled (from end-of-life tyres) steel fibres (RTSF) at different dosages and blends (Hu et al., 2018). Two total fibre dosages were assessed: 30 kg and 45 kg per m^3 of concrete, which are typically used for slabs-on-grade and suspended slabs, respectively. An intermediate dosage at 35 kg/m^3 was also evaluated for comparison purposes. Two undulated steel manufactured fibres were used (MSF1: 0.8/55 and MSF2: 1/60) and RTSF (0.1/25) (Table 4). Prisms were tested using a three-point load setup (EN 14651:2005) in Crack Mouth Opening Displacement (CMOD)-control (Figure 9).

Table 4. Experimental programme and compressive results.

Total fibre dosage (kg/m^3)	Mix	MSF1 dosage (kg/m^3)	MSF2 dosage (kg/m^3)	RTSF dosage (kg/m^3)	Avg. f_{cu} (MPa) SFRC/Plain	Stdev. (MPa) SFRC/Plain
30	A	-	30	-	43.9/42.0	1.8/0.9
	B	-	20	10	42.6/46.1	2.2/2.0
	C	-	15	15	44.3/47.5	1.9/1.1
	D	-	10	20	44.6/47.5	1.9/1.1
	E	-	-	30	41.8/37.6	1.9/3.7
35	F	35	-	-	42.9/42.0	1.9/0.9
45	G	45	-	-	41.9/42.0	1.0/0.9
	H	35	-	10	42.8/46.1	0.2/2.0
	I	22.5	-	22.5	50.3/47.5	2.4/1.1
	J	10	-	35	44.5/39.9	0.7/1.0

Figure 9. 3-point bending test.

Figures 10 and 11 show the load-deflection curves for SFRC mixes at 30 kg/m^3, and 45 kg/m^3, respectively. Load-deflection curves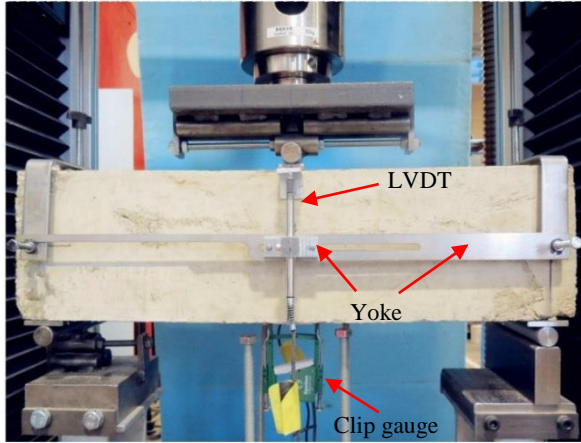 for single-fibre-type reinforced concrete and plain concrete prisms are shown in solid lines, while hybrid SFRC prisms are shown in dashed lines (red curves: plain concrete). The 35 and all 45 kg/m^3 mixes exhibited deflection hardening behaviour, which was only found from hybrid mix B [MSF2 (20) + RTSF (10)] at the total fibre dosage of 30 kg/m^3.

The best flexural performance was found from hybrid mixes B [MSF2 (20) + RTSF (10)] and H [MSF1 (35) + RTSF (10)] in the two groups of mixes, indicating that hybrid SFRC mixes containing 10 kg/m^3 of RTSF can show better flexural performance than MSF-only mixes at the same fibre dosage. Compared to other SFRC mixes, a sharper descending gradient occurs for mixes containing more than 22.5 kg/m^3 of RTSF (RTSF-only mix E and hybrid mixes I and J) starting at a deflection of approximately 1.5 mm. This may be due to the fact that shorter RTSF can debond or even pull out at large crack widths, leading to progressive damage. This also suggests that RTSF, due to their geometrical characteristics, are less effective at controlling macrocracks than MSF.
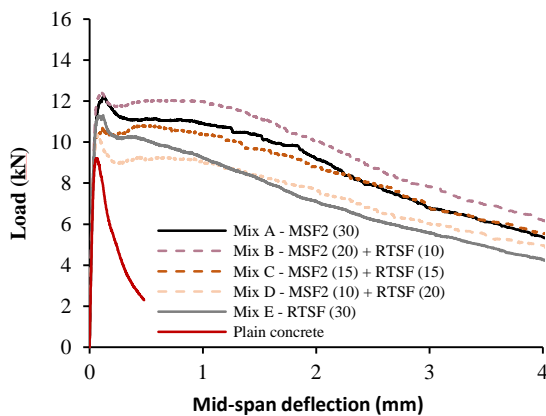
Figure 10. Load-deflection curves for SFRC mixes at 30 kg/m^3.
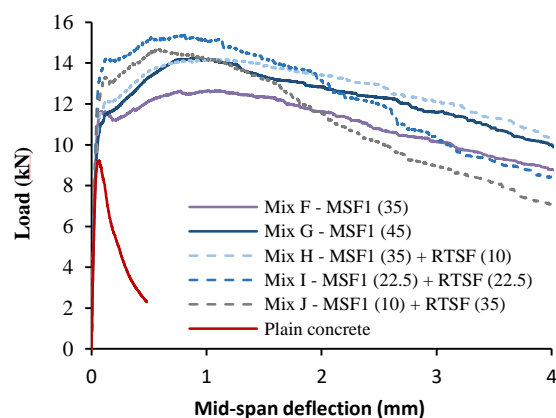
Figure 11. Load-deflection curves for mixes at 35 and 45 kg/m^3.

2.5 *Mechanical behaviour and long-term performance of Steel Fibre Reinforced Rubberised Concrete (SFRRuC)*

RuC reinforced with recycled steel fibres (RTSF) can offer a concrete pavement system that has similar flexibility to flexible pavements, flexural strength similar to rigid concrete pavements and

good durability properties and freeze&thaw resistance (Alsaif et al., 2018a, Alsaif et al., 2018b, Alsaif et al., 2019). This study examined the resistance of SFRRuC to chloride corrosion and freeze-thaw effects. The mixes contained various rubber aggregate contents (0, 30 and 60% by volume of both fine and coarse aggregates) and were reinforced with 20 kg/m^3 of MSF (undulated steel manufactured fibres) and 20 kg/m^3 of RTSF. Table 5 shows the details of the experimental programme.

Table 5. Experimental programme.

| Concrete mixes ID | % Rubber replacing aggregates by volume | | MSF (kg/m^3) | RTSF (kg/m^3) |
	Fine	Coarse		
0P	0	0	0	0
0BF	0	0	20	20
30BF	30	30	20	20
60BF	60	60	20	20

For the chloride corrosion test, specimens were first exposed to intermittent wet-dry cycles in 3% NaCl solution for 150 and 300 days. Then, uniaxial compression tests (100x100mm cubes) and three-point bending tests (100x100x500mm concrete prisms) were performed according to EN 12390-3:2009 (BSI, 2009) and RILEM (2002), respectively. For the freeze-thaw tests, 100x100x500mm concrete prisms were subjected to continuous freeze&thaw cycles ranging from -15℃ to 20℃ (in 24 hours) as specified in PD CEN/TR15177 (BSI, 2006). The internal damage of concrete was assessed through its Relative Dynamic Modulus of elasticity (RDMs) using measurements obtained from ultrasonic pulse transit times (UPTT) after 7, 14, 28, 42 and 56 freeze-thaw cycles.

Figure 12 presents the compressive and flexural strength in terms of mean values for all mixes: a. after 28 days of mist curing, b. after 150 and 300 days of wet-dry chloride exposure. Compared to the observed compressive strength reduction, the steel fibres significantly mitigated the loss in flexural strength associated with the rubber replacement increase. Regarding the chloride exposure, in most cases, both compressive and flexural strength increased after 150 and 300 days of wet-dry cycles, compared to the 28-day values. This increase is mainly attributed to the absence of corrosion attack, as evidence of rust in the fibres embedded in these specimens was not observed. It is also justified by the continuous hydration of the cementitious material over the period of exposure.

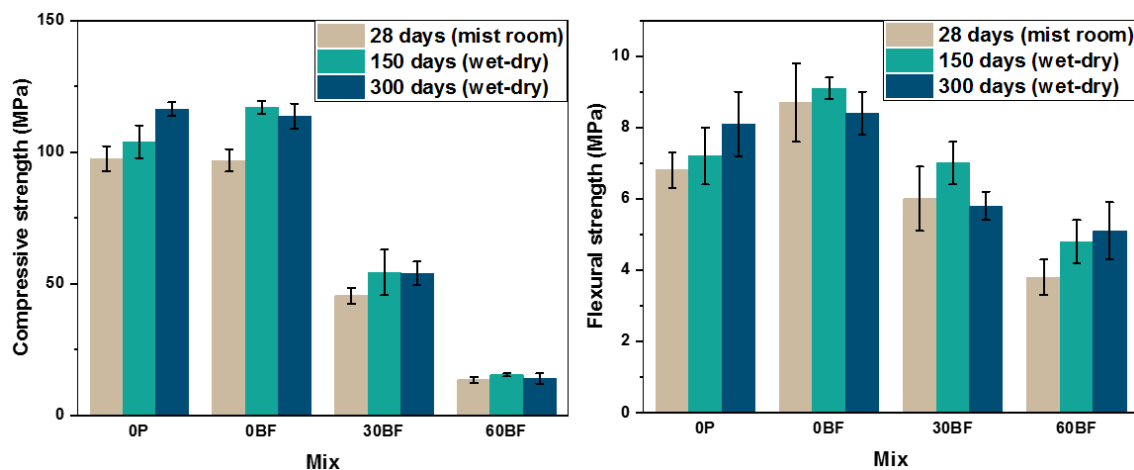Figure 12. Compressive strength (left) and flexural strength (right) of concrete mixes exposed to a wet-dry chloride environment.

Figure 13 shows the mean values of RDMs as a function of freeze-thaw cycles. Although the rate of reduction in RDM values increases with the rubber content, the RDM values of all concrete prisms are way above the threshold value of 80% defined by RILEM (2004) that cause the internal

damage. Hence, SFRRuC mixes can be considered as durable concrete mixes because they survived 56 freeze-thaw cycles with good resistance to freeze thaw actions. This shows that the incorporation of blend fibres into SFRRuC make a positive contribution to its mechanical and long term performance as the fibres help in maintaining the concrete integrity by restraining the development of micro-cracks.
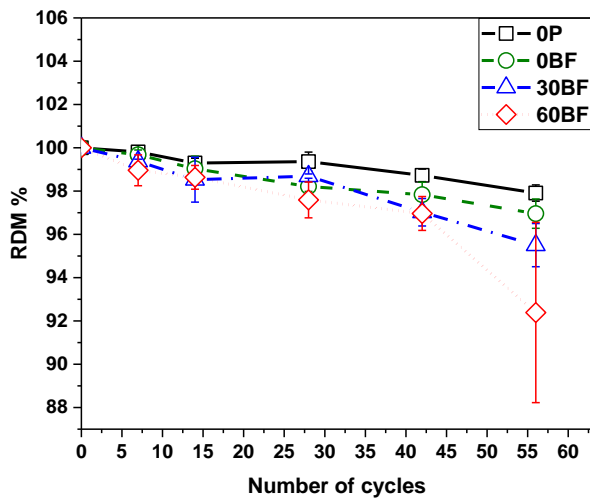
Figure 13. Change in RDMs during freeze/thaw cycles.

2.6 Development of a specialised radiant heating panel to investigate concrete spalling

A specialised Radiant Panel Heating System (RPHS) was designed and manufactured to assess the fire spalling behaviour of concrete reinforced with Recycled Tyre Polymer Fibres (RTPF), as a replacement of manufactured Polypropylene fibres (PP). The RPHS is based on an electric radiant heating vertical panel. The thermal loading is controlled by measuring the exposed surface of the specimen using a plate thermometer.

The fire-spalling behaviour of concrete with RTPF was assessed by performing six fire tests on concrete panels with dimensions of 250x500x500mm. Three specimens were made of plain concrete whilst another three specimens were reinforced with 2 kg/m^3 of RTPF. The specimens were subjected to an axial stress of 10 MPa, which was 20% of their compressive strength at ambient-temperature. The specimens were exposed to the ISO fire curve. A heat transfer analysis was conducted in Abaqus to model the temperature in a concrete specimen and a numerical model was developed which was also verified by the experimental results.

All three plain concrete specimens experienced severe spalling. The specimens with 2 kg/m^3 RTPF did not spall showing good evidence that RTPF can prevent fire-induced spalling in concrete (Figueiredo et al., 2019). Figure 14 shows the aftermath of example specimens after the spalling tests.

Figure 14. Specimens after the fire-induced spalling tests. a) plain concrete b) RTPF reinforced concrete.

3   MAIN CONCLUSIONS

The EU-funded Anagennisi project demonstrated that all tyre components can be used efficiently in construction. Rubber aggregates can be used to replace mineral aggregates up to 60% by volume to produce a more ductile concrete, especially when confined by internal (steel stirrups) or external (FRP sheets) reinforcement. Concrete compressive strains exceeding 6% can be achieved and this can lead to more flexible structural elements, such as, base isolation units, low moment connections and high dissipation connections for seismic applications. RSTF were found to work best in blends (together with manufactured steel fibres), where they exhibit superior behaviour to conventional SFRC in terms of mechanical, fatigue and environmental performance. RuC can be reinforced with RTSF and produce a flexible pavement with flexural strength similar to rigid concrete pavements; this type of pavement is chloride resistant and can withstand extreme environmental conditions (freeze and thaw). Clean RFPF were produced in sufficient quantities and when used in moderate quantities in concrete were shown to control plastic shrinkage and prevent fire spalling.

Although the experimental studies presented in this paper included only laboratory work, the project demonstrated this technology in various in-situ applications through several demonstration projects, and developed the first design recommendations for these materials. The main demonstration projects dealt with applications such as sprayed concrete reinforced with RTSF for tunnel linings, casting of life-size slabs-on-grade using hybrid RTSF (+ manufactured steel fibres) reinforced concrete and mortar application using short RTSF.

REFERENCES

Alsaif A., Koutas L., Bernal S.A., Guadagnini M., and Pilakoutas K., Mechanical performance of steel fibre reinforced rubberised concrete for flexible concrete pavements, Construction and Building Materials 172 (2018a) 533-543.

Alsaif A., Bernal S.A., Guadagnini M., and Pilakoutas K., Durability of steel fibre reinforced rubberised concrete exposed to chlorides, Construction and Building Materials 188 (2018b) 130-142.

Alsaif A., Bernal S.A., Guadagnini M., and Pilakoutas K., Freeze-thaw resistance of steel fibre reinforced rubberised concrete, Construction and Building Materials 195 (2019) 450-458.

Bompa D.V., Elghazouli A.Y., Xu B., Stafford P.J. and Ruiz-Teran A.M., 2017. Experimental assessment and constitutive modelling of rubberised concrete materials. Construction and Building Materials, 137, pp.246-260. https://doi.org/10.1016/j.conbuildmat.2017.01.086.

BSI, EN 12390-3, Testing hardened concrete, Part3: Compressive strength of test specimens, BSI 389 Chiswick High Road, London W4 4AL, UK, 2009.

BSI, PD CEN/TR15177, Testing the freeze-thaw resistance of concrete – Internal structural damage, BSI 389 Chiswick High Road, London W4 4AL, UK, 2006.

Elghazouli A.Y., Bompa D.V., Xu B., Ruiz-Teran A.M. and Stafford, P.J., 2018. Performance of rubberised reinforced concrete members under cyclic loading. Engineering Structures, 166, pp.526-545. https://doi.org/10.1016/j.engstruct.2018.03.090.

European Tyre and Rubber manufacturers' association, 2015, End-of-life Tyre Report, Brussels, Belgium.

Figueiredo F., Huang S., Angelakopoulos H., Pilakoutas K., Burgess I., Mitigation of concrete spalling in fire using recycled fibres from waste tyres, 2017, IFireSS 2017 – 2nd International Fire Safety Symposium, Naples, Italy, June 7-9.

Figueiredo F., Huang S., Angelakopoulos H., Pilakoutas K., Burgess I., Effects of Recycled Steel and Polymer Fibres on Explosive Fire Spalling of Concrete, 2019, Fire Technology,55, 5, https://doi.org/10.1007/s10694-019-00817-9, pp1495-1516.

Hu H., Papastergiou P., Angelakopoulos H., Guadagnini M., Pilakoutas K., Mechanical properties of SFRC using blended manufactured and recycled tyre steel fibres, Construction and Building Materials. 163 (2018) 376–389. doi:10.1016/j.conbuildmat.2017.12.116.

Mander J.B., Priestly M.J.N. and Park R., Theoretical Stress-Strain model for Confined Concrete, 1988, J.Struct.Eng, 114(8): 1804-1826.

Pilakoutas K., Raffoul S., Papastergiou P., Garcia R., Guadagnini M. and Hajirasouliha I., 2015, Innovative reuse of all tyre components in concrete: The Anagennisi project, International Conference on Sustainable Structural Concrete, 15-18 Sep 2015, La Plata, Argentina.

Raffoul, S., Escolano-Margarit, D., Garcia, R., Guadagnini, M., Pilakoutas, K. (2019). 'Constitutive model for rubberised concrete passively confined with FRP laminates', Journal of Composites for Construction 23 (6): 04019044.

Raffoul, S., Garcia, R., Escolano-Margarit, D., Guadagnini, M., Hajirasouliha, I., Pilakoutas, K. (2017). 'Behaviour of unconfined and FRP-confined rubberised concrete in axial compression', Construction and Building Materials 147: 388-397.

Raffoul, S., Garcia, R., Pilakoutas, K., Guadagnini, Flores Medina, N. (2016). 'Optimisation of rubberised concrete with high rubber content: An experimental investigation', Construction and Building Materials 124: 391-404.

RILEM, TC 162-TDF, Test and design methods for steel fibre reinforced concrete, Bending test, Final Recommendation, Materials and Structures 35, 579-582, 2002.

RILEM, TC 176-IDC, Internal damage of concrete due to frost action, Final Recommendation, Prepared by L. Tang and P.-E. Petersson SP Swedish National Testing and Research Institute, Boras, Sweden. Materials and Structures / 2ⁿᵈ International Workshop on Advanced Materials and Innovative Systems in Structural Engineering: Novel Researches, Materiaux et Constructions, Volume 37, December 2004, pp 754-759 in Slab test: Freeze/thaw resistance of concrete Internal deterioration 2004.

2ⁿᵈ International Workshop on Advanced Materials and
Innovative Systems in Structural Engineering:
Novel Researches

ISTANBUL
fib IWAMISSE
Turkey 2019

Performance-based optimisation of RC frames with friction wall dampers

Neda Nabid[1], Iman Hajirasouliha[2], and Mihail Petkovski[3]

[1] Visiting Researcher, The University of Sheffield, Sheffield, UK
[2] Senior Lecturer, The University of Sheffield, Sheffield, UK
[3] Lecturer, The University of Sheffield, Sheffield, UK

ABSTRACT: This study aims to develop a computationally efficient method for optimum performance-based design of friction-based dampers based on the concept of Uniform Distribution of Deformation (UDD) and also propose a simplified method for preliminary design of these systems subjected to near and far-field earthquakes. In the proposed approach, the computational cost is considerably reduced by using an adaptive convergence factor modified based on the level of performance violation. The efficiency of the method is investigated for 3, 5 and 10-storey RC frames and the results are compared with Genetic Algorithm (GA) and a coupled UDD-GA approach. It is shown that the proposed method can lead to optimum design solutions with significantly lower computational costs (up to 300 times) compared to both GA and coupled UDD-GA methods. Optimum solutions are shown to be more sensitive to Peak Ground Velocity (PGV) than Peak Ground Acceleration (PGA), especially for near-field earthquakes with high velocity pulses. Based on the results of this study, a new design equation is proposed for the preliminary design of RC frames with friction wall dampers.

1 INTRODUCTION

Friction and metallic dampers dissipate considerable amounts of seismic input energy through yielding metal and friction between two or more solid bodies, respectively. Both dampers exhibit hysteretic behaviour that can be idealised by an elastic perfectly plastic load-displacement relationship. Due to their high energy dissipation capacity, the hysteretic dampers are considered as potentially efficient passive control systems to enhance seismic performance of substandard structures. However, optimum design of energy dissipation devices for earthquake resistant structures can be a challenging task due sensitivity of the responses to the characteristics of the seismic excitation as well as the complexity and high nonlinearity of these systems.

Several research studies have been carried out on optimum design of friction dampers under earthquake excitations using different optimisation techniques such as Genetic Algorithm (GA) (Mohammadi et al., 2019), backtracking search optimisation algorithm (BSA) (Miguel et al., 2016) and Uniform Distribution of Deformation (UDD) (Nabid et al., 2018). However, most of the aforementioned optimisation methods are computationally expensive and/or based on only a single design earthquake event require, and therefore, may not be suitable for practical applications. A design slip load spectrum was developed by Filiatrault and Cherry (1990) to obtain the best slip load distribution for friction dampers by minimising an energy performance index. They showed that the optimum slip load is not only a structural property but also depends on the frequency and amplitude of the ground motion (linearly proportional to the PGA of the input earthquake). In a study performed by Xu et al. (2007), the performance of yielding and viscous

passive energy dissipation systems were investigated subjected to near-field ground motions by using an analytical ground velocity pulse model. They concluded that the performance of different passive energy dissipation systems depends significantly on the period of the pulse excitation.

Moghaddam and Hajirasouliha (2004, 2005, 2006 and 2008) used the concept of Uniform Distribution of Deformation (UDD) to determine the optimal distribution of stiffness in shear-buildings by developing a practical iterative procedure. This approach has been later adopted for optimum seismic design of different passive control systems such as viscous dampers (Levy and Lavan, 2006), tuned mass dampers (Lavan and Daniel, 2013), buckling restrained brace dampers (Mohammadi et al., 2019) and friction dampers (Nabid et al., 2018). Previous studies showed that using UDD approach, the convergence factor is one of the key parameters to determine the speed of the optimisation. The value of this factor depends on the type of structure, number of storeys and adopted optimisation algorithm. However, all the above mentioned studies on UDD optimisation are based on a constant predefined convergence parameter, which may potentially cause instability in the optimisation process or result in a low convergence rate.

This study aims to improve the computational efficiency of UDD optimisation methods by using an adaptive convergence parameter, which is a function of performance violation level. The computational efficiency of the proposed method is then demonstrated through optimisation of 3, 5 and 10-storey frames and comparison with the results obtained from standard UDD optimisation with constant convergence factors as well as a Genetic Algorithm (GA) and a coupled UDD-GA approach. More over the effects of near-field and far-field ground motions is evaluated on optimum design of friction wall dampers leading to a maximum amount of energy dissipation efficiency in friction devices. Based on the results, an empirical equation is proposed to obtain the optimum slip load values by considering the effects of number of storeys and earthquake PGV.

2   MODELLING AND DESIGN ASSUMPTIONS

The benchmark structures used in this study consist of 3, 5 and 10-storey RC frames equipped with friction dampers with the typical geometry shown in Figure 1. The details of the friction damper are also shown in this figure. The employed assembly comprises a concrete wall panel, a friction device at the top, horizontal supports at the bottom, and vertical supports at the sides. The lateral connections can prevent transferring extra shear forces to the adjacent columns and the floor beams by using appropriate slot direction. This arrangement ensures that the displacement of the friction device at the top of the panel is equal to the inter-storey drift at each level. A Slotted Bolted Connection (SBC) is used as the friction device, and the friction mechanism is provided by the relative movement between the two external steel plates attached to the wall, and a T-shape central steel plate attached to the beam with brass plates inserted at the interfaces.
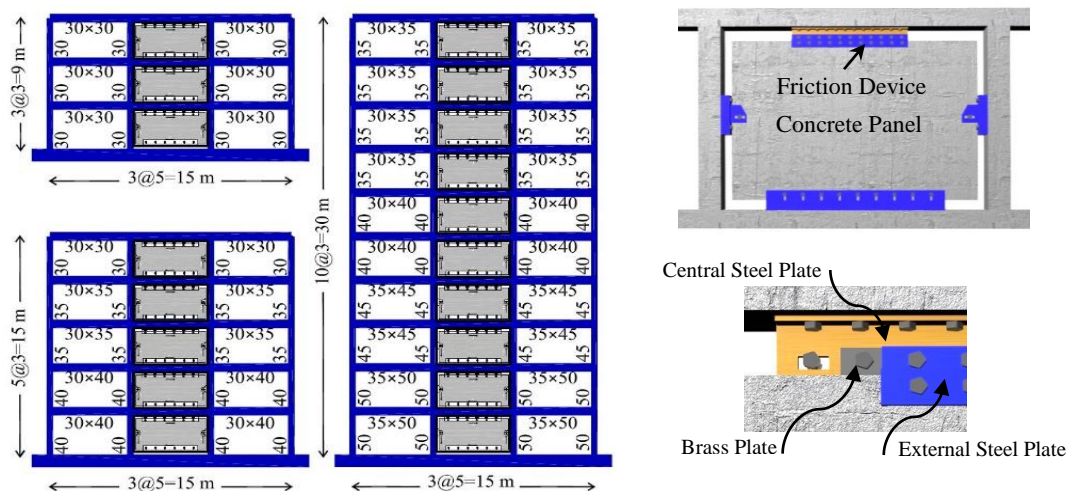

Figure. 1. Geometry of the reference RC frames equipped with friction wall dampers and schematic view of the friction wall damper (adopted from Nabid et al. (2017))

The studied RC frames were assumed to be located on a soil type C of EC8 (2004a) category and were designed based on low-to-medium seismicity regions using PGA of 0.2g. The uniformly distributed live and dead loads were considered to be 1.0 kN∕m² and 5.3 kN∕m² for the roof level; and 2.5 kN∕m² and 5.5 kN∕m² for all the other floors. The reference frames were initially designed in accordance with EC8 (2004a) and EC2 (2004b) for moment-resisting RC frames with medium ductility (DCM). The concrete compressive strength (f_c') and the yield strength of steel reinforcement bars (f_y) were assumed to be 35 MPa and 400 MPa, respectively.

3   GROUND MOTION DATASETS

In this study, two sets of 10 near-field and 10 far-field ground motions were selected correspond to soil class C of EC8 with surface magnitudes ranging from 6.5 to 7.4 (see Tables 1 and 2). The rupture distances (R: distance from the fault rupture plane to the site) are within 10 km for the near-field records and between 12 and 30 km for the selected far-field ground motions.

A synthetic Design Basis Earthquake (DBE) level compatible with the EC8 design response spectrum was also generated using the TARSCTHS (Papageorgiou at al., 2002) software, assuming PGA=0.4g and soil class C. In this study, the optimisation process is conducted for the studied RC frames under the DBE representative spectrum compatible earthquake to satisfy Life Safety (LS) performance limit with 2% allowable maximum inter-storey drift ratio.

Table 1. Properties of the selected near-field ground motions

No.	Earthquake	Ms	Station	Abr.	R (km)	PGA (g)	PGV (cm/s)	PGV/PGA (s)
1	1999 Duzce	7.14	Duzce	DUZ	6.58	0.515	84	0.166
2	1992 Erzincan	6.69	Erzincan	ERZ	4.38	0.387	107	0.282
3	1994 Northridge	6.69	Rinaldi Receiving Sta	RIN	6.50	0.874	148	0.173
4	1994 Northridge	6.69	Newhall - Fire Sta	NEW	5.92	0.590	97	0.168
5	1994 Northridge	6.69	LA - Sepulveda VA Hospital	SEP	8.44	0.932	76	0.083
6	1995 Kobe	6.9	KJMA	JMA	0.96	0.630	76	0.123
7	1995 Kobe	6.9	Takatori	TAK	1.47	0.671	123	0.187
8	1995 Kobe	6.9	Port Island	POR	3.31	0.290	51	0.179
9	1979 Imperial Valley	6.53	Meloland Geot. Array	MEL	0.07	0.298	93	0.168
10	1979 Imperial Valley	6.53	El Centro Array #4	ARR4	7.05	0.484	40	0.084

Table 2. Properties of the selected far-field ground motions

No.	Earthquake	Ms	Station	Abr.	R (km)	PGA (g)	PGV (cm/s)	PGV/PGA (s)
1	1994 Northridge	6.69	Canoga Park-Topanga Can	CAN	14.70	0.358	34	0.097
2	1994 Northridge	6.69	Northridge-Saticoy St	SAT	12.09	0.459	60	0.133
3	1994 Northridge	6.93	Capitola	CAPIT	15.23	0.511	38	0.076
4	1989 Loma Prieta	6.93	Sunnyvale-Colton Ave.	SUN	24.23	0.207	37	0.182
5	1989 Loma Prieta	6.93	Gilroy Array #3	GIL3	12.82	0.559	36	0.066
6	1987 Superstition Hills	6.54	El Centro Imp. Co. Cent	COC	18.20	0.357	48	0.137
7	1987 Superstition Hills	6.54	Westmorland Fire Station	WES	13.03	0.211	32	0.155
8	1971 San Fernado	6.61	LA - Hollywood Stor Lot	HOLL	22.77	0.225	22	0.100
9	1992 Landers	7.28	Desert Hot Springs	LAN	21.78	0.171	19	0.113
10	1978 Tabas	7.35	Boshrooyeh	TAB	28.79	0.106	13	0.125

4   EFFECT OF NEAR-FIELD AND FAR-FIELD EARTHQUAKES ON OPTIMUM DESIGN OF FRICTION DAMPERS

To evaluate the effect of near-field and far-field ground motions on optimum design solutions, the 3, 5 and 10-storey frames with friction wall dampers are subjected to the natural records listed

in Tables 1 and 2. Figures 2 presents the energy dissipation parameter (RW), as a function of slip load ratio under the selected near-field and far-field earthquakes for 5 and 10-storey frames.
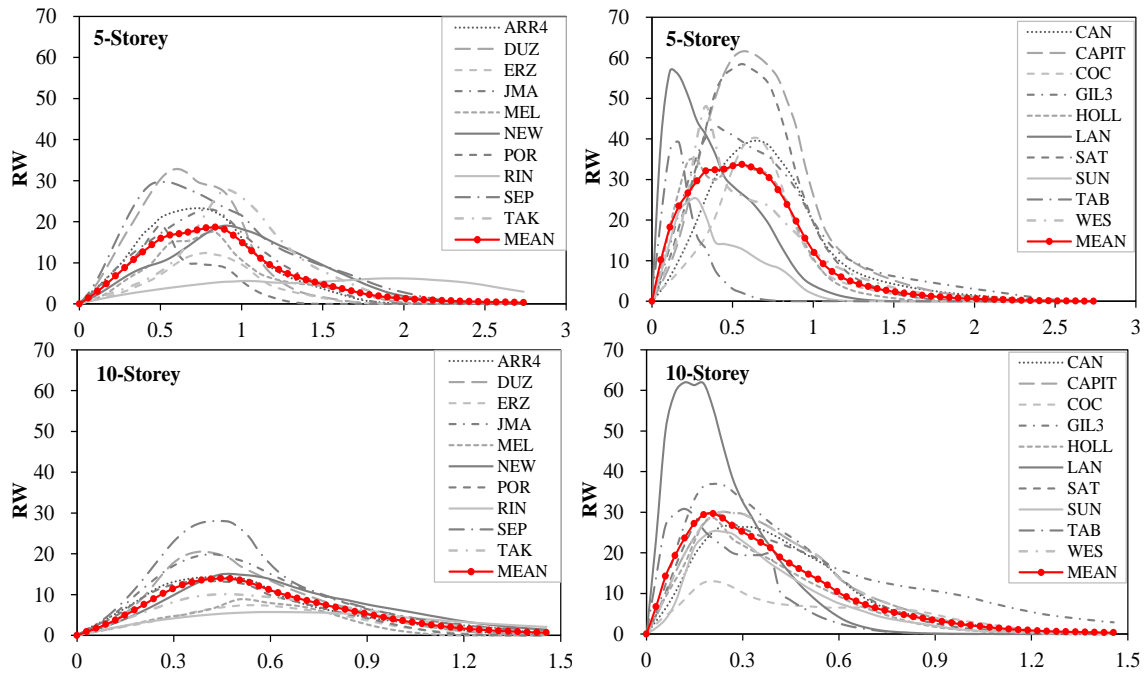

Figure. 2. Variation of energy dissipation parameter, RW, of 5 and 10-storey frames as function of slip load ratio under (left) near-field and (right) far-field ground motions

The comparison of mean-value curves shows almost twice higher energy dissipation efficiency for far-field earthquakes, while near-field earthquakes generally lead to higher and wider optimum ranges of slip load ratios for the supplemental friction-based energy dissipation devices. By considering no more than 10% reduction in the maximum of the mean RW curves, the range of optimum slip load ratios for the selected near-field earthquakes was obtained as 0.89-1.51, 0.56-0.95 and 0.34-0.54 for the 3, 5 and 10-storey frames, respectively. The corresponding optimum slip load ratio ranges obtained for the far-field earthquakes were 0.31-0.67, 0.33-0.73 and 0.16-0.27. The following equation calculates the optimum slip load ratios for all types of earthquakes, giving an average error of less than 18% (Nabid et al., 2019 (a)):

$$R_{EQ} = \left(4.75 \times e^{-0.09n} \times (a_v)^{0.75}\right)/100 \tag{1}$$

where R_{EQ} is the optimum slip load ratio for both near-field and far-field earthquakes and a_v is the PGV of the earthquake. By using a previously defined uniform cumulative pattern (Nabid et al., 2017) for the height-wise distribution of slip loads, the equation below can be used to find the slip load values at each storey level:

$$F_{s,i} = \frac{\sum_{1}^{n} F_{y,i} \times 4.75 \times e^{-0.09n} \times (a_v)^{0.75}}{100 \times n(n+1)/2} \times (n+1-i) \tag{2}$$

Figure 3 compares the individual optimum slip load ratios obtained for the selected natural near-field and far-field earthquakes with the curves resulting from Equation 1. The proposed equation curve is the best fit to the series of optimum slip load ratios obtained for the selected earthquakes. R-squared values corresponding to Equation 1 are reasonably high which confirms the accuracy of the proposed equation to predict the optimum slip load ratio under both near and far-field earthquakes. It can be observed from Figure 3 that the upper parts of the data sets with higher optimum slip load ratios are associated with the results of the near-field earthquakes, whereas the lower parts correspond to those of the far-field records. The dispersion of the results and

discrepancy between the data sets and the proposed equation curve can be caused by different pulse periods and frequency contents of the design earthquakes.
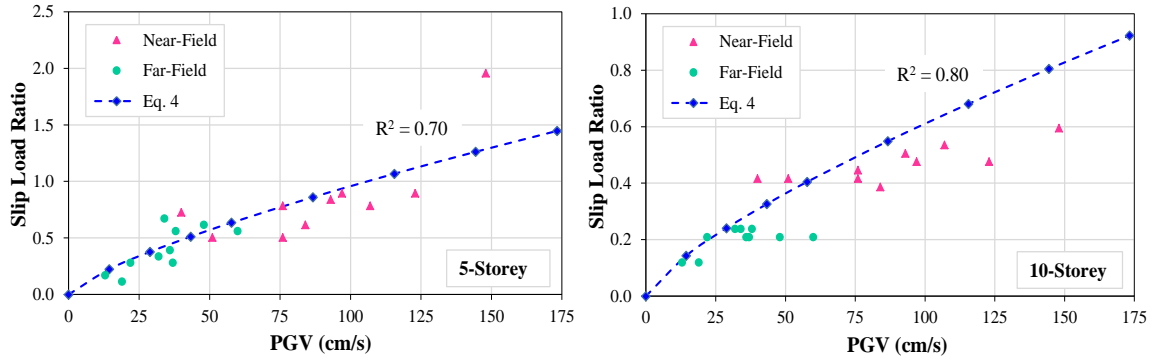

Figure. 3. Comparison of optimum slip load ratios for the selected near and far-field earthquakes with the proposed empirical equation (Equation 1) as functions of earthquake PGV level

5   ADAPTIVE UDD OPTIMISATION ALGORITHM

In this study, the designed structures are assumed to satisfy the Life Safety (LS) and Collapse Prevention (CP) performance levels under DBE and MCE events, respectively. In the proposed iterative optimisation method, the slip load values of the friction devices are gradually modified until these pre-defined performance targets are satisfied. Maximum inter-storey drift is considered as the main design parameter to control the required performance limits. Unlike conventional UDD optimisation algorithms, the proposed method employs an adaptive equation in which the convergence factor is modified in proportion to the level of performance violation. The suggested optimisation algorithm comprises the following iterative steps:

1. A uniform slip load distribution with identical slip load values for all the storey levels is assumed for the initial design of the friction devices. Previous studies showed that the final optimum design is independent of the initial values; however, the optimisation rate can be affected (e.g. Hjirasouliha and Moghaddam 2009; Hajirasouliha and Pilakoutas 2012). Also studies by Hajirasouliha et al. (2016) indicated that the optimum design solutions are not generally very sensitive to small variations in the stiffness and strength of the system.

2. The initial structure is then subjected to the selected spectrum-compatible DBE record and the value of maximum inter-storey drift is obtained at each storey level and compared with the performance target value (e.g. LS).

3. The slip loads are changed so that all of the relative displacements reach the predefined objective. To satisfy this, the slip load is increased in the storeys where the inter-storey drift exceeded the target, and reduced in the storeys with inter-storey drifts below the target value. The process continues until all inter-storey drifts are close to the performance target within a predefined tolerance, where the structure is considered to be practically optimum. The following equation was used to obtain the optimum distribution of slip loads:

$$\left(F_{s,i}\right)_{n+1} = \left(F_{s,i}\right)_n \times \left(\frac{\Delta_i}{\Delta_{target}}\right)_n^{\alpha} \tag{3}$$

where Δ_i and Δ_{target} are maximum and target inter-storey drifts of ith storey for n^{th} iteration, respectively; $F_{s,i}$ is defined as the slip load of the friction device at the ith storey; α is the convergence parameter. The value of this factor depends on several parameters such as the type of structure and number of storeys. Previous studies have proposed different ranges for the convergence parameter including: 0.1 to 0.2 proposed by Hajirasouliha et al. (2011, 2012) for truss like structures and RC frames, 0.2 used by Moghaddam et al. (2005) for steel braced frames,

0.2 to 0.5 suggested by Nabid et al. (2018) for friction dampers, and 0.5 recommended by Lavan (2015) for nonlinear structures with viscous dampers.

To provide the best convergence rates, in this study an adaptive equation (Equation 4) is proposed for the convergence factor, which depends on the maximum relative displacement obtained at each step to the predefined target displacement. The aim is to accelerate the optimisation by increasing the α value where the difference between the maximum drift and the performance target is smaller, and also to decrease the α value where the ratio between the drift and the target displacement is larger. The proposed equation can achieve a good convergence during the optimisation process irrespective to the size of the selected frame.

$$\alpha_i = Abs\left(Ln(\frac{\Delta_i}{\Delta_{target}}) \right)^{-0.25} \tag{4}$$

In every optimisation iteration, the coefficient of variation of the inter-storey drifts (COV_Δ) is also calculated. The optimisation algorithm continues from step 2 until an acceptable level of COV_Δ is achieved (e.g. less than 0.1). Since the initial structure is designed for gravity and seismic loads based on a seismic design code (here EC8), at some storey levels the target inter-storey drift may be satisfied without using friction dampers. Therefore, it is not usually possible to reach a very uniform inter-storey drift distribution (i.e. very low COV_Δ), especially when the effect of gravity loads is dominant. However, as will be discussed in the following sections, the proposed algorithm is capable of removing the unnecessary dampers during the optimisation process.

In this section, the efficiency of the proposed adaptive UDD optimisation algorithm is compared to the standard UDD method with constant values of the convergence factor for the selected 3, 5, and 10-storey frames under the representative DBE event. In case of standard UDD optimisation, the convergence factors are selected between 0 and a value which leads to the fluctuation of the results and divergence of the iterations. As an example, Figure 4 compares the convergence rate of the adaptive and standard UDD in terms of maximum drift ratio (drift scaled to storey height) and total slip load value required to satisfy LS performance target under the DBE representative earthquake for the 3-storey frame. The results in general show that the small values of the convergence factor lead to very slow convergence rates of both maximum drift and slip load, while the higher values of this factor may result in divergence of the iterations. The proposed adaptive α factor, however, leads to a convergence in only a few steps (i.e. less than 10 steps). Pit should be mentioned that previous studies conducted by Hajirasouliha et al. (2012) and Nabid et al. (2018) indicated that UDD optimisation may not converge by using convergence factors higher than 0.5 and 1, respectively. However, the results of the current study show that for the optimisation of friction wall dampers, only α factors greater than 2, 3 and 5 lead to fluctuation of the results for the 3, 5, and 10-storey frames, respectively. This indicates that these systems are generally less sensitive to the rate of variations in the design parameters. Using the adaptive approach, the efficient range of convergence factor will not be limited to a specific even if similar structural systems are used.
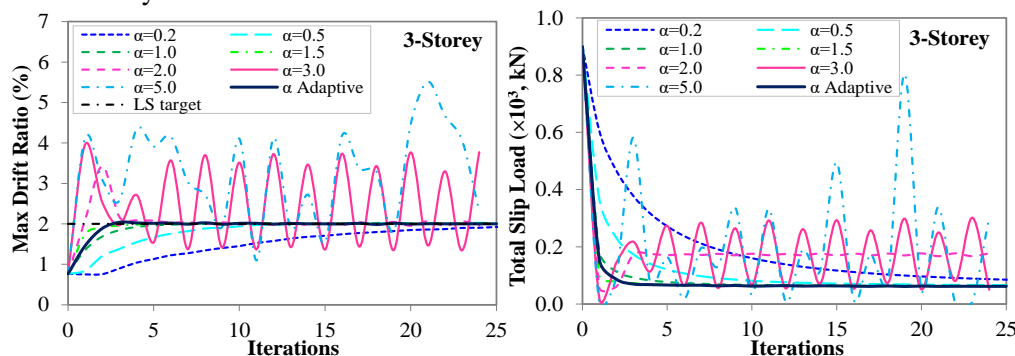

Figure. 4. Variations of maximum inter-storey drift ratio (scaled to the storey height) and total slip load value for 3-storey frame, DBE event

6   COMPUTATIONAL EFFICIENCY OF ADAPTIVE UDD OPTIMISATION METHOD

To investigate the efficiency of the proposed optimisation approach, the following Genetic Algorithm (GA) optimisation procedure is also employed for optimum design of the 3, 5 and 10-storey frames with friction dampers, using a MATLAB (2016) code developed for this purpose:

1. The initial population of 50 individuals is randomly selected from a wide range of slip loads starting from 0 to a relatively high value.

2. Non-linear time-history dynamic analysis is performed using the representative earthquake design event as input, and the maximum inter-storey drift of all the storeys is determined.

3. The maximum inter-storey drift is compared with the predefined performance target (here LS performance level under DBE) and a penalty is applied to the slip loads of the storeys which exceed that value. Then, the objective function (defined as a summation of the slip loads required for all the friction devices) and the penalty function is calculated. Exploration of the optimal result is then performed according to the fitness of the objective function. Equations 5 and 6 are used for calculating the penalty function (PF) and objective function (OF), respectively:

$$PF = a \times \left(\frac{\Delta_{\max}}{\Delta_{t\,arg\,et}} - 1 \right) \qquad\qquad (5)$$

$$OF = \sum_{i=1}^{N} F_{s,i} + PF \qquad\qquad (6)$$

where a is an empirical scale factor considered to be equal to 1000, 1500 and 3000 for the 3, 5 and 10-storey frames, respectively. These numbers were found to be sufficient to scale the penalty value to the same order with the objective function. Δ_{max} and Δ_{target} are the maximum and target inter-storey drifts, and N is the number of storeys. In this algorithm, steps 2 and 3 are repeated for the entire population of samples. More detailed information about the adopted algorithm can be found in Nabid et al. (2019 (b)).

4. Using the above mentioned GA operators, a new population is generated from the best individuals of the previous generation.

5. The algorithm is then repeated from step 2 to 4 for each generation until the mean value of the objective function converges to the best fitness function in the same generation or the maximum number of generations is achieved.

Figure 5 (a) illustrates the variation of the mean and best values of the fitness function (objective function, Equation 6) for the 3, 5, and 10-storey frames subjected to the representative DBE event as the generations proceed during the GA optimisation. For better comparison, the optimisation was repeated three times for each frame using different sets of random initial populations (slip load values) and the answer with the lowest fitness values was retained as the optimum solution. Based on the results, the optimisation procedures converged to the fittest values after about 40 generations for the 3, 5 storey frames and about 60 generations for the 10-storey frame. To demonstrate the efficiency of the proposed adaptive optimisation method in terms of convergence speed and optimum design solutions, the results are compared with those obtained from the optimisation using the Genetic Algorithm (GA) technique. In addition, the GA optimisations are repeated for the selected frames by considering the optimum slip load values obtained from the adaptive UDD algorithm as the initial slip load values (i.e. initial population) rather than using random selections. Figure 5 (b) illustrates the height-wise distribution of slip load values for the 3, 5 and 10-storey frames optimised frames optimised using (1) the proposed adaptive UDD method, (2) GA optimisation starting with random values (i.e. GA) and (3) GA optimisation starting with optimum values obtained from the adaptive UDD (i.e. UDD-GA) under the representative DBE event. The slip load distributions follow almost similar patterns for all the

selected optimisation approaches. The only exception is the 10-storey frame with higher number of variables, where the slip load distribution obtained from the GA optimisation after 3000 analyses is slightly different with the UDD and UDD-GA results. This implies that there are at least two different slip load distributions that lead to very similar objective functions in this case.
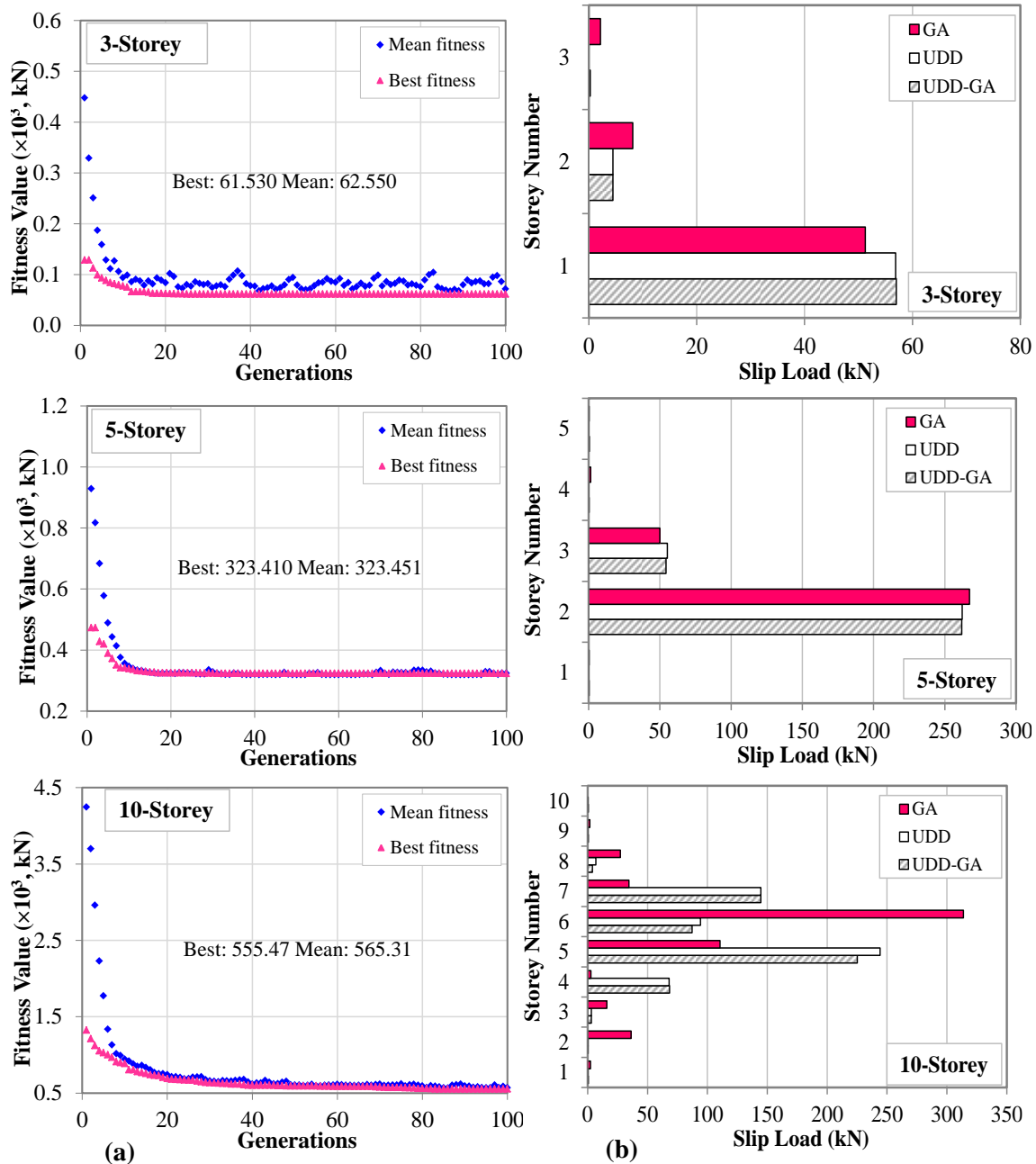

Figure 5. (a) Variations of fitness function of 3, 5, and 10-storey frames versus optimisation generation during GA optimisation, and (b) Height-wise distribution of optimum slip loads for 3, 5 and 10-storey frames optimised using adaptive UDD, GA and UDD-GA optimisation methods, DBE event

Table 3 compares the objective functions and the total number of non-linear dynamic analyses of the 3, 5 and 10-storey frames optimised using the proposed adaptive UDD, GA and the coupled UDD-GA optimisation methods under the representative DBE event. It can be noted that the number of non-linear dynamic analyses required for the GA optimisation is significantly higher than those needed for the adaptive UDD (by up to 300 times), while these two methods lead to almost similar objective functions. It is shown in Table 3 that using the optimum results from the UDD as the initial population of the GA (i.e. UDD-GA) considerably decreases the number of

2nd International Workshop on Advanced Materials and
Innovative Systems in Structural Engineering:
Novel Researches

ISTANBUL
IWAMISSE
2019

required analyses (by up to 65%), which means that the UDD-GA combination is a significant improvement in terms of computational costs compared to the standard GA optimisation.

Table 3. Comparison of GA, adaptive UDD, and UDD-GA methods in terms of total number of non-linear dynamic analyses and objective function, DBE event

	Adaptive UDD		GA		UDD-GA	
	No. of analyses	Objective function (kN)	No. of analyses	Objective function (kN)	No. of analyses	Objective function (kN)
3-Storey	6	61.8	2000	61.5	700	61.4
5-Storey	10	318.0	2000	323.4	800	313.4
10-Storey	14	556.9	3000	556.6	1450	541.8

7   SUMMARY AND CONCLUSIONS

An efficient simplified model was proposed for optimum seismic design of friction-based dampers by considering the effects of near-field and far-field ground motions. To obtain the optimum slip load ranges, a parametric study was performed on 3, 5, and 10-storey RC frames with friction wall dampers under a set of 20 near and far-field earthquake records. Subsequently, an empirical equation was proposed to obtain the optimum slip loads based on the number of storeys and Peak Ground Velocity (PGV) of the design earthquake. In addition, an adaptive performance-based optimisation methodology based on the theory of Uniform Distribution of Deformation (UDD) was developed as a tool for optimum design of friction-based dampers in RC structures under seismic excitations by using a convergence factor that is modified in proportion to the performance violation level. The efficiency of the proposed adaptive UDD method was demonstrated through optimisation of the studied frames with friction dampers to satisfy LS performance limit under DBE representative spectrum compatible earthquake. The results were then compared with those obtained from the standard UDD, standard GA and a combination of UDD and GA methods under a synthetic spectrum-compatible earthquake. Based on the results of this study, the following conclusions can be drawn:

- Friction wall dampers exhibit, on average, 118% higher energy dissipation efficiency under far-field earthquakes compared to the near-field records. In general, the optimum ranges of slip load ratios obtained for the frames under the near-field earthquakes are also noticeably wider and higher (about 1.5 times) compared to those achieved under the far-field ground motions.

- The range of the most efficient convergence factors for the standard UDD method can be different for different types of structures. The proposed adaptive convergence factor, which was used for three different multi-storey buildings, was shown to be significantly more computationally efficient than standard UDD method with constant convergence factors.

- The optimum solutions obtained from the proposed adaptive UDD after a small number of iterations (generally less than 15 nonlinear dynamic analyses) are either very close or even slightly better than those obtained from the GA approach after at least 2000 nonlinear dynamic analyses. This demonstrates the significant advantage of the proposed adaptive UDD method over heuristic optimisation methods such as GA, in terms of computational efficiency and simplicity.

- Using optimum results obtained from the adaptive UDD as a starting point of the GA can considerably increase the optimisation speed (up to 3 times faster) compared to the standard GA using a random initial set.

- The optimum results obtained from the UDD-GA approach were only slightly better (less than 3%) than those achieved with the proposed adaptive UDD method alone. This indicates that the new adaptive UDD method is sufficiently accurate for practical applications.

REFERENCES

CEN (Comité Européen de Normalization), 2004a, Eurocode 8: Design of structures for earthquake resistance-Part 1: General rules, seismic actions and rules for buildings. EN 1998-1-1, Brussels.

CEN (Comité Européen de Normalization), 2004b, Eurocode 2: Design of concrete structures -Part 1-1: General rules and rules for buildings. EN 1992-1-2, Brussels.

Filiatrault, A. and Cherry, S. 1990, Seismic design spectra for friction-damped structures. *Journal of Structural Engineering,* 116(5): 1334-1355.

Hajirasouliha I and Moghaddam H. 2009, New Lateral Force Distribution for Seismic Design of Structures. *Journal of Structural Engineering ASCE*, 135(8): 906-915.

Hajirasouliha I and Pilakoutas K. 2012, General Seismic Load Distribution for Optimum Performance-Based Design of Shear-Buildings. *Journal of Earthquake Engineering*, 16(4): 443-462.

Hajirasouliha I, Asadi P and Pilakoutas K., 2012, An efficient performance-based seismic design method for reinforced concrete frames. *Earthquake Engineering and Structural Dynamics*, 41: 663–679.

Hajirasouliha I, Pilakoutas K and Moghaddam H. 2011, Topology optimization for the seismic design of truss-like structures. *Computers and Structures*, 89(7-8): 702-711.

Hajirasouliha I, Pilakoutas K and Mohammadi RK. 2016, Effects of uncertainties on seismic behaviour of optimum designed braced steel frames. *Steel and Composite Structures*, 20(2): 317-335.

Lavan O and Daniel Y., 2013, Full resources utilization seismic design of irregular structures using multiple tuned mass dampers. *Structural and Multidisciplinary Optimization*, 48: 517–532.

Lavan O. 2015, A methodology for the integrated seismic design of nonlinear buildings with supplemental damping. *Structural Control and Health Monitoring*, 22: 484–499.

Levy R and Lavan O. 2006, Fully stressed design of passive controllers in framed structures for seismic loadings. *Structural and Multidisciplinary Optimization*; 32(6): 485–498.

MATLAB, 2016, version R2016b. The Math Works, Inc., Natick, Massachusetts, USA.

Miguel, LFF, Miguel, LFF and Lopez, RH, 2016, Simultaneous optimization of force and placement of friction dampers under seismic loading. *Engineering Optimization,* 48: 586-602.

Moghaddam H and Hajirasouliha I. 2004, A new approach for optimum design of structures under dynamic exciation. *Asian Journal of Civil Engineering*, 5 (12): 69-84.

Moghaddam H and Hajirasouliha I. 2005, Fundamentals of optimum performance-based design for dynamic excitations. *Scientia Iranica*, 12(4): 368-378.

Moghaddam H and Hajirasouliha I. 2006, Toward more rational criteria for determination of design earthquake forces. *International Journal of Solids and Structures*, 43(9): 2631-2645.

Moghaddam H and Hajirasouliha I. 2008, Optimum strength distribution for seismic design of tall buildings. *Structural Design of Tall and Special Buildings*, 17(2): 331-349.

Moghaddam H, Hajirasouliha I and Doostan A. 2005, Optimum seismic design of concentrically braced steel frames: concepts and design procedures. *Journal of Constructional Steel Research*, 61(2): 151-166.

Mohammadi RK, Garoosi MR and Hajirasouliha I., 2019, Practical method for optimal rehabilitation of steel frame buildings using buckling restrained brace dampers. *Soil Dynamics and Earthquake Engineering*, 123: 242-251.

Nabid N, Hajirasouliha I and Petkovski M. 2017, A practical method for optimum seismic design of friction wall dampers. *Earthquake Spectra,* 33(3): 1033-1052.

Nabid N, Hajirasouliha I and Petkovski M. 2018, Performance-based optimisation of RC frames with friction wall dampers using a low-cost optimisation method. *Bulletin of Earthquake Engineering,* 16(10): 5017-5040.

Nabid N, Hajirasouliha I and Petkovski M. 2019 (a), Simplified method for optimal design of friction damper slip loads by considering near-field and far-field ground motion. *Journal of Earthquake Engineering,* In-Press; DOI: 10.1080/13632469.2019.1605316.

Nabid N, Hajirasouliha I and Petkovski M. 2019 (b), Adaptive low computational cost optimisation method for performance-based seismic design of friction dampers, *Engineering Structures*, 198, 109549.

Papageorgiou A, Halldorsson B and Dong G. 2002, TARSCTH (Target Acceleration Spectra Compatible Time Histories), Engineering Seismology Laboratory at the State University of New York at Buffalo.

Xu Z, Agrawal AK, He WL and Tan P. 2007, Performance of passive energy dissipation systems during near-field ground motion type pulses. *Engineering Structures:* 29(2): 224-236.

2nd International Workshop on Advanced Materials and
Innovative Systems in Structural Engineering:
Novel Researches

ISTANBUL
fib IWAMISSE
Turkey 2019

Seismic strengthening of substandard buildings with composite materials

Maurizio Guadagnini[1], Kypros Pilakoutas[1], Iman Hajirasouliha[1], Reyes Garcia[2], Nicholas Kyriakides[3], and Mihaela Anca Ciupala[4]

[1] The University of Sheffield, Sheffield, UK
[2] The University of Warwick, Coventry, UK
[3] Cyprus University of Technology, 3036, Limassol, Cyprus
[4] University of East London, 4-6 University Way, Beckton, London

ABSTRACT: This paper discusses the results from experimental programmes including shaking table tests on full-scale one-bay two-storey RC frames with poor detailing in the beam-column joints. The tests were performed on the AZALEE shake table at the Commissariat à l'Énergie Atomique (CEA) Laboratory in Saclay, France, as part of two EU-funded Projects that aimed to investigate the effectiveness of externally bonded carbon fibre reinforced polymer (CFRP) reinforcement in improving the seismic behaviour of substandard RC buildings. To simulate typical substandard construction, the reinforcement of columns and beam-column joints of the full-scale structures had inadequate detailing. After an initial series of shake table tests were carried out to assess the seismic behaviour of the bare buildings, columns and joints were repaired and subsequently retrofitted using CFRP for the ECOLEADER building, and a retrofitting solution consisting of CFRP and Post-Tensioned Metal Straps for the BANDIT building. The buildings were then subjected to incremental seismic excitations to assess the effectiveness of the retrofitting solutions at improving the global and local building performance. Whilst the original bare buildings were significantly damaged at a peak ground acceleration (PGA) of 0.15-0.20g, the retrofitted buildings resisted severe shake table tests up to PGA=0.50-0.60g without failure. Moreover, the retrofitting intervention enhanced the interstorey drift ratio capacity and has proven to be very effective at addressing the seismic deficiencies of substandard buildings.

1   INTRODUCTION

Much of the existing building stock in Europe, as well as in developing countries, has been designed according to old standards with little or no seismic provisions, and often suffers from poor material and construction practices. As a result, many existing buildings have deficient lateral load resistance, insufficient energy dissipation and can rapidly lose their strength during earthquakes, leading to collapse. Extensive human and financial losses in recent major earthquakes (China, 2008; Indonesia and Italy, 2009; Haiti and Chile, 2010; Nepal, 2015) have highlighted the seismic vulnerability of substandard reinforced concrete (RC) buildings.

The retrofit of seismically deficient structures provides a feasible and cost-effective approach to improve their load carrying capacity and reduce their vulnerability. Over the last decade, the use of externally bonded fibre composite materials (FRPs) has offered engineers a new solution for strengthening seismically deficient buildings (Pendhari et al. 2008). Comparatively to other traditional strengthening techniques, FRP materials possess advantages such as high strength to weight ratio, high resistance to corrosion, excellent durability, ease and speed of in-situ application and flexibility to strengthen selectively only those members that are seismically deficient (Gdoutos et al. 2000).

Several experimental tests have been conducted to investigate the behaviour of deficient full-scale RC buildings strengthened with FRPs using pseudo-dynamic (Pinto et al. 2002, Balsamo et al. 2005, Balsamo et al. 2005, Di Ludovico et al. 2008) or quasi-static lateral load tests (Della Corte et al. 2006). Based on the results of these experiments, some analytical models were developed to predict the seismic behaviour of deficient and strengthened RC buildings (Jeong et al. 2004, Kosmopoulos and Fardis, 2007). The results from these studies have confirmed the effectiveness of FRP materials at preventing the occurrence of brittle failures and improving the seismic behaviour of the strengthened buildings. However, none of the above studies investigated the efficiency of FRPs at improving the seismic behaviour of deficient full-scale RC frames using shaking table tests.

This paper discusses the results from experimental programmes including shaking table tests on full-scale one-bay two-storey RC frames with poor detailing in the beam-column joints. The tests were performed on the AZALEE shake table at the Commissariat à l'Énergie Atomique (CEA) Laboratory in Saclay, France, as part of two EU-funded Projects that aimed to investigate the effectiveness of carbon fibre reinforced materials (CFRPs) in improving the seismic behaviour of substandard RC buildings.

2   ECOLEADER PROJECT

2.1   Project overview

The main objective of this project was to study experimentally the performance of existing substandard RC frames and different retrofitting configurations using CFRPs. The frame was designed and built according to typical old pre-seismic construction practice of southern Europe and is representative of substandard buildings typically found in developing countries. Initial shaking table tests were carried out until significant damage was observed. Subsequently, the damaged frame was repaired, and columns and beam-column joints were retrofitted using externally bonded CFRPs and additional tests were performed.

2.2   Geometry of the RC frame, material properties and set-up of tests

The tested building was a one-bay two-storey frame regular in plan and elevation, and was designed using old European earthquake-resistant provisions from the 60's (Chaudat et al. 2005). Consequently, columns and beam-column joints were expected to experience significant damage during the initial shaking tests. The frame was 4.26×4.26 m in plan and had a constant storey height of 3.30 m. A general view of the frame along with details of the general geometry, element sections and corresponding reinforcement are shown in Figure 1.
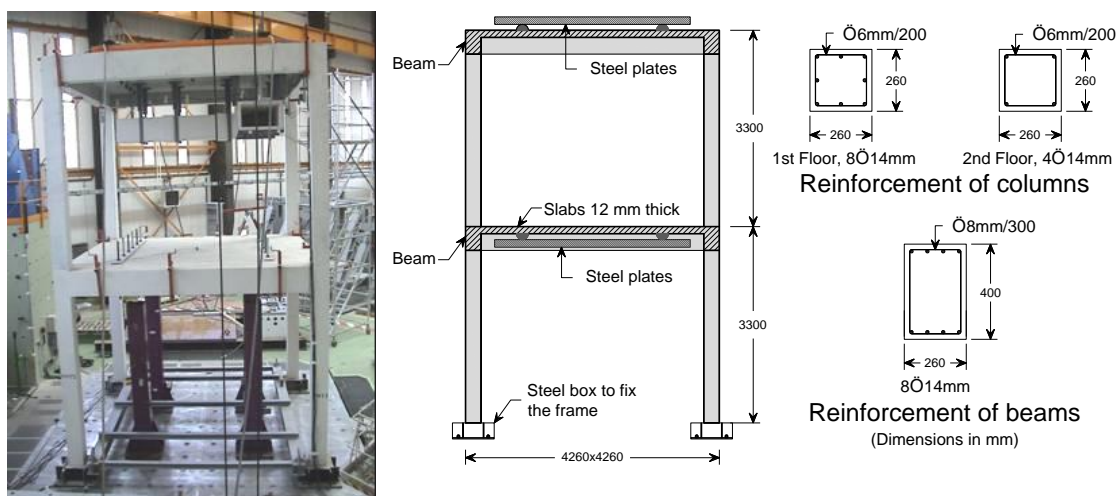

Figure 1. General view and geometry of the ECOLEADER frame and structural elements.

2nd International Workshop on Advanced Materials and
Innovative Systems in Structural Engineering:
Novel Researches

ISTANBUL
fib IWAMISSE
Turkey 2019

The detailing of the reinforcing steel in beam-column joints is shown in Figure 2. The material properties were obtained based on the average of the results for 12 bar specimens and 24 concrete cylinders. Yield and ultimate strength of steel reinforcement were f_y=551 MPa and f_u=656 MPa, and concrete compressive strength and modulus of elasticity were f_c=20 MPa and E_c=25545 MPa, respectively. The manufacturer specifications of the utilised unidirectional CFRPs composites were tensile strength f_{FRP}=1350MPa, modulus of elasticity E_{FRP}=105GPa, and layer thickness of 0.48 mm. An additional mass of 9.0 ton was attached to each slab to simulate real loading conditions as shown in Figure 1.
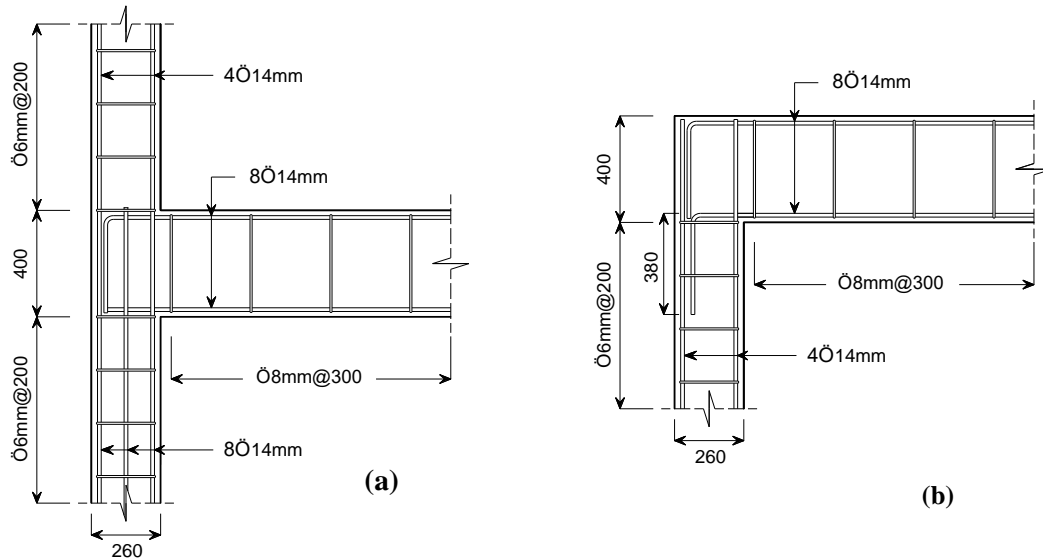

Figure 2. Detailing of reinforcing steel in beam-column joints at (a) 1st storey and (b) 2nd storey.

The structure was instrumented with displacement and acceleration transducers at each storey to monitor the response history during the shaking tests. The displacement transducers were attached to an external rigid frame to facilitate the measurements and quantify the residual displacements after each test.

The experimental programme consisted of unidirectional horizontal input shaking using increasing peak ground accelerations (PGA) levels ranging from 0.05g to 0.4g. A single ground motion record was used based on the Eurocode 8 (EC8) soil profile type C spectrum (CEN 2004). Natural frequencies of the structure were obtained using white noise as input signal before the start and after each test. For this purpose, a low intensity excitation containing a frequency range of 0.5-50 Hz was used. The accelerations recorded at the base and at each storey were then post-processed to identify the natural frequencies of the first two modes of vibration.

2.3   Tests results and discussion

The initial series of tests (PGAs 0.05g to 0.40g) produced significant but repairable damage on the building. After these tests, the damaged frame was retrofitted locally with externally bonded CFRP composites using a wet lay-up technique. The main purpose of the rehabilitation was to produce a beam mechanism, which is in line with modern seismic design philosophy. Before the retrofitting intervention, the damaged concrete was repaired using repair mortar and the main cracks injected with epoxy resin. Concrete surfaces at the application zones were smoothed and prepared to improve the adherence between the existing concrete and the fibre sheets. One vertical CFRP sheet (parallel to the columns axes) was attached at the interior and exterior faces of

columns ends to enhance their flexure strength (Figure 3a). Beam-column joints at both storeys were also retrofitted using one orthogonal sheet to avoid a premature shear failure, as shown in Figure 3b. Two thin strips of CFRPs were wrapped around the beams ends to prevent premature debonding of the sheets applied to retrofit the joints (Figure 3b). Additionally, it was decided to use CFRP confinement to increase further the column capacity and avoid possible buckling and premature debonding of the longitudinal sheets along the columns axes (Figure 4). The existing transverse reinforcement was sufficient to prevent shear failure in beams and columns; therefore, no additional CFRP was required to prevent this type of failure.
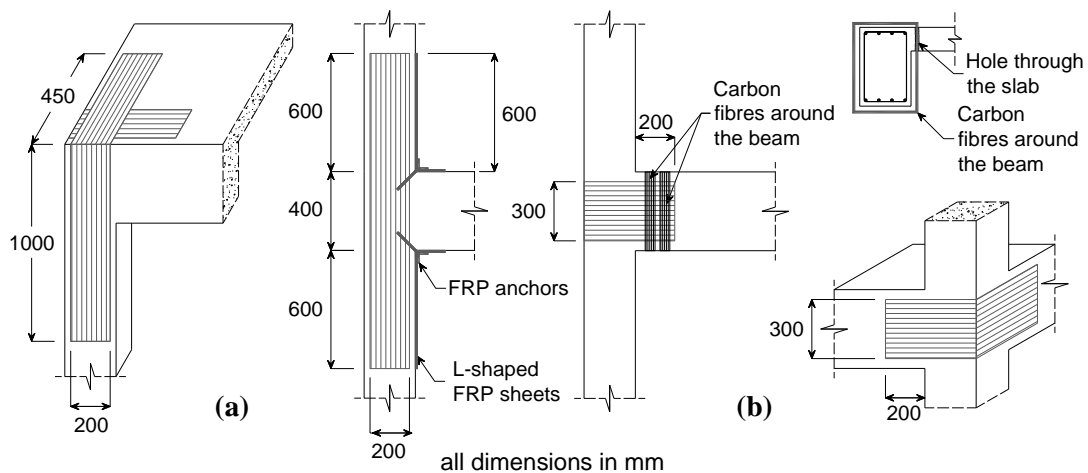

Figure 3. Rehabilitation of the frame using CFRPs at (a) exterior faces of columns, and (b) exterior zone of beam-column joints.
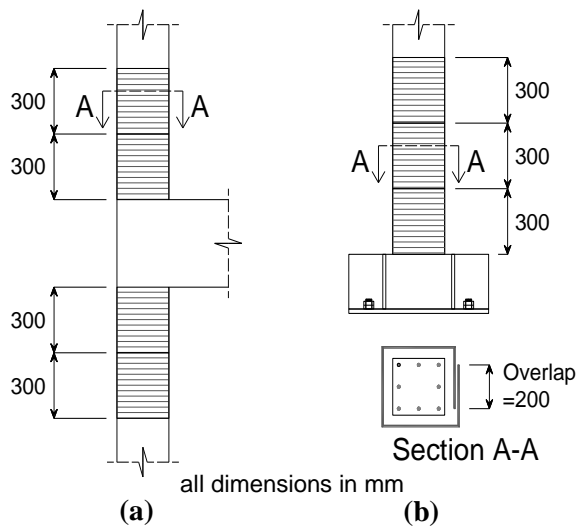

Figure 4. Confinement of the columns using CFRPs at (a) columns ends, and (b) bottom of 1st storey columns.

Following the CFRP-retrofitting of the frame, a second series of shaking table tests were conducted with PGA levels ranging from 0.05g to 0.50g. No evident damage appeared during the test at PGA= 0.05g. A visual inspection detected the first damage at the CFRP sheets at the 2nd storey columns after the tests at PGA level of 0.20g. No further damage was observed at columns or CFRP sheets until after the final tests, however, some fracture of the sheets occurred at beam-column joints. The adopted retrofitting strategy was effective at preventing debonding of the

CFRP sheets as this type of failure was not observed during the tests. However, after the tests at
a PGA of 0.50g, significant cracking occurred at the beams ends (Figure 5). Figure 6 shows the
deformed shape at maximum deformation for the frame in bare and CFRP-retrofitted conditions.
It can be seen that the use of CFRP composites resulted in a considerable reduction of inter-storey
drift at the second floor since it delayed the deterioration of the building due to bond-slip of the
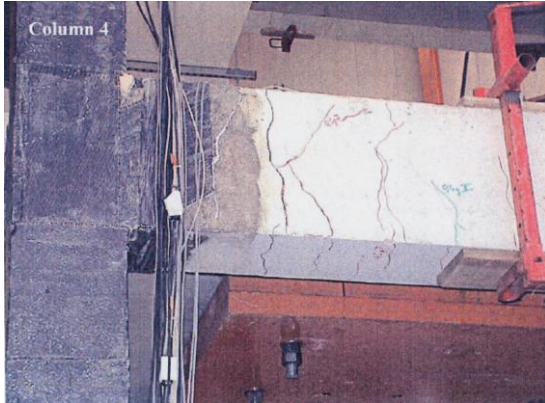reinforcing steel at beams and columns.

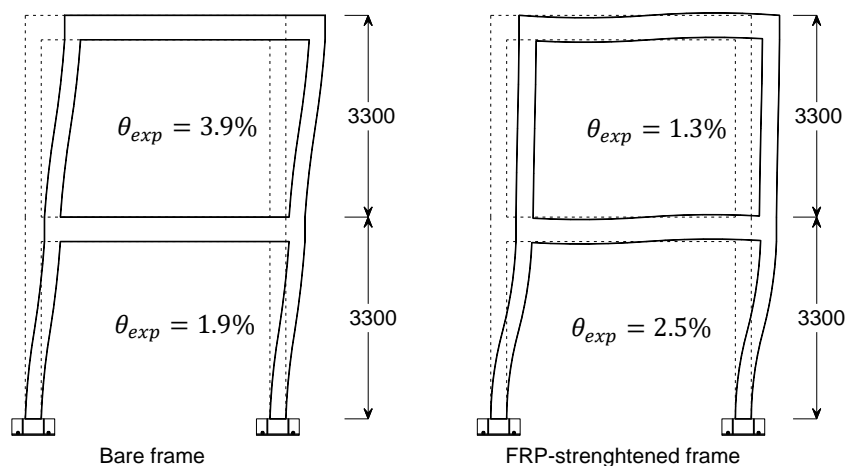Figure 5. Damage at beam ends after the tests on the retrofitted frame.

Figure 6. Deformed shape for the frame in bare and CFRP-retrofitted conditions at PGA=0.40g.

3 BANDIT PROJECT

3.1 Project overview

The EU-funded BANDIT project examined the effectiveness of a 'dual' retrofitting solution using
CFRPs and Post Tensioned Metal Straps (PTMS) at improving the performance of a previously
damaged full-scale RC building with deficient beam-column joints. As for the building discussed
above, the structure was tested at the CEA/EMSI laboratory facilities (Saclay) in France and
subjected to an intensive experimental programme, including five phases of shaking table tests.
Only test phases 4 and 5 of the project, which focused on assessing the performance of the 'dual'
retrofitting solution combining CFRP and PTMS, are described in the following, whilst the initial
test phases are reported in Garcia et al. (2014). The proposed 'dual' retrofitting solution allowed

a direct comparison of the effectiveness of the two techniques using full-scale shaking table tests
at high PGA levels.

3.2   Geometry of the RC frame, material properties and set-up of tests

The geometry of the full-scale two-storey one-bay building was similar to that of the structure
tested as part of the ECOLEADER project and discussed in Section 2 (see also Garcia et al. 2010).
The building had a regular plan of 4.26×4.26 m and a constant floor height of 3.30 m (Fig. 7a-b).
The columns had a cross section of 260×260 mm (Figure c) and longitudinal column bars of Ø14
mm (Ø is the bar diameter). These column bars were lapped over a length l_b=25Ø=350 mm just
above the 1st floor joints to represent old construction practices, as shown in Figure d.
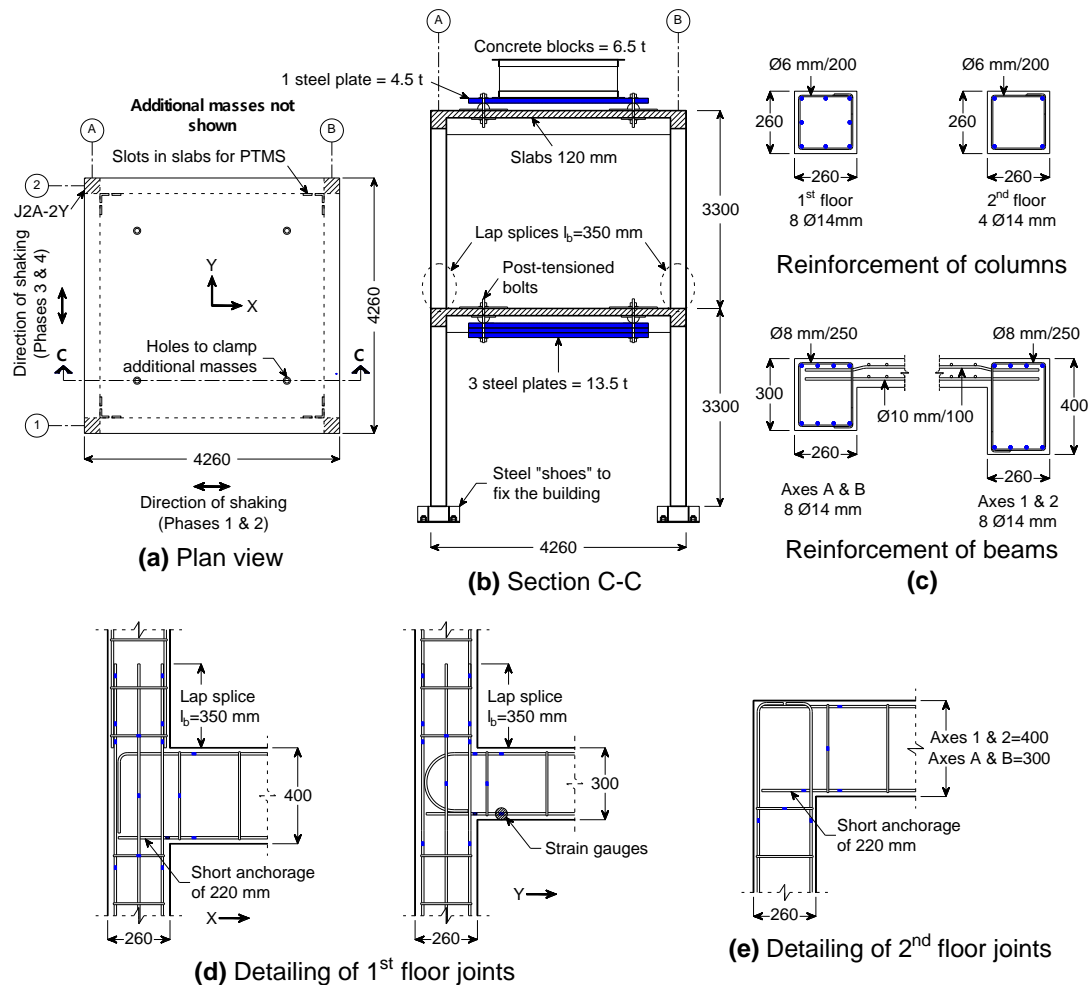

Figure 7. General geometry and reinforcement detailing of BANDIT building (units: mm), partially
adapted from Garcia et al. (2014a)

The beams had a cross section of 260×400 mm in the X direction and 260×300 mm in the Y
direction (see Fig. 7c). The smaller beam depth was selected to increase the flexibility of the
building in the Y direction, thus promoting large interstorey drifts (and therefore damage) in such
direction during the tests at higher PGA levels. The longitudinal beam reinforcement consisted of
Ø14 mm bars. The bottom beam reinforcement was anchored into the joints with no hooks/bends
for a length of 220 mm (approximately 16Ø) to study the effect of deficient bar anchorage, as
shown in 7d. This short anchorage length would be considered insufficient to develop the full
capacity of the Ø14 mm bars according to Eurocode 2 (CEN 2004a). The top beam reinforcement
of the 1st floor joints was anchored using 90° bends and U-shaped hooks, which provided adequate

2nd International Workshop on Advanced Materials and
Innovative Systems in Structural Engineering:
Novel Researches

ISTANBUL
fib IWAMISSE
Turkey 2019

anchorage according to Eurocode 2 requirements. The top and bottom beam reinforcement was anchored into the 2nd floor joints for 220 mm in both X and Y directions, as shown in Figure 7e. It should be mentioned that the beam reinforcement at the 2nd floor joints were welded to the longitudinal column reinforcement to repair the building after the initial damage. The column-to-beam relative flexural strength ratio ($\Sigma MR_{col}/\Sigma MR_{beam}$) in the bare condition did not satisfy the strong column-weak beam strength philosophy recommended in current seismic design codes. To prevent shear failures outside the joints, the columns were reinforced with Ø6 mm stirrups spaced at 200 mm centres, whereas the beams were reinforced with Ø8 mm stirrups spaced at 250 mm centres. The stirrups were closed with 90° hooks instead of 135° hooks typically required by current seismic codes. As no confining stirrups were provided in the beam-column joint cores and, significant damage was expected in these components. The top and bottom of the 120 mm thick slabs were reinforced with 10 mm bars spaced at 100 mm centres in both directions.

The building was cast using two batches of ready-mixed normal-strength concrete, one for each floor. Each floor was cured for seven days in the formwork and then kept under standard laboratory conditions. The mean properties of the concrete compressive strength (f_{cm}) and elastic modulus of each batch were determined from tests on nine concrete cylinders and found to be 30.7 MPa and 24.300 GPa, respectively for the 1st floor and 24.6 MPa and 21.2 GPa, respectively for the 2nd floor. Although the resulting concrete stenghts are higher than often encountered in existing substandard RC buildings ($f_{cm}<20$ MPa), the strength of the concrete used in this study is representative of typical constructions built during the 1970-80s in the Middle-East, Latin America and Mediterranean regions. Due to difficulties in finding low-strength plain bars, the building was reinforced using ribbed bars grade S500 complying with NF A 35-016-1 (AFNOR 2007). Commercially available high-strength (f_u=1100 MPA) metal straps with nominal cross section 0.8×25 mm and zinc corrosion-resistant surface coating were used for the PTMS retrofitting. The bidirectional (0°-90°) CFRP sheets used for the retrofitting had 70% of the fibres oriented in the main longitudinal direction of the sheets. According to the manufacturer's data, the CFRP had a tensile strength f_{FRP}=1350MPa and a modulus of elasticity E_{FRP}=105GPa, and layer thickness of 0.48 mm.

The dual retrofitting intervention aimed to provide a strong column-weak beam mechanism by preventing the premature failure of the joints and by enhancing the flexural capacity of the columns, thus complying with current seismic design philosophy. Fig. 8 shows a general view of the retrofitted building. Fig. 8a shows that the PTMS was installed so as to create a confining 'mesh' around the beam-column joints. The layout of CFRP sheets was similar to that used to retrofit the ECOLEADER building presented above (see also Garcia et al. 2010, Garcia et al. 2014).
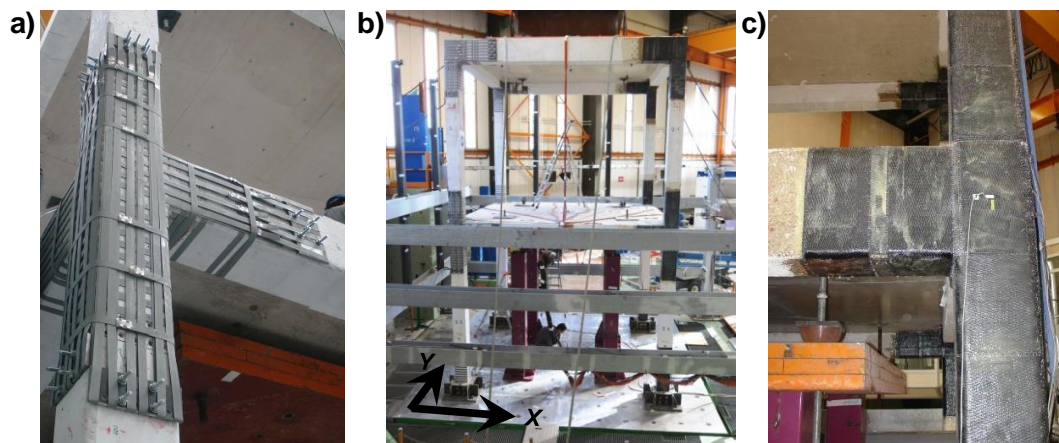

Figure 8. View of the building after the CFRP/PTMS retrofitting: (a) PTMS-retrofitted joint; (b) general view on shaking table, and (c) CFRP-retrofitted joint

The full testing programme is reported in Garcia et al. (2015) and consisted of 30 shaking table tests conducted in five phases. The building was tested up to a PGA=0.35g during the first three phases of testing, which examined the seismic performance of the substandard RC structure and the effectiveness of the PTMS retrofitting technique. The performance of the two retrofitting solutions using CFRP and PTMS was compared in testing phase 4, during which the building was subjected to input records in the direction parallel to frames A and B in Figure a. Finally, a subsequent testing phase (Phase 5) allowed to investigate the behaviour of the retrofitted building under severe 3D shaking.

Only the results from Phase 4 are described below to highlight the potential of the examined retrofitting solutions. The full set of results from all phases of testing is discussed in Garcia et al. (2015).

3.3   Test results and discussion

The seismic excitation applied to the building after the repairs and dual CFRP/PTMS retrofitting (Phase 4) ranged from PGA 0.05g to 0.35g. In general, as the CFRP sheets and metal straps covered the concrete surfaces, damage at the joints could not be observed during the tests. However, popping and metallic sounds during tests (especially after the test at PGA=0.20g) indicated that the CFRP and metal straps were effectively carrying considerable tension forces. After the tests were halted, a visual inspection revealed that no apparent damage was caused on the straps or on the CFRP sheets. Overall, the metal straps maintained most of the post-tensioning force, with the exception of some longitudinal straps placed along the columns of the 1st floor joints. Some cracking was also evident at the beam-column joints, but only on frame B where the PTMS retrofitting was applied. The damage observed in the building in Phase 4 indicated that the repairs and CFRP/PTMS retrofitting intervention prevented the premature shear failure of the deficient joints.

The analysis of the global lateral stiffness of the structure (K) during testing Phase 4, which was estimated based on the implementation of an equivalent SDOF model, shows that the repairs and retrofitting restored the stiffness of the building from K=1430 kN/m (end of Phase 3) to 2510 kN/m (beginning of Phase 4), i.e. an enhancement of 75% (Figure). At the end of Phase 4 (PGA=0.35g), damage accumulation degraded the stiffness of the original bare building by 77% (from 6600 kN/m at the beginning of Phase 1 to 1500 kN/m). Despite this severe stiffness reduction, the limited structural damage observed after Phase 4 indicated that the building was capable of sustaining seismic shaking at higher intensities. Further tests confirmed that the stability of the building was never compromised even during the shake table tests at PGA=0.60g. However, at such high levels of PGA shaking, some push type seals started to shear off. Despite of this, the metal straps maintained 70-80% of their initial post-tensioning force, thus confirming the reliability of the PTMS technique at high seismic excitation levels.
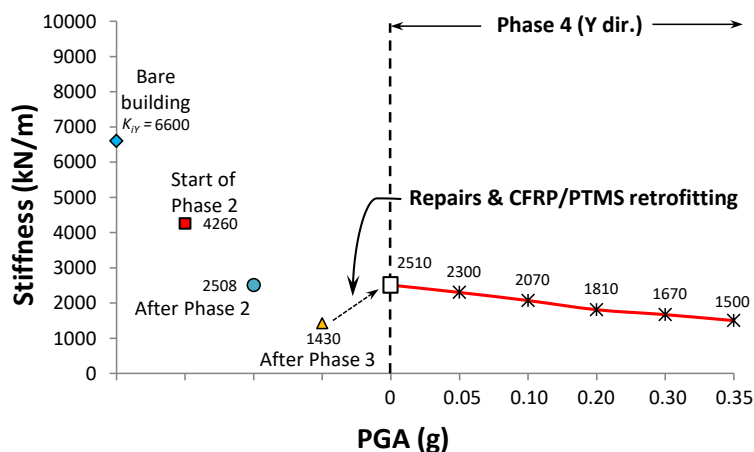

Figure 9. Evolution of lateral stiffness during testing Phase 4 (Y direction)

3.4   Performance levels

Existing guidelines for seismic assessment and retrofit of existing buildings such as ASCE/SEI 41-06 (ASCE 2007) establish limits on acceptable values of maximum interstorey drift ratios, implying that exceeding these limits is a violation of a performance objective. According to ASCE/SEI 41-06, maximum transient drift ratios of δ=1.0%, 2.0% and 4.0% correspond to Immediate Occupancy (IO), Life Safety (LS), and Collapse Prevention (CP) performance levels, respectively.

Fig. 10 compares the maximum interstorey drift ratios of the 1st and 2nd floor of the CFRP and PTMS-retrofitted frames. The figure includes the results from two equidistant displacement transducers fixed on each exterior face of the slabs, labelled as "CFRP" and "PTMS" according to the retrofitting technique used on each frame. It is shown that the 1st and 2nd floors of the retrofitted building had similar δ_s at all PGA levels. This implies that both CFRP/PTMS retrofitting solutions led to a more uniform damage distribution over the building height, which allowed a better exploitation of the available members' capacity. The building remained safely within the CP performance level during the last test at PGA=0.35g (δ=2.92%). Overall, maximum drift values of the "PTMS" frame were only 2-6% larger than those of the "CFRP" frame, thus indicating that some negligible in-plane torsion occurred during the tests.
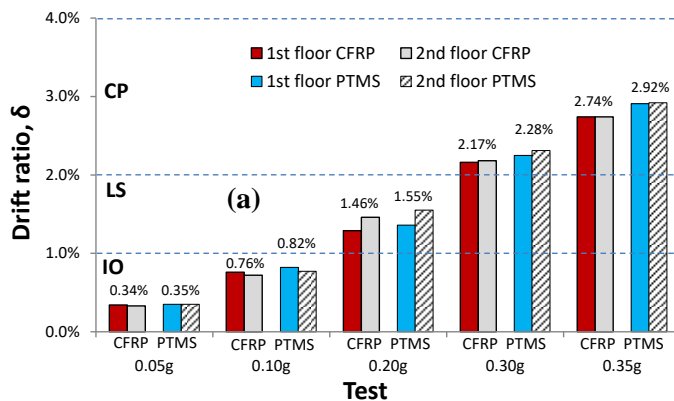

Figure 10. Interstorey drift ratio of 1st and 2nd floors during Phase 4 (Y dir.)

4   CONCLUSIONS

The two projects discussed in this paper investigated experimentally the effectiveness of externally bonded CFRPs at improving the behaviour of seismically deficient full-scale two-storey RC frames. A novel cost-effective retrofitting system using post tensioned metal straps was also tested in the BANDIT building and its performance compared to that of CFRP. From the experimental results, the following conclusions are drawn:

1. The results of the shaking table tests demonstrated that the adopted local retrofitting strategy using CFRP materials was effective at changing the plastic hinge mechanism from column-sway to beam-sway, which is in line with modern seismic design philosophy. The epoxy-injection of cracks and the adopted retrofitting strategy were also effective at restoring the lateral stiffness and the initial dynamic characteristics of the RC frames.

2. The proposed CFRP and dual CFRP/PTMS retrofitting intervention also led to a more uniform damage distribution and, therefore, to a better exploitation of the available capacity in the structure.

3. In comparison to the original bare building, the retrofitting intervention enhanced the interstorey drift ratio capacity of the 1st and 2nd floors. Both of the examined buildings

remained safely within the Collapse Prevention performance level and without evidence of potential collapse.

4. Although some push type seals sheared off during the tests at high PGA levels, the metal straps used in the BANDIT building maintained 70-80% of their initial post-tensioning force, thus confirming the reliability of the PTMS technique at high seismic excitation levels. Comparatively, the CFRP sheets sustained only local minor debonding. The adopted retrofitting solution also led to a strong column-weak beam behaviour and yielding of the beams at the 1st floor, which is in line with current seismic design philosophy.

REFERENCES

Balsamo A, Colombo A, Manfredi G, Negro P, Prota A. Seismic behavior of a full-scale RC frame repaired using CFRP laminates. Eng Struct 2005; 27(5): 769-80.

Balsamo A, Manfredi G, E M, Negro P, Prota A. Seismic rehabilitation of a full-scale structure using GFRP laminates. ACI Struct J, SP230-75. 2005: 1325-44.

CEN (2004) EN 1998-1:2004 Eurocode 8 - Design of structures for earthquake resistance Part 1: General rules, seismic actions and rules for buildings. Comité Européen de Normalisation, Lausanne

Chaudat T, Garnier C, Cvejic S, Poupin S, Le Corre M, Mahe M. ECOLEADER Project No. 2: Seismic tests on a reinforced concrete bare frame with FRP retrofitting - Tests Report. SEMT/EMSI/RT/05-006/A, CEA, Saclay, France; 2005.

Della Corte G, Barecchia E, Mazzolani FM. Seismic upgrading of RC buildings by FRP: full-scale tests of a real structure. J Mater Civ Eng 2006; 18(5): 659-69.

Di Ludovico M, Prota A, Manfredi G, Cosenza E. Seismic strengthening of an under-designed RC structure with FRP. Earthq Eng Struct Dyn 2008; 37(1): 141-62.

Garcia R, Hajirasouliha I, Guadagnini M, Helal Y, Jemaa Y, Pilakoutas K, Mongabure P, Chrysostomou C, Kyriakides N, Ilki A, Budescu M, Taranu N, Ciupala MA, Torres L, Saiidi M (2014) Full-scale shaking table tests on a substandard RC building repaired and strengthened with Post-Tensioned Metal Straps. J Earthq Eng 18 (2):187-213. doi:10.1080/13632469.2013.847874

Garcia R, Hajirasouliha I, Pilakoutas K (2010) Seismic behaviour of deficient RC frames strengthened with CFRP composites. Eng Struct 32 (10):3075-3085. doi:10.1016/j.engstruct.2010.05.026

Garcia, R., Pilakoutas, K., Hajirasouliha, I., Guadagnini, M., Kyriakides, N., & Ciupala, M. A. (2015). Seismic Retrofitting of RC Buildings Using CFRP and Post-Tensioned Metal Straps: Shake Table Tests. Bull Earthq Eng, 15(8), 3321-3347.

Gdoutos EE, Pilakoutas K, Rodopoulos CA. Failure analysis of industrial composite materials. 1st ed. New York: McGraw-Hill; 2000.

Jeong SH, Elnashai AS. Analytical assessment of an irregular RC full scale 3D test structure. Mid-America Earthquake Center, Dept. of Civil and Environmental Engineering, University of Illinois at Urbana-Champaign, Urbana, Illinois, USA; 2004, p. 146.

Kosmopoulos AJ, Fardis MN. Estimation of inelastic seismic deformations in asymmetric multistorey RC buildings. Earthq Eng Struct Dyn 2007; 36(9): 1209-34.

Pendhari SS, Kant T, Desai YM. Application of polymer composites in civil construction: a general review. Comp Struct 2008; 84(2): 114-24.

Pinto AV, Verzeletti G, Molina J, Varum H, Pinho R, Coelho E. Pseudodynamic tests on non-seismic resisting RC frames (bare and selective retrofit frames). Report EUR 20244, JRC-IPSC, Ispra, Italy; 2002.

2nd International Workshop on Advanced Materials and
Innovative Systems in Structural Engineering:
Novel Researches

ISTANBUL
fib IWAMISSE
Turkey
2019

Seismic vulnerability assessment of substandard RC buildings

Soheil Khoshkholghi[1], Dan Ciucu[2], Zuhal Ozdemir[3], Ilya Sianko[4], Iman Hajirasouliha[5], and Kypros Pilakoutas[6]

[1,3,4,5,6] The University of Sheffield, Sheffield, United Kingdom
[2] Imperial College London, London, United Kingdom

ABSTRACT: Extensive losses and mortality rates observed during recent major earthquakes in developing countries (1999 Kocaeli, 1999 Duzce, 2003 Bam, 2004 Sumatra Indonesia, 2005 Kashmir, 2011 Van, 2015 Nepal, 2017 Iran/Iraq and 2018 Sulawesi Indonesia) highlight the high seismic vulnerability of existing RC buildings. This work will investigate the effect of common deficiencies in substandard RC structures on vulnerability/fragility curves by considering the effect of different brittle failure modes analytically. Initially, the results of shaking table tests on a full-scale two-storey RC frame with poor detailing in the beam-column joints are used for validation of the analytical model. Then, a case study building in Marmara region, Turkey, which represents the characteristics of the Turkish building stock, is selected. Finally, a realistic 3D finite element model of the building is developed to investigate the parameters affecting vulnerability of the structure. In future, this model will be used to derive novel advanced vulnerability curves accounting for key parameters of different class of buildings. The developed methodology will be incorporated in a comprehensive framework on the Earthquake Risk Assessment (ERA) specifically developed for areas, where generally limited information related to seismic risk parameters exist.

1   INTRODUCTION

The impact of earthquakes on the economy and social welfare of developing countries is often more devastating and longer lasting than in developed countries. As an example, the 2010 Haiti earthquake (M_w= 7.0) caused more than 220,000 deaths and 300,000 injuries, while almost 300,000 houses were destroyed and damaged by the earthquake leaving in total 1.3 million people homeless (Eberhard et al., 2010). The total damages of this tragedy have reached an estimated total of $7.8 billion (65% of Haiti's GDP). The much bigger 2011 Tohoku (M_w= 9) earthquake and tsunami in Japan resulted only in 15,500 death and economical loss was $130 billion (2% of Japan's GDP). Another example is, the 1999 Kocaeli earthquake (M_w= 7.4) which caused more than 17,000 death and around $20 billion financial loss (approximately 10% of Turkey's GDP) (Erdik et al., 2012) . On the other hand, the estimated death toll and economic losses due to the 1995 Kobe (M_w= 6.9) earthquake was 5,500 death and $130 billion (2% of Japan's GDP) (Leng, 2015).

The primary action of earthquakes, ground shaking, does not cause loss of life. It is the vulnerability of the built environment and lack of resilience of the society that turn earthquakes into catastrophes. The majority of the existing buildings in developing countries is either pre-code, or has not been designed and/or constructed according to seismic codes. As a result, deficient lateral load resistance systems, insufficient energy dissipation capacity, and rapid strength degradation during reversal load make substandard structures highly vulnerable to

seismic actions. Images of deficiencies related to substandard RC buildings are presented in Figure 1.

Figure 1. Common deficiencies of substandard RC buildings a) improper hooking and usage of plain bars, b) pull out failure and c) low concrete quality.

High vulnerabilities may be attributed to poor quality of construction and materials as well as poor detailing in critical locations, such as columns and beam-column joints, which can lead to brittle failure. Current vulnerability curves are in general empirically derived and do not capture specific deficiencies. Analytical vulnerability curves underestimate damage from common brittle modes of failure since they mostly consider flexural failure modes during modelling.

Analytical vulnerability analysis methods can overcome some of the issues associated with empirical and judgement based approaches. Analytical methods are based on the analysis of a large number of buildings created by changing their selected structural parameters statistically, through increasing seismic demand levels using appropriate simplified (Calvi, 1999, and Demartinos and Dritsos 2006) or refined analytical or numerical methods (Rossetto and Elnashai, 2005 and Kappos et al., 2008).

In case of substandard RC buildings, analytical methods theoretically could address the common deficiencies (shear, local buckling, slip-bond failure, beam-column joint failure etc.) found in such structures to represent their damage potential. However, most existing analytical vulnerability curves ignore brittle failure modes and the natural variability in materials and geometrical characteristics. Therefore, there is an urgent need to develop more realistic analytical vulnerability curves for substandard buildings and update existing risk assessment frameworks in order to achieve more accurate damage estimations.

This paper presents the analytical tool selected for this study (OpenSees) for the development of vulnerability curves and its ability to capture the behaviour of deficient beam column joints by considering steel-concrete bond-slip and bond-strength degradation. The results of shaking table tests on a full-scale two-storey RC frame with poor detailing in the beam-column joints are used for validation of the analytical model. Then, the RC building data collected from different areas of the Marmara region, Turkey is grouped into sub-classes according to their ductility and strength characteristics. Finally, a case study building, which represents the typical geometrical, functional and material characteristic of Turkish building stock, is selected to develop vulnerability curves. This work formed part of a bigger research effort. The develop vulnerability curves will be integrated in a comprehensive earthquake risk assessment and management framework for developing countries, where little or no information is available related to seismic risk parameters.

2   APPROACHES FOR SEISMIC VULNERABILITY ASSESSMENT OF BUILDINGS

Seismic vulnerability is defined as the probability of earthquake loses at a specific ground motion intensity level. Seismic vulnerability of structures is, in general, presented in the form of the variation of mean damage ratio (e.g. the ratio of cost of damage to cost of replacement) with the

level of ground motion intensity (such as macroseismic intensity, peak ground acceleration, spectral acceleration and spectral displacement for 5% damping, or inelastic spectral displacement for a displacement based damping values). Uncertainties in construction materials, structural geometries, damage indicators and ground motion parameters leads to variations in damage states of structures at a specific ground motion level, which can be represented with a lognormal mean and standard deviation values. Based on these mean and standard deviation values, a lognormal cumulative distribution functions can be formed to represent fragility of structures. Therefore, fragility curves define the probability of exceedance of a certain degree of earthquake performance limit state for a specified building type due to a given ground motion level.

There are three main approaches for seismic vulnerability/fragility assessment of structures: 1) empirical, 2) expert opinion and 3) analytical. Hybrid methods also exist by combining two of these methods aiming to benefit from their advantages while reducing their drawbacks.

2.1   Empirical Vulnerability Assessment

Empirical vulnerability curves are developed by performing statistical evaluation of data collected during post-earthquake damage surveys. Therefore, they can account not only the strong ground motion but also, the earthquake source, path, site, exposure, structural and non-structural components (Rossetto et al., 2014). Damage Probability Matrices (DPM) and continuous vulnerability functions are two main empirical vulnerability assessment methods. The reliability of the empirical vulnerability curves directly depends on quality and completeness of the database, and is usually related to the data collection method. If the data is based on only the damage recorded after a single earthquake then, the ground motion intensity values in the database may be limited. In addition, it is highlighted in the literature, that there is a large variation in the empirical fragility assessment procedures, which result from differences in the damage observation databases used, functional forms chosen to fit to the data, the selected ground motion intensity measure, and the statistical modelling technique used (Rossetto et al., 2013).

2.2   Vulnerability Assessment based on Expert Judgment

Because of the limitations on past earthquake damage data for various building types and cost of analytical vulnerability assessment methods, expert judgment can be used to evaluate the vulnerability of structures. This technique has no real scientific basis and has a lot of limitations in its use. The experience level of each expert can affect the reliability of the outcome. If the panel has experience of a particular set of structures, then their predictions cannot be applied to a different set of structures.

2.3   Analytical Vulnerability Techniques

The three main approaches for deriving analytical fragility curves are: (1) Correlation between damage index and damage states, (2) Correlation between capacity curves (for buildings) and spectral response curves (capacity spectrum method), and (3) Correlation between capacity curves (for buildings) and acceleration time histories.

The first approach was popular in the past decade. The damage indices can be either global (structural level), local (element level) or combination of both (Rossetto et al., 2014). The most commonly used local damage index (Park and Ang, 1985) is defined by linearly combining dissipated energy of an element with the maximum displacement. The robustness of the fragility curves derived using damage indices are closely related to damage model/damage index and the level of complexity of the structural model, the type of analysis, and the damage indicator to which the damage level is correlated (Rossetto et al., 2014). The second approach, the capacity spectrum approach is based on running a pushover nonlinear static analysis for a given structure, producing a pushover curve (base shear versus roof displacement) which describes the global behaviour of certain structure when subjected to combination of gravity loads and monotonically increasing lateral forces, to statically represent the seismic action. Usually pushover curves are idealized to be a series of linear branches of constant stiffness and expressed in the pseudo-

acceleration/displacement spectral space (capacity curves). The capacity curve is then intersected with a spectral demand curve in order to determine the performance point. A performance point for a structure can be calculated for different intensity levels, from which fragility curves can be constructed. This method is favoured by many seismic codes and researchers (Fajfar, 2000 and FEMA-356) due to the simplicity and prompt of application specially for large population of structures. The third approach is adopted in the simplified version of incremental dynamic analysis proposed by Vamvatsikos and Cornell (2002) and Rossetto and Elnashai (2005). Both procedures allow the performance and, hence, damage of a structure to be calculated for a set of record.

The accuracy of the fragility curves derived by analytical approaches depends on both the level of detailing considered in the modelling procedure and the type of analysis (IDA or Pushover, etc.) used for deriving fragility curves. To derive vulnerability curves for a specific class of building in the probabilistic way it is necessary to perform many analyses. Moreover, various types of analysis have different time and detailing demands. Therefore, one of the main steps during analytical fragility analysis is, to define a relatively simple but accurate modelling procedure that can be done quickly.

2.4 Hybrid methods

This method is a combination of post-earthquake damage statistics and analytical damage statistics from a mathematical model. Various types of uncertainties exist in the vulnerability curves derived from the above mentioned techniques due to limited post-earthquake damage data, judgemental data subjectivity and modelling issues in analytical vulnerability. In order to reduce these uncertainties in curves, hybrid vulnerability curves have been derived by researchers (Kappos et al., 1998) which use data from various sources. The benefit of this method is the freedom provided by testing any building type for which data are needed. The limitations are due to scale of model, loading type and laboratory equipment capacity.

3 VERIFICATION OF THE ANALYTICAL TOOL USED FOR THE VULNERABILITY ANALYSIS OF BUILDINGS

In this work, OpenSees (Mazzoni et al., 2009) Finite Element software is selected for performing the vulnerability analysis of the case study building due to the fact that the software has the necessary elements to represent substandard detailing. Before deriving the vulnerability curves, an existing experimental programme is used to verify to analytical tool.

3.1 The experimental program

A full scale two-storey RC structure, which was designed according to the old version of European earthquake-resistant provisions from the 60's, is used to verify the numerical models. It is expected that significant damage will develop in columns and joints of the structure.

The tested structure is a symmetric two-storey one-bay RC frame, which has a dimension of 4.26 x 4.26 m in plan and 3.3 m of storey height at both levels (Garcia et al., 2010). All column sizes are 260 mm by 260 mm and all beam sizes are 260 mm by 400 mm. The main reinforcement for the columns consist of 8 vertical bars of 14 mm in diameter at the first floor and 4 vertical bars of 14 mm in diameter at the second floor. The main reinforcement for the beams consist of 8 vertical bars of 14 mm in diameter. 6 mm transverse reinforcement with 200 mm spacing was used in columns and 8 mm transverse reinforcement with 300 mm spacing was used in beams. The average material properties obtained based on material tests are as follow: Yield and ultimate strength of steel reinforcement were f_y=551 MPa and f_u=656 MPa, and concrete compressive strength and modulus of elasticity were f_c =20 MPa and E_c=25,545 MPa, respectively. An additional mass of 9.0 ton was attached to each floor to simulate real loading conditions.

External displacement transducers and accelerometers at each storey were used during the shaking table test to monitor the response history. The displacement transducers were attached to an external rigid frame to facilitate the measurements and quantify the residual displacements after each test. ing peak ground accelerations (PGA) levels ranging from 0.05g to 0.4g. A single artificial ground motion record, that matches the Eurocode 8 (2005) soil profile type C spectrum was used in the tests.

3.2   Analytical modelling

The 3D model of the frame was developed using OpenSees software. Beams and columns are modelled using the "Nonlinear Beam Column Element", which considers the spread of plasticity along the element and the integration along the element is based on Gauss-Lobatto quadrature rule (two integration points at the element ends). The mass of the system was assigned to elements as mass density (per unit length). The additional mass for the steel plates on each floor was considered by putting 25% of the plate's mass (2.25 tons) as a distributed mass along each beam. For assigning the sections to the elements first material properties for concrete and steel needed to be defined.

Concrete02 concrete model of OpenSees was used for modelling concrete. For modelling steel rebar, reinforcing Steel Material model of OpenSees was employed used with the integrated buckling model based on Gomes and Appleton (1997). Figure 2 shows the stress-strain curves for both concrete and steel employed in the analytical model. Three different configuration of sections for columns of 1st, 2nd floor and beams are assembled using fiber section. Once it is done, the sections are assigned to the elements and the full 3D frame assembled with the boundary condition of totally fixing all degrees of freedom for nodes at the basement.

After creating the model, gravity and modal analysis was performed to check the loading and the initial period of the frame, respectively. Moreover, to make sure that the loads are transferring correctly from the local axis to the global axis after applying the gravity loads, reaction forces were checked at the base nodes and fund to be correct. The period for the first mode was estimated as 0.52 sec while, from the experiment it was 0.53 sec. After performing modal analysis, time history analyses (THA) are carried out for a series of shaking table displacement histories as shown in Figure 3 recorded during experiment. These displacement records were imposed simultaneously to all four nodes at the basement level using Multiple Support Pattern in OpenSees. THA was performed for the developed model with five different input record which the PGA levels are 0.05g, 0.1g, 0.2g, 0.3g and 0.4g one after each other while the damage was accumulated after each analysis.
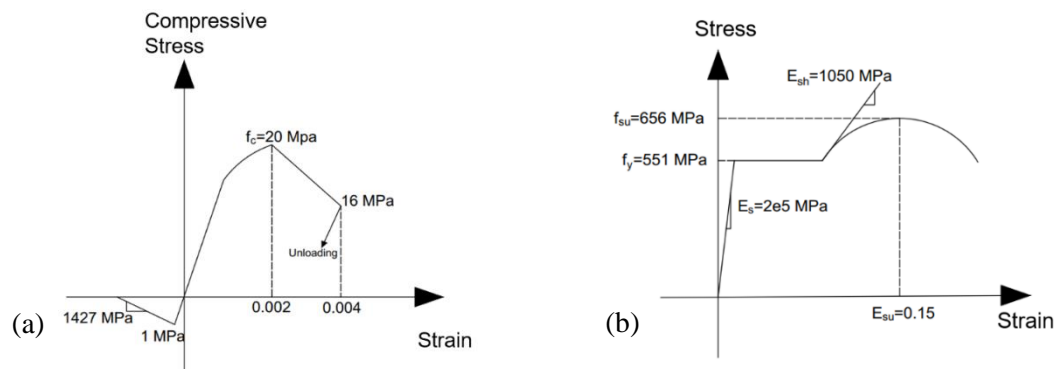

Figure 2. Stress-strain curve for (a) concrete and (b) reinforcing steel.

For monitoring the structural behaviour displacement at each level plus strains in the reinforcement at different sections according to the instrumentation of experiment recorded and compared with experimental results. The strain-gage readings of column 3, just 13cm below the

1st floor's joint (see Figure 4), and the first floor's displacement histories from both analysis and experiment for 0.05g and 0.3g are compared.
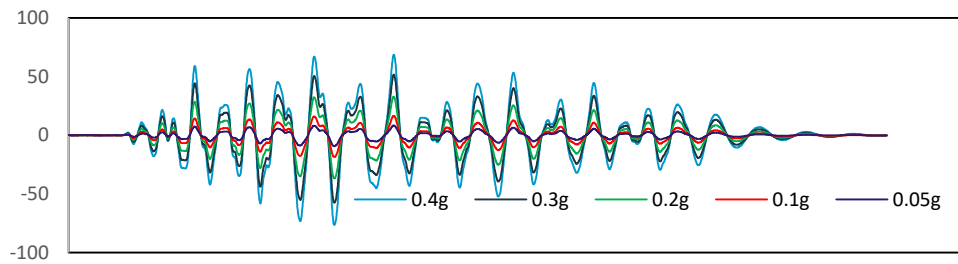

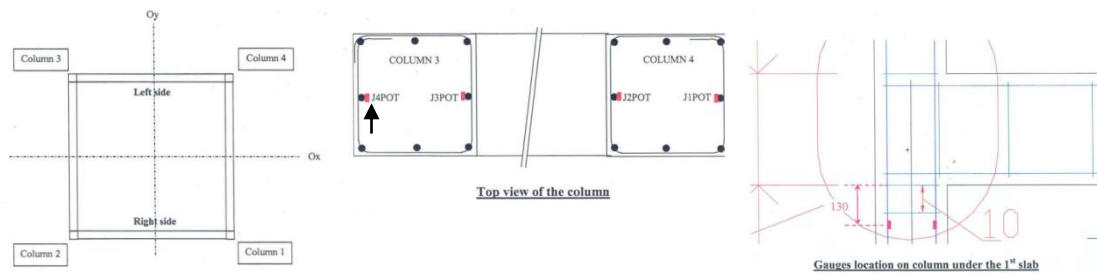Figure 3. Input shaking table displacement (mm) histories.

Figure 4. The strain-gage location used for comparison with analysis results.

One of the challenges with the modelling of this substandard RC frame was to introduce the bar slippage deficiency due to inadequate bond anchorage. Although, there are various ways to model bar slip, recent studies proposed using a zero length element where bond is inadequate by defining the bond stress versus bond slip behaviour between steel reinforcements and surrounding concrete (Zhao and Sritharan, 2007). In the analytical model the Zero Length Section element command was used with the same cross section. However, the bond stress and slip deformation was calculated according to Braga et al. (2012) and assigned to the section using Hysteretic Uniaxial material command. The assigned bond slip versus bar slip deformation is presented in Figure 5. Zero length elements are used at column-joint connections. Connection of the columns to the foundation did not have bar slip because, the reinforcements were all welded to the foundation.

After introducing the bar-slip behaviour to the model, the displacement history of both storeys and strain-gage readings showed good agreement with the experiment. The 1st floor's displacements and strain-gage readings for 0.05g and 0.3g are presented in Figure 6. It can be concluded from performing this modelling exercise, that the OpenSees software is suitable for purposes of modelling substandard RC buildings.

Figure 5. (a) Bond stress versus slip displacement model and (b) locations of zero length section elements.
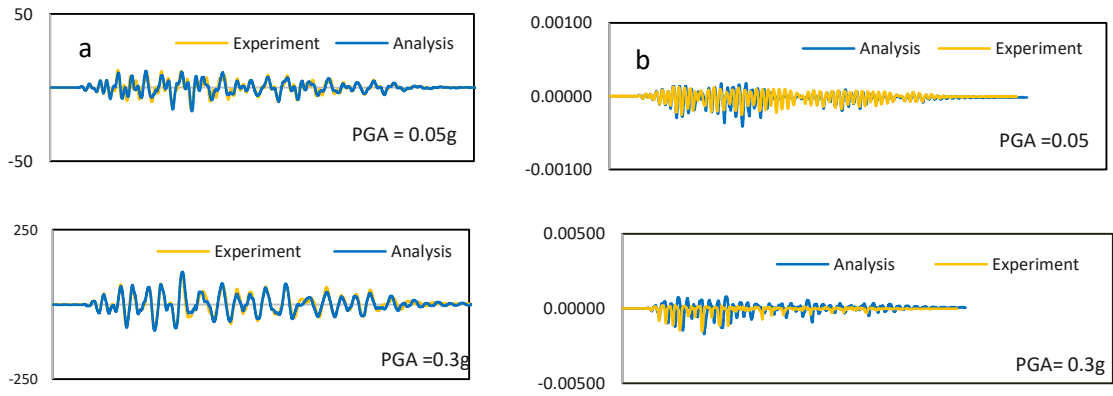
Figure 6. (a) 1st floor displacement (mm) histories and (b) strain readings after addressing the bond slip behaviour into model.

4   VULNERABILITY ANALYSIS OF THE CASE STUDY BUILDING

To develop vulnerability curves for the typical substandard Turkish buildings, data regarding geometrical, functional and material properties of RC buildings were collected from different areas of the Marmara region. Then, these buildings are grouped into sub-classes according to their ductility and strength characteristics. A case study building, which falls into one of these categories, is selected to develop vulnerability curves.

4.1   The case study structure

The selected structure is located in Izmit, Kocaeli. The structural system of the building is a reinforced concrete frame with concrete slabs and rest on a mat foundation. The building was constructed in 1975. It has three storeys and a total height of 9 m. Typical floor plan, façade and cross-sections of the building along shorter and longer directions are shown in Figure 7.
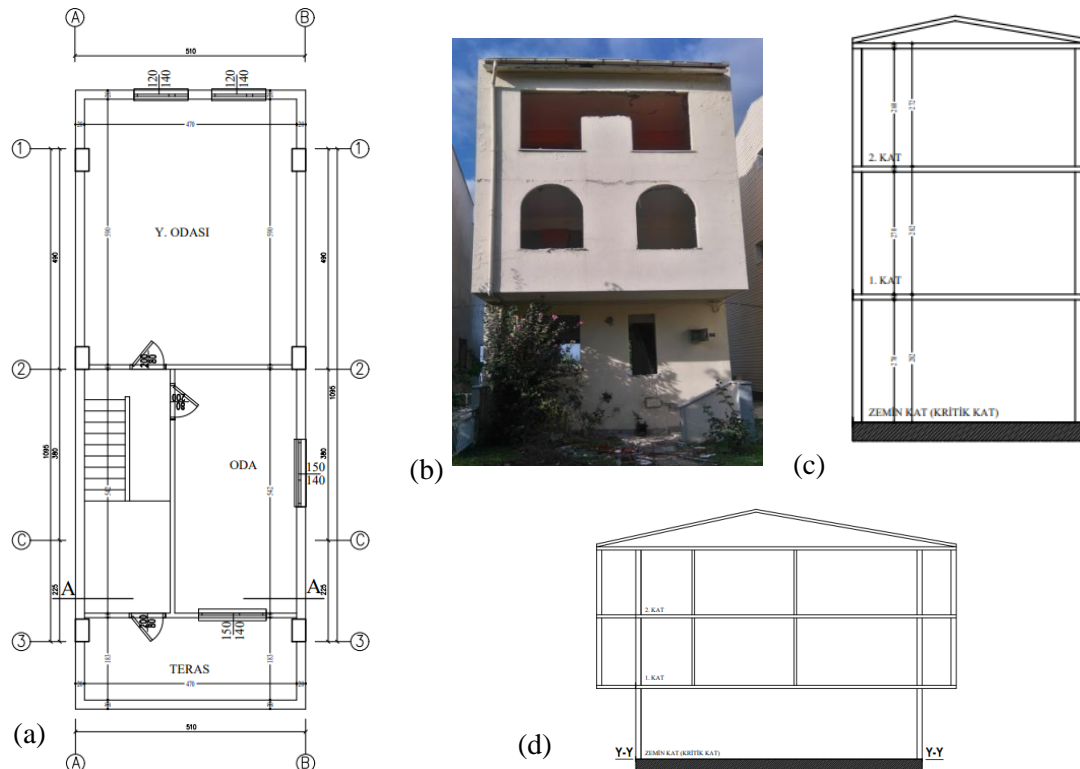

Figure 7. (a) Typical floor plan, (b) facade, (c) cross-section along the shorter direction, and (d) cross-section along the longer direction of the case study building.

The plan length of the building in the shorter direction is 5.1m along the height of the structure. The plan length in the longer direction is 10.95 and 13.95 m at the ground floor and at the 2nd and 3rd floors, respectively. All column sizes are 300 mm by 500 mm and all beam sizes are 250 mm by 500 mm. The thickness of cover concrete is 30 mm in both columns and beams. The main reinforcement for the columns consist of 6 vertical bars of 14 mm in diameter. Floor heights at all levels are 3 m. Slab thickness is 0.12 m. 14 mm transverse reinforcement with 200 mm spacing was used in columns and beams. The total mass of the building is calculated as 180.353 tones.

A series of material tests were performed on the building to determine concrete strength, steel grade, number, diameter and spacing of reinforcement bars. The mean concrete strength was obtained as 13.1 MPa by testing the cylindrical specimens taken from the structure. In the analytical model, Chang and Mander (1994) concrete model is employed for the confined concrete. Experimental data collected by researchers of Istanbul Technical University, Turkey, is used to developed a material model parameters for steel reinforcement. Stress-strain curves for concrete and reinforcing steel are shown in Figure 8a and 8b, respectively. An Eigen value analysis is performed for the building. The fundamental period of the building is obtained as 0.751 sec in x direction. Buckling failure mode is incorporated in steel material model based on the study of Dhakal and Maekawa (2002). Bond-slip model and parameters, which are calculated based on the experimental data collected by Ahmad (2011), are integrated into the analytical model of the case study building as defined in Section 4.2. The assigned bond slip versus bar slip deformation is presented in Figure 8c.
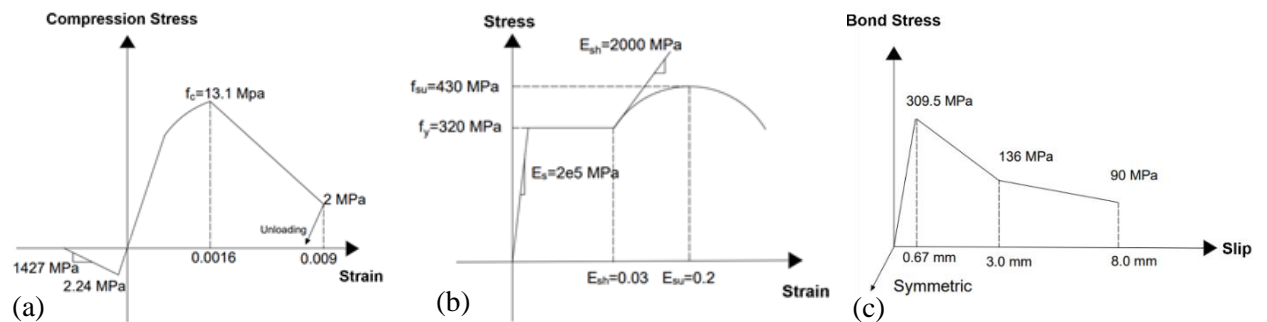

Figure 8. Stress-strain curve for a) concrete and b) reinforcing steel and (c) Bond stress versus slip displacement curve for the case study building

4.2 Elastic design spectra and Pushover Analysis of the building

Two distinguished Turkish seismic design codes are used for the development of vulnerability curves: the code was in effect at the time of the construction of the building and the code is in effect today. According to Turkish Seismic Design codes of 1975 and 2018 (TSDC, 1975 and TSDC, 20018), the structure is assumed to rest on soil class III and ZE, respectively. For the Horizontal elastic design spectra derived based on both codes are shown in Figure 9a.

In order to develop vulnerability curves, pushover analysis is performed for the structure. An inverted triangular lateral load pattern is used to represent the distribution of the inertia forces along the height of the structure. To assess the effect of concrete compressive strength on the vulnerability of the building, the pushover analysis of the structure is repeated for a series concrete compressive stress values (5MPa, 10 MPa, 15 MPa, 20 MPa and 25 MPa). Improved Capacity Spectrum Method of FEMA 440 (2005), is employed to convert the obtained pushover curves to capacity curves. The elastic design spectra are also converted to acceleration-displacement response spectrum (ADRS) format. Figure 9b shows base shear-roof displacement curves obtained from pushover analyses for a series of concrete compressive stress values for the building. Low concrete compressive strength shows very brittle behaviour. The increase in ductility and strength are very remarkable, when concrete compressive strength increases from 5 MPa to 10 MPa. The strength and ductility slightly improve with the increase in concrete compressive strength after 13.1 MPa.
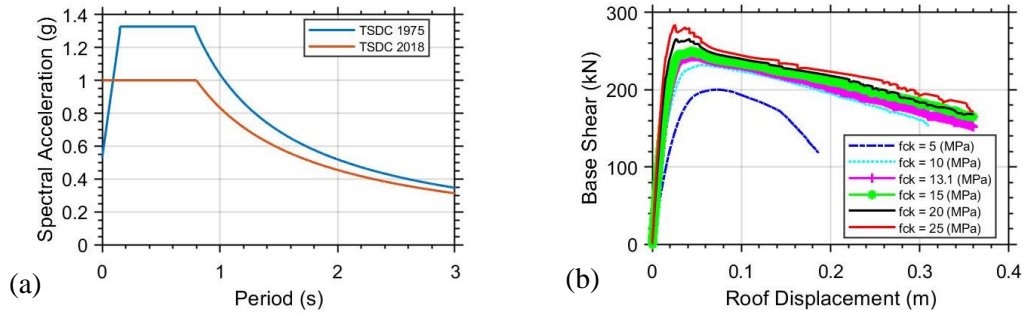
Figure 9. (a) Elastic design spectra of TSDC-1975 and TSDC-2018 and (b) pushover curves for the case study building for different

4.3 Vulnerability curves

Vulnerability curves are pretty sensitive when it comes to which design spectrum is used. Using TSDC-1975, the vulnerability curves developed present for all the classes of the concrete a stronger building, that can take higher PGA values. By using TSDC-2018, the old buildings wont comply with it, hence they will present many deficiencies such as bond-slip, corrosion and poor quality of concrete. Therefore, the new vulnerability curves developed based on the design spectrum TSDC-2018 will present weaker buildings that will fail in early stages.

The procedure proposed by Kyriakides (2007) is employed for the development of the vulnerability curves. In this method, period variation in the structure is used as a global damage index. Every point on the capacity spectrum is treated as a performance point and MADRS method (FEMA 440, 2005) is applied in a reverse way to develop vulnerability curves. Figure 10 shows vulnerability curves developed using TSDC-1975 and TSDC-2018 response spectra assuming different concrete compressive stress values for the building. It can be observed from this figure that very low concrete compressive strength highly affects the vulnerability of the structure. For the concrete compressive strength values larger than 10MPa, vulnerability curves show slight variations. As expected, the structure is more vulnerable when TSDC-2018 response spectra is employed. According to TSDC-2018, PGA is 0.53 g for the site where the case study building was constructed. However, the building reaches 100% damage at around PGA of 0.37 g. Therefore, total collapse of the building is expected for an earthquake with probability of exceedance 10% in 50 years according to new Turkish Seismic Design Code (TSDC-2018).
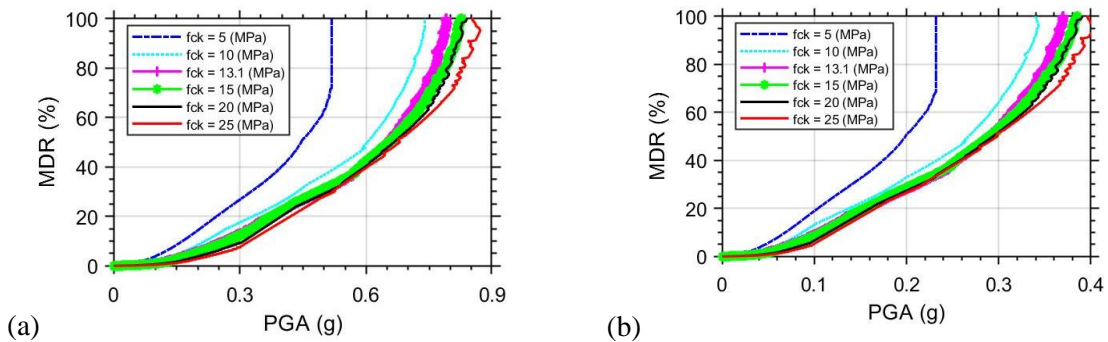

Figure 10. Vulnerability curves developed using (a) TSDC 1975 and (b) TSDC 2018 spectra.

5 CONCLUSIONS

This work focusses on the effect of deficiencies of substandard RC buildings on the vulnerability curves of such structures. First, the results of an existing experimental study carried out on a full-scale two storey RC frame with poor detailing in the beam-column joints are used to validate analytical tool. Both storeys displacements and strain-gage readings taken during the experiments

are predicted well with the numerical model. Then, 3D finite element model of a case study building, which represents the characteristics of the Turkish building stock, is built to derive vulnerability curves of the building using TSDC 1975 and TSDC 2018 response spectra assuming different concrete compressive stress values for the building. Vulnerability analysis results showed that the concrete compressive strength value of less than 10 MPa highly affects the vulnerability of the structure. The vulnerability curves show slight variations for the concrete compressive strength values of larger than 10MPa. According to TSDC 2018, total collapse of the building is expected for an earthquake with probability of exceedance 10% in 50 years.

REFERENCES

Ahmad, S., 2011, Seismic Vulnerability of Non-Ductile Reinforced Concrete Structures in Developing Countries, PhD dissertation, University of Sheffield.

Braga, F., Gigliotti, R, Laterza, M, D'Amato, M, 2012, Modified Steel Bar Model Incorporating Bond-Slip for Seismic Assessment of Concrete Structures, *Journal of Structural Eng*, 138(11): p. 1342-1350.

Calvi, G. M., 1999, A displacement-based approach for vulnerability evaluation of classes of buildings. Journal of Earthquake Engineering, 3(03): 411-438.

Chang, GA, and Mander, JB, 1994, Seismic energy based fatigue damage analysis of bridge columns: Part I –Evaluation of seismic capacity, *NCEER-94-0006*.

Dhakal, RP and Maekawa, K, 2002, Modeling for Postyield Buckling of Reinforcement, *Journal of Structural Engineering*, 128 (9).

Demartinos, K., and Dritsos, S., 2006. First-level pre-earthquake assessment of buildings using fuzzy logic. Earthquake spectra, 22(4): 865-885.

Eberhard, M.O., Baldridge, S., Marshall, J., Mooney, W., and Rix, G. J., 2010. The Mw 7.0 Haiti earthquake of Jan 12, 2010: *USGS/EERI advance reconnaissance team report*. USGS Open-File Report, 1048, 58.

Erdik, M., Kamer, Y., Demircioğlu, M., and Şeşetyan, K., 2012, 23 October 2011 Van (Turkey) earthquake. Natural hazards, 64(1): 651-665.

Eurocode 8, 2005, design of structures for earthquake resistance, ed. Fardis, M.N. Eurocodes. London.

Fajfar, P., 2000, A nonlinear analysis method for performance-based seismic design, *Earthquake spectra*, 16(3): p. 573-592.

FEMA-356, 2000, Commentary for the seismic rehabilitation of buildings. FEMA-356, Federal Emergency Management Agency, Washington, DC.

FEMA-4402005, Improvement of nonlinear static seismic analysis procedures. Washington, DC.

Garcia, R., I. Hajirasouliha, and K. Pilakoutas, 2010, Seismic behaviour of deficient RC frames strengthened with CFRP composites. Engineering Structures, 32(10): p. 3075-3085.

Gomes, A. and J. Appleton, 1997, Nonlinear cyclic stress-strain relationship of reinforcing bars including buckling. Engineering Structures, 19(10): p. 822-82

Kappos, A., K. Stylianidis, and K. Pitilakis, 1998, Development of seismic risk scenarios based on a hybrid method of vulnerability assessment. Natural Hazards, 17(2): p. 177-192.

Kappos, A. J., Panagopoulos, G., and Penelis, G. G., 2008. Dev. of a seismic damage and loss scenario for contemporary and historical buildings in Thessaloniki, Greece. Soil Dyn and Eq Eng, 28: 836-850.

Kyriakides N, Seismic vulnerability assessment of RC structures. 2007, PhD Thesis, UOS, UK.

Leng, R., 2015, Japan's Civil Society from Kobe to Tohoku. Journal of contemporary Japanese studies.

Mazzoni S, M.F., Scott MH, Fenves GL., 2009, *Open System for Earthquake Engineering Simulation User Command-Language Manual*, Pacific Earthquake Engineering Research Center, Berkeley, USA.

Park, Y.-J. and A.H.-S. Ang, 1985, Mechanistic seismic damage model for reinforced concrete. Journal of structural engineering, 111(4): p. 722-739.

Rossetto, T., and Elnashai, A., 2005. A new analytical procedure for the derivation of displacement-based vulnerability curves for populations of RC structures. Engineering structures, 27(3): 397-409.

Rossetto, T., Ioannou, I., & Grant, D. N., 2013, Existing empirical fragility and vulnerability relationships: compendium and guide for selection. GEM Foundation, Pavia.

Rossetto, T., et al., 2014, Evaluation of existing fragility curves, in SYNER-G: Typology definition and fragility functions for physical elements at seismic risk, Springer. p. 47-93.

Vamvatsikos, D. and C.A. Cornell, 2002, Incremental dynamic analysis. Eq Eng & Str Dyn, 31:491-514.

TSDC-1975, Turkish Seismic Design Code, 1975, Ministry of Public Works and Settlement. Specification for structures to be built in disaster areas. Government of Republic of Turkey. 1975.

TSDC-2018, Turkish Seismic Design Code, 2018, Disaster and Emergency Management Presidency, Ankara.

Zhao, J. and Sritharan, S., 2007, Modeling of strain penetration effects in fiber-based analysis of reinforced concrete structures. ACI Structural Journal, 104(2): p. 133-141.

Development of a Framework for Rapid Earthquake Risk Assessment for Substandard Buildings in Turkey

Alper Ilki[1], Ufuk Yazgan[2], Cem Demir[3], Ali Osman Ates[4], Uğur Demir[4], Eren Kupcu[5], Goktug Unal[6], Mehmet Akif Altinok[7], Büsranur Karakaya[7], Furkan Narlitepe[7]

[1] Prof. Dr., Istanbul Technical University, Istanbul, Turkey
[2] Assoc. Prof. Dr., Istanbul Technical University, Istanbul, Turkey
[3] Doctor, Istanbul Technical University, Istanbul, Turkey
[4] PhD Candidate, Istanbul Technical University, Istanbul, Turkey
[5] MSc, Structural Engineer, Istanbul, Turkey
[6] PhD Student, Istanbul Technical University, Istanbul, Turkey
[7] MSc Student, Istanbul Technical University, Istanbul, Turkey

ABSTRACT: The building stock in many developing countries including Turkey comprises substandard buildings. Such buildings are known to be highly vulnerable and have experienced catastrophic damage during past earthquakes leading to extensive life and economic losses. To mitigate the seismic vulnerability of this kind of buildings and execute effective post-earthquake disaster management, there is an urgent need for reliable earthquake risk assessment and post-earthquake disaster management strategies that take the specific characteristics of substandard buildings into account.

This paper presents a part of the methodology of an international collaboration project between the UK and Turkey entitled "Development of a Framework for Rapid Earthquake Risk Assessment and Post-Earthquake Disaster Management for Substandard Buildings in Turkey" funded by the Research Councils UK (RCUK) and The Scientific and Technological Research Council of Turkey (TUBITAK). The framework includes a rapid assessment procedure considering primary and secondary seismic hazards (e.g. landslides and liquefaction), structural vulnerability and financial aspects as well as communication and knowledge modeling for crisis management. Moreover, investigations on different retrofitting techniques to develop vulnerability mitigation strategies for substandard buildings are also integrated into the framework.

1   INTRODUCTION

Poor seismic behavior of substandard buildings arising from distinctive deficiencies such as low quality of concrete, large spacing of transverse reinforcement and lack of seismic detailing of reinforcement has resulted in catastrophic life and economic losses during earthquakes. These deficiencies lead to undesired premature/brittle failure of structural members that may cause partial or total collapse of buildings during major earthquakes. To execute a realistic seismic risk assessment for this kind of buildings, realistic consideration of failure modes that occur on substandard building structural members should be accommodated in the structural models.

In developed countries, a number of generic tools such as HAZUS-MH (USA) [1], ELER [2] and QLARM [3] (EU) have been developed to conduct seismic risk assessment and loss estimation. These tools are more convenient to conduct large scale assessments in specific regions, and

2nd International Workshop on Advanced Materials and
Innovative Systems in Structural Engineering:
Novel Researches

IWAMISSE
2019
ISTANBUL
fib
Turkey

contain generic hazard determination (using maps) and loss assessment based on generic vulnerability/fragility curves. In these methods, the buildings are generally classified into vulnerability classes based on their year of construction which defines the code that they comply with. However, in many developing countries (including Turkey), since the existing buildings generally do not comply with the codes of their construction periods, this sole parameter may lead to inaccurate classification of the substandard buildings. Therefore, the utilization of these tools for Turkish substandard buildings in seismic risk assessment can lead to unrealistic results. On the other hand, some other tools have been developed for supporting integrated risk management strategies such as KOERILOSS [4] and AFAD-RED [5] in Turkey; as well as other attempts such as Earthquake Risk Assessment (ERA) framework [6 and 7] which were developed for developing countries considering substandard building stock. The main issue with these tools is the assumption of vulnerability of substandard buildings which is not diversified enough to allow an accurate risk assessment. Basically, they assign all substandard buildings into a single building class (i.e. pre-code building class) whose definition is expected to vary for each region of interest due to the variations in the construction practice. Consequently, there is a need for an assessment tool that considers the distinctive structural properties of substandard buildings.

In this project, it is aimed to integrate the actual fragility/vulnerability curves particularly obtained for substandard buildings into the AFAD-RED (developed by the project partner Gebze Technical University) and ERA (developed by the project partner University of Sheffield). The project also contains communication and knowledge modeling for crisis management to ensure an efficient use of the data obtained from the high-level earthquake risk assessment. A novel approach will be used to combine field/experimental observations and real-time data from mobile devices and advanced apps widely used for social networking to coordinate search/rescue actions and to increase situational awareness during crisis. The use of social media data analysis for post-crisis management of stress, trauma, and recovery will help to create a more resilience society in Turkey.

This research collaboration project between the UK (United Kingdom) and Turkey is supported by RCUK and TUBITAK within Newton and Katip Çelebi Funds to contribute to the economic development and social welfare of Turkey. The institutions involved in the project are Istanbul Technical University (ITU, principal investigator in Turkey) and Gebze Technical University (GTU) from the Turkish side and The University of Sheffield (UoS, principal investigator in the UK) and Sheffield Hallam University (SHU) from the UK side. The developed framework is planned to be used to build up an efficient and innovative seismic risk assessment and mitigation tool, specifically designed considering the structural properties of substandard buildings in the Marmara region of Turkey. Besides, the framework will significantly improve the country's capacity for earthquake disaster management. The project will also expand seismic risk mitigation research and help establish new capabilities for the insurance industry, such as Turkish Catastrophe Insurance Pool (TCIP also known as DASK in Turkish).

2   SCOPE AND THE OBJECTIVES OF THE PROJECT

The scope of this international research project is to develop, an innovative and efficient framework of seismic risk assessment and disaster mitigation for substandard buildings in Turkey. The project also contributes to the coordination of post-earthquake search and rescue actions and enhance situational awareness. The project objectives are to:

- categorize the building stock in the Marmara region according to their strength and ductility characteristics: Classification is performed utilizing a modified version of the PERA Method [8] previously developed by the project research group for performance-based rapid seismic assessment of reinforced concrete (RC) frame buildings.
- obtain vulnerability relationships for key substandard building classes incorporating the specific characteristics and failure modes of substandard buildings in the structural models.

- enhance the GTU and UoS rapid assessment tools (AFAD-RED for GTU and ERA for UoS) by integrating the fragility/vulnerability relationships particularly obtained for substandard buildings.
- extend the ERA framework to cover the secondary seismic hazards (landslides and liquefaction) using existing local geological and geotechnical information.
- Validate selected retrofitting solutions with laboratory tests by conducting reversed cyclic loading tests on nearly full-scale reinforced concrete columns for optimal retrofitting options to determine their effectiveness on the enhancement of the seismic behavior of substandard members.
- develop vulnerability mitigation strategies based on seismic retrofit. The efficacy of different retrofitting methods on the seismic performance enhancement will be integrated into the vulnerability assessment models.
- develop an Earthquake Information Processing and Analysis Centre: An Earthquake Information Processing and Analysis Centre (EIPAC) will be established to gather, process and analyze all data and reports from a mobile application that will be specially developed for this purpose. Furthermore, EIPAC will also search social media to determine the information related to the impact of an earthquake.
- develop a Mobile Application for Earthquake Management: A mobile application in Turkish and English will be developed. The information about the situation of the earthquake affected area will be collected in EIPAC from eyewitness, rescue workers, structural engineers, and other personnel on the ground via developed mobile application.
- develop a Post-Earthquake Control Centre Dashboard (PECCD): The PECCD will be a web-based application utilized to capture and screen earthquake-related information. It will receive data from the Earthquake Information Processing and Analysis Centre. Using the information from the Earthquake Information Processing and Analysis Centre, the areas where the search-rescue actions and humanitarian aid most needed will be determined. Moreover, the users of PECCD will also be able to explore the data through map based displays.
- integrate the post-earthquake social/disaster management framework with the ERA framework: The developed earthquake management framework will be integrated with ERA to provide real-time information on expected critical damage, rehabilitation priorities, and casualties for rescue and recovery operations.
- validate the integrated frameworks using scenario simulation: Scenario simulation will be implemented for strong ground motion scenarios in selected urban areas of Marmara.

To reach these objectives, the framework fundamentally contains two-phases: Pre- and post-earthquake cases. Accordingly, for these two phases, the general flowchart of the project is shown in Figure 1.

The first phase contains the tasks for pre-earthquake predictions. To classify the building stock in the Marmara region, the structural characteristics and geometric properties of the buildings in selected areas are compiled. After that, buildings are classified using PERA method considering their seismic force and deformation capacities and representative buildings for each building class are chosen. Then, incremental dynamic analyses (IDA) are performed to obtain fragility/vulnerability relationships for each building. During the nonlinear finite element (FE) analyses, particular approaches for modeling of substandard building characteristics are obtained through a literature survey, so that uncertainty of the material characteristics and effects such as longitudinal bar buckling and slip are considered. Thereafter, loss estimation is carried out using probabilistic risk assessment considering obtained fragility/vulnerability relationships and site-specific seismic hazard. It should be noted that seismic hazard data also contains secondary hazards such as landslides and liquefaction. The vulnerability assessment models are to be further developed to include the effects of different retrofitting techniques and retrofitting decision is to be made after the comparison of the loss before and after retrofitting. In addition, the optimum retrofitting techniques will be validated with full-scale column tests. The second phase of the project is mainly related to disaster response using real-time data from smart devices

to contribute to the coordination of post-earthquake search and rescue actions, and enhance situational awareness.
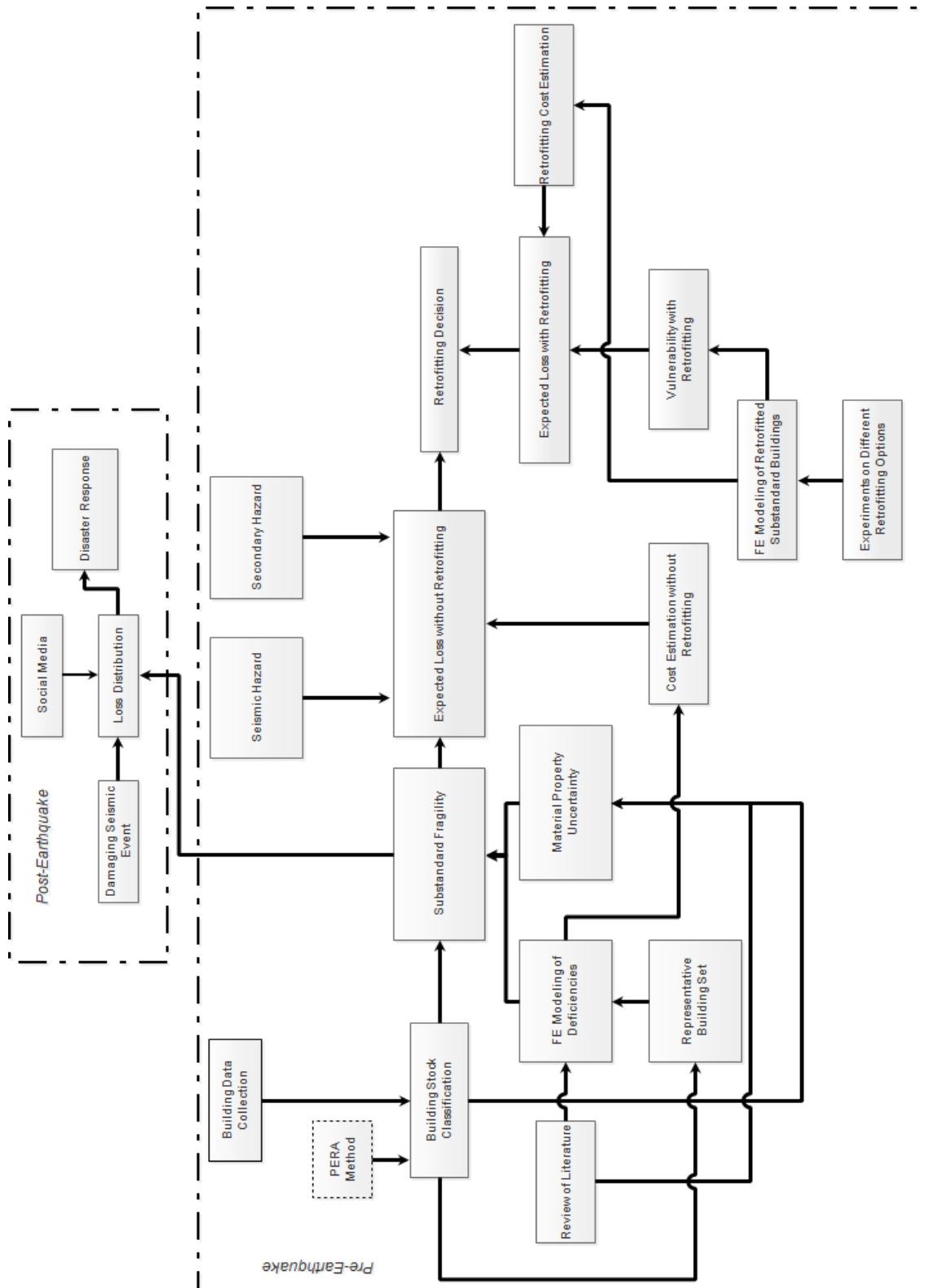

Figure 1. General flowchart of the project

3   BUILDING DATABASE AND THE APPROACH FOLLOWED BY ITU

3.1   Building Data Collection

Floor plans, number of stories, story heights, material properties, reinforcement details and soil classes of a total number of 156 existing reinforced concrete buildings located in the Marmara Region were collected and compiled in a comprehensive database. The distribution of the collected buildings with respect to their number of stories, year of construction, reinforcement type and concrete compressive strength is shown in Figure 2. As it can be inferred from Figure 2, the number of stories varies from three to five (56% of buildings), the compressive strength of concrete varies between 10-20 MPa (48% of buildings), and the reinforcing steel type is S220 (79% of buildings) for majority of the buildings. Moreover, the buildings were mostly constructed between the years 1975 and 2000 (58% of buildings). For each of the buildings in the building database, modified PERA method was applied and buildings were sorted with respect to their lateral load and deformation capacities so that five representative buildings which are to be analyzed with the Incremental Dynamic Analysis (IDA) approach could be selected. It should be noted that, a series of analyses that included 54 different cases were derived from these five buildings. These cases aimed to investigate several deficiencies, uncertainties and retrofitting approaches which are explained in the following pages. Further details about the building selection for vulnerability analysis are provided in the companion paper (Yazgan et. al [9]).
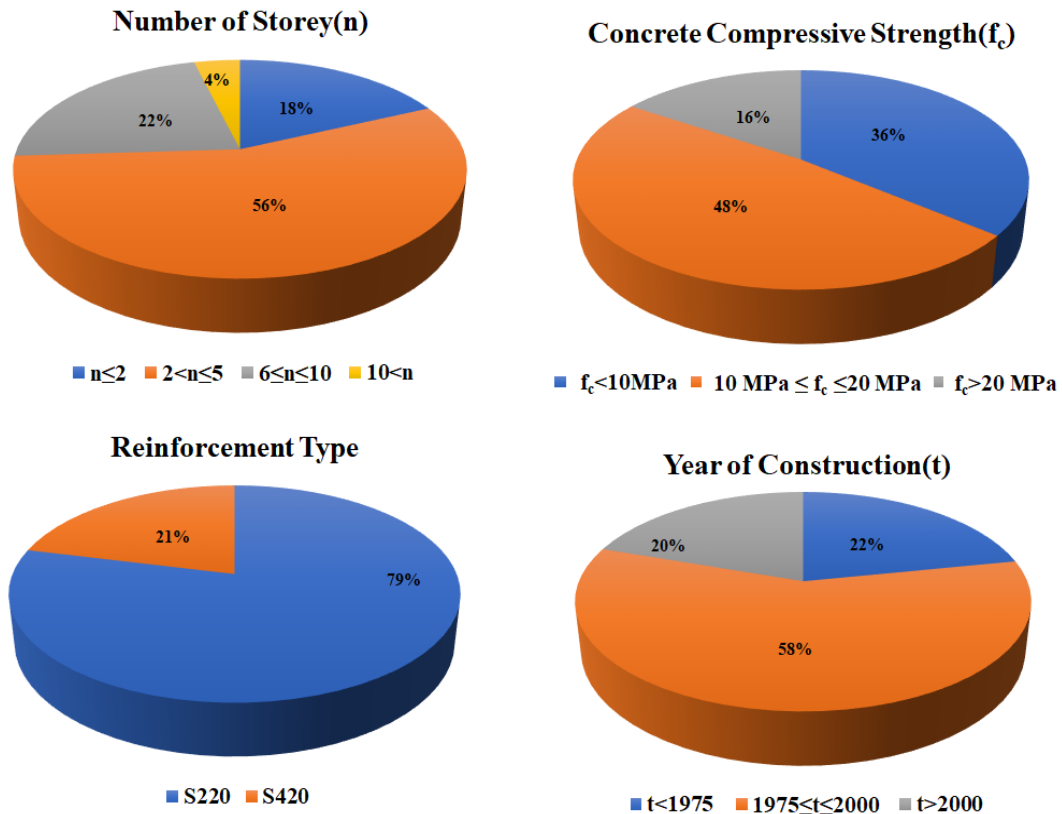

Figure 2. Distribution of number of stories, concrete compressive strength, reinforcement type and year of construction for the building database

3.2 *Fragility Analysis of the Selected Buildings*

A series of Incremental Dynamic Analysis (IDA) was conducted to obtain the fragility curves of the representative buildings. Spectral accelerations and maximum inter-story drift ratios were used as intensity and damage measures, respectively. Seven earthquake records with two components were applied in the X and Y directions of each building separately. At each step of the IDA, earthquake records were scaled to the target spectral acceleration by considering the first dominant period of the building. The target spectral accelerations were increased step by step from 0.05g to 1.5g with a typical step size of 0.05g. Finally, fragility curves were obtained with respect to spectral acceleration, peak ground acceleration and peak ground velocity. Buckling of longitudinal reinforcing bars, lap splice deficiencies and the variation of material properties (concrete and steel qualities) were taken into account in structural models. Moreover, the effect of structural system irregularities such as torsional irregularity, soft story and some retrofitting options on the fragility relationships were also investigated. The parameters considered during the analyses are summarized in Figure 3. Typical fragility curves for an investigated substandard building including lap-splice and bar buckling deficiencies can be seen in Figure. 4. It should be noted that, the challenges emerging from the specific characteristics and deficiencies of substandard buildings for vulnerability modeling is discussed in the companion paper (Yazgan et. al [9]).

In addition to the analysis for the selected substandard buildings in their original unretrofitted state, the vulnerability assessment models are further developed to include the effects of different strengthening and retrofitting techniques emphasizing the effectiveness on enhancing the seismic performance. For this purpose, various retrofitting approaches are evaluated and conventional and novel methodologies (such as shear wall addition, column reinforced concrete jacketing, fiber-reinforced polymer composite (FRP composite) jacketing, thin reinforced concrete jacketing with FRP confinement and sprayed glass fiber reinforced mortar jacketing with textile reinforcement) are considered for one of the buildings. With this analysis series, the efficacy of these retrofitting approaches and their potential effects on the vulnerability of substandard buildings is investigated.
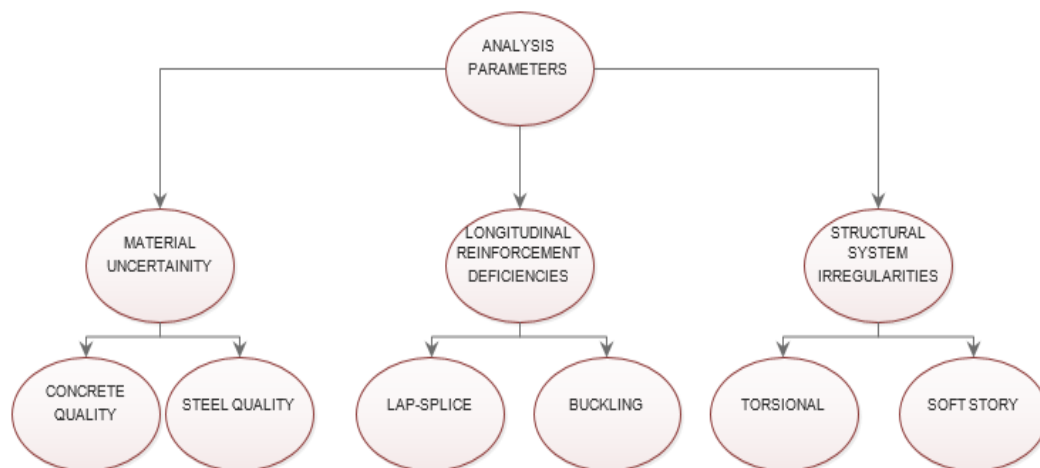

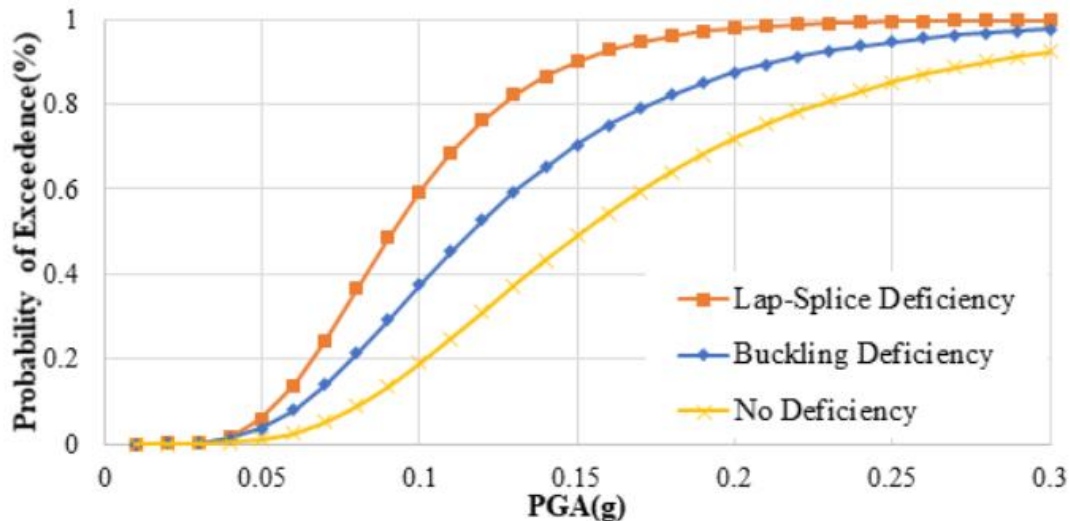Figure 3. Considered parameters for incremental dynamic analyses.

Figure 4. Typical fragility curves obtained by considering lap splice and longitudinal bar buckling deficiencies.

3.3 Validation of Selected Retrofitting Techniques

Effectivenesses of three of analytically investigated retrofitting techniques (FRP composite jacketing, thin reinforced concrete jacketing with FRP confinement, and sprayed glass fiber reinforced mortar jacketing with textile reinforcement) for the enhancement of seismic behavior of substandard reinforced concrete columns are tested experimentally under high axial load ratios and reversed cyclic lateral loading. Based on test results and using an available database, retrofitting design methodology will be proposed for the new generation of earthquake-resilient structures, which will also guide the further development of the Turkish seismic design code.

4 CONCLUSIONS

Developing of fragility/vulnerability relationships considering the specific deficiencies is essential for an accurate seismic risk assessment and loss estimation in the regions where the major part of the building stock consists of substandard buildings. In this paper, the general outline and the followed approach for an international research project entitled "Development of a Framework for Rapid Earthquake Risk Assessment and Post-Earthquake Disaster Management for Substandard Buildings in Turkey" are presented. In this project, the building stock is classified with a rational classification method that takes into account the strength and deformability characteristics of structures rather than the coarse building construction date and number of stories approach which is followed by many of the earthquake risk assessment approaches. In the developed framework, expected losses after an earthquake are determined by using fragility/vulnerability curves specially derived for substandard building classes for which certain deficiencies are considered. During the risk assessment, secondary hazards (such as landslides and liquefaction) are also taken into account. In this study, it is also aimed to integrate an optimal retrofitting scheme to the framework for the seismic risk mitigation of substandard buildings. Moreover, usage of real-time data from smart devices for disaster response is also included in the project.

ACKNOWLEDGEMENTS

REFERENCES

[1] FEMA (2018). HAZUS-MH technical manual. Federal Emergency Management Agency, Washington, DC.

[2] Hancilar, U., Tuzun, C., Yenidogan, C. and Erdik, M. (2010). ELER software-a new tool for urban earthquake loss assessment. Natural Hazards and Earth System Sciences, 10(12), 2677.

[3] Trendafiloski, G., Wyss, M. and Rosset, P. (2011). Loss estimation module in the second generation software QLARM. In Human Casualties in Earthquakes (pp. 95-106). Springer Netherlands.

[4] Kandilli Observatory and Earthquake Research Institute (2003). Earthquake risk assessment for the Istanbul Metropolitan area. Final report. Boğaziçi University Press.

[5] Fahjan,Y., Kara, F.İ. and Pakdamar, F. (2013). Disaster and emergency management authority of Turkey (AFAD) and Gebze Technical University (GTU), Earthquake damage estimation system software development project final report, Istanbul, Turkey.

[6] Kythreoti, S. (2002). Earthquake risk assessment and management case study: Cyprus Doctoral Dissertation, The University of Sheffield, Sheffield, UK.

[7] Ahmad, S., Kyriakides, N., Pilakoutas, K., Neocleous, K. and uz Zaman, Q. (2015). Seismic fragility assessment of existing sub-standard low strength reinforced concrete structures. Earthquake Engineering and Engineering Vibration, 14(3), 439-452.

[8] Ilki, A., Comert, M., Demir, C., Orakcal, K., Ulugtekin, D., Tapan, M., and Kumbasar, N. (2014). Performance based rapid seismic assessment method (PERA) for reinforced concrete frame buildings. Advances in Structural Engineering, 17(3), 439-459.

[9] Yazgan, U., Ilki, A., Demir, C., Demir, U., Ates, A.O., Kupcu, E., Unal, G., Altinok, M.A., Karakaya, B. And Narlıtepe, F. (2019). Challenges in Developing Seismic Vulnerability Models for Substandard Building Stocks in Turkey. 2nd International Workshop on Advanced Materials and Innovative Systems in Structural Engineering: Novel Researches, IWAMISSE 2019, Istanbul, TURKEY.

Challenges in Developing Seismic Vulnerability Models for Substandard Building Stocks in Turkey

Ufuk Yazgan[1], Alper İlki[1], Cem Demir[1], Uğur Demir[1], Ali Osman Ateş[1], Eren Küpçü[1], Göktuğ Ünal[1], Mehmet Akif Altınok[1], Büşranur Karakaya[1], Furkan Narlıtepe[1]

[1] Istanbul Technical University, Istanbul, Turkey

ABSTRACT: Substandard buildings comprise the seismically most critical portion of the existing building stock. Past earthquakes have shown that large majority of losses are due to poor seismic performance of these buildings. For the purpose of estimating damage and expected loss for the substandard buildings in the Marmara region (Turkey), development of reliable methods are urgently needed. Existing approaches for vulnerability classification of buildings rely heavily on the design-code level of the buildings. In the regions where the predominant type is substandard buildings with poor seismic resistance, this approach results in clustering of large portions of the existing stock into a single vulnerability class. This leads to lack of granularity in the loss estimates. In order to tackle this issue, a new strategy for the vulnerability-based classification of building stock is proposed here. Unlike the existing schemes, proposed approach is based on utilization of rapid assessment methods. For this purpose, a modified version of the rapid assessment method known as PERA method (Ilki et al. 2014) is utilized. The method developed is for performance-based rapid seismic assessment of reinforced concrete (RC) frame buildings. Envisioned vulnerability modeling framework is based on development of specific vulnerability models for the groups of substandard buildings that are found to have similar performance characteristics based on rapid assessment results. This will allow some level of differentiation between substandard buildings while still keeping the amount of required information related to the building stock at a manageable level. Vulnerability relationships that represent average characteristics of each substandard vulnerability class will be developed by means of numerical simulations. These models are expected to provide the major contributors of the expected loss with a higher degree of granularity compared to existing vulnerability models.

1 INTRODUCTION

Seismic vulnerability models are critical components of the seismic risk assessment tools. Vulnerability models relate the expected level of economic loss due to the damage sustained by a specific type of structure to the intensity of strong ground motion that is exhibited at the site of the structure. The efforts for characterizing the relationship between intensity of shaking and the damage grade sustained by specific types of structures for the purpose of estimating future losses, had started more than 80 years ago (Freeman, 1932). Even in those early studies by Freeman (1932), the need for categorizing buildings into vulnerability classes was understood and substandard buildings, being the main driver of the seismic losses was recognized. One of the first to remark this fact was Freeman (1932):

> "In nine cases out of ten, the terrible happenings that involve the loss of life and property are the result of inexcusably bad design or of bad construction."

Very similar conclusions were reported after numerous post-earthquake reconnaissance investigations up until today. Nowadays, it is a well-established fact that the large majority of structural damages are sustained by the substandard buildings within the affected building stock. Therefore, it is crucial to capture the seismic vulnerability characteristics of the substandard buildings in developing accurate estimates of losses due to future earthquakes.

The importance of capturing the differences in the vulnerability characteristics of different types of buildings within a building stock was recognized in the early '70s. This lead to initial attempts to established vulnerability-based building classification schemes (e.g. Whitman, 1973). Even in those early classification schemes, the importance of the utilized design code, in addition to the structural system type, was admitted. Whitman (1973) proposed classifying buildings classified into 3 three classes in terms of the utilized design standard: pre-11a building classification scheme that takes into account the time interval (i.e. pre-1933, post-1947, others). The proposed date limits correspond to the specific years when the seismic design code in U.S. was revised significantly. Also today, the structure classification schemes take into account the dates of revision of the seismic design standards.

Classification of building stock into vulnerability classes simply based on their year of design and construction is a suitable strategy if the structures are designed/constructed properly by complying with the codes at the time of their construction. Unfortunately, this is not the case in the large majority of the megapols in developing countries, such as Istanbul. The enforcement of the code conditions is typically insufficient in those regions. As a result, it can be very misleading to assume that all buildings constructed enactment of a seismic design code, all have the targeted safety against seismic actions. Unfortunately, it takes time for the new and improved construction practices to be adopted by the practitioners. This fact should be taken into account when defining categorization schemes for substandard buildings.

Another key challenge in the assessment of seismic vulnerability of substandard buildings is the development of the basis data for the assessment. Typically, three types of data sources are considered in the development of vulnerability models: (1) expert-opinion, (2) empirical observations, and (3) analytical/numerical models. The overall objective in establishing vulnerability models for a specific group of structures is to predict both the mean value and the dispersion of the expected losses for that type of structure subjected to a given level of strong ground motion. Particularly, evaluation of the likely dispersion of the extent of losses within the set of substandard structures that belong to the same class is a challenging issue. Since the construction practices for substandard buildings do not comply with the codes, the spectrum of probable irregularities and deficiencies are almost boundless. As a result, it is a highly challenging task to assess the dispersion of damages that may be sustained by a group of substandard buildings that belong to the same category and that are subjected to the same ground motion intensity level.

The research presented in this manuscript is part of a research project entitled "Development of a Framework for Rapid Earthquake Risk Assessment and Post-Earthquake Disaster Management for Substandard Buildings in Turkey" which is jointly supported by the Scientific and Technological Research Council of Turkey (TUBITAK) and the Research Councils UK (RCUK). Further information about the objectives and the methodology of this project is presented by İlki *et al.* (2019). The main objective of this proceeding is to remark the major challenges associated with estimation of vulnerability of substandard buildings. In addition, some recommendations are provided for overcoming these challenges.

2   VULNERABILITY MODELS IMPLEMENTED IN EXISTING LOSS ASSESSMENT PLATFORMS

There is a vast amount of literature on development of vulnerability models for structures. Their benefits and limitations have already been discussed elsewhere (GFDRR, 2014). These are not repeated here. Instead, specifically the strategies utilized for capturing the vulnerability

characteristics of substandard buildings in the existing loss modeling frameworks, are investigated.

One of the most well-established seismic loss assessment tools, is the HAZUS-MH developed by Federal Emergency Management Agency (Schneider and Schauer, 2006). HAZUH-M consists of a number of modules which are interdependent with output of some modules acting as input to others. It provides estimates of potential building and infrastructure losses from earthquakes, riverine and coastal floods, and hurricane winds. More specifically, it provides estimates of the structural and nonstructural repair costs caused by building damage and the associated loss of building contents and business inventory and the indirect economic losses are also treated as an extension of this module. In order to model the vulnerability of structures within a given region, two main inputs are required as i) model building type including height and seismic design level (High-Code, Moderate-Code, or Low-Code seismic standards, or not seismically designed and referred to as Pre-Code buildings) ii) response spectrum (or PGA) at building's site. This type of an approach is a suitable strategy for the regions where enforcement of the revised design codes are taken up in the practice without significant delay.

Earthquake Loss Estimation Routine (ELER) framework that was developed for the rapid estimation of earthquake shaking and losses in the Euro-Mediterranean region, is a tool that is frequently utilized (Hancılar et al. 2010). It is capable of incorporating regional variability and uncertainty generated from ground motion prediction equations (GMPE), fault finiteness, site modifications, and inventory of physical and social elements subjected to earthquake hazard and the associated vulnerability relationships. The European building taxonomy developed by Giovinazzi (2005) within the EU-FP5 RISK-UE project is utilized in ELER. This classification scheme is a modified version of the original scheme adopted in EMS-98 (Grunthal, 1998). In this scheme, three code levels are defined for the classification of RC buildings. These are designated as "Earthquake Resistant Design (ERD)" levels. Since the seismic design code applicable in Turkey improved particularly after 1975, the buildings are classified as pre-1979 (included) and post-1980 reflecting the state of seismic design applications.

EarthQuake Loss Assessment for Response and Mitigation (QLARM) tool is based on the ERD-based vulnerability differentiation approach, similar to ELER. The methodology estimates percent of buildings as well as the total number of fatalities and injured, casualties by settlement and a map showing mean damage by settlement (Trendafiloski et al. 2011). QLARM evaluates the building damage using the European Macroseismic Method (Giovinazzi, 2005) and EMS-98 vulnerability classes. The vulnerability classes are assigned mostly depending on the level of ERD provided.

In essence, the ERD based classification -utilized in most of the existing frameworks- has a bit different aim than capturing the differences in the seismic vulnerability based on adoption of different construction practices. ERD-based schemes aim at differentiating between the (non-seismic action dominated) design principles utilized in regions with high seismicity and those in seismically active regions. Inevitably, the level of separation among the substandard buildings that suffer from construction related deficiencies is not much. This precludes the capability of the loss modeling framework to provide detailed and accurate loss estimates for the case of substandard buildings in developing countries.

Another noteworthy approach is the Earthquake Risk Assessment Methodology (EQRAM) developed by Khan et al. (2012). This approach consists of three main parts. Part I of the model estimates the seismic hazard. Part II of the model involves the Earthquake Risk Assessment (ERA) framework. Part III estimates the fatalities and injuries depending on the population distribution. A general framework for determining the vulnerability of structures in developing countries (Ahmad et al., 2015) was used to generate input data for the vulnerability module of EQRAM. The risk module of EQRAM also includes the building inventory and population assessment which is based on a GIS. The probability of damage and consequent loss of elements at risk is calculated from the results of risk module.

Meanwhile in Turkey, Disaster and Emergency Management Authority of Turkey (AFAD) and Gebze Technical University (GTU) have developed Rapid Earthquake Damage and Loss Estimation Software AFAD-RED (Fahjan et al., 2013). AFAD-RED uses existing building, geology, lifeline and similar databases as an input parameter as well as vulnerability curves and attenuation relationships alike analysis parameters. As a result, it generates intensity, PGA, PGV and spectral displacement maps and potential damage and fatality losses at county, district and town levels. RISK-UE and HAZUS99 building classifications are used in AFAD-RED (Fahjan et al., 2013). Similar to ELER, seismic vulnerability is considered in the building database as being: none, poor or well-engineered. The basic outputs of the analyses are structural damage level (Light, Medium, Heavy, and Complete Damage), number of injured people, number of life loss and number of people requiring temporary shelter. AFAD-RED also estimates structural damage rates of lifelines and critical facilities and calculates the direct economic losses. In AFAD-RED, the user can either use the predefined attenuation relationships and fragility curves or define new ones. Fahjan et al. (2013) indicates the obvious need for creating specific vulnerability curves for Turkey.

Based on the review of the state-of-the-art seismic risk assessment tools and frameworks, following limitations were identified:

- Existing frameworks utilize a very crude classification for the buildings within the overall class of substandard buildings.
- The impact of presence/absence of specific structural deficiencies are not reflected directly in the results, and
- Existing frameworks do not allow for disaggregation of expected losses and optimization of mitigation efforts (e.g. retrofitting)

Tackling this issue is one of the main objectives of the project entitled "Rapid Earthquake Risk Assessment and Post-Earthquake Disaster Management Framework for Substandard Buildings in Turkey". For this purpose, establishing an improved vulnerability modeling framework for the substandard buildings in Turkey.

3   MAIN CHALLENGES

Assessment of seismic vulnerability of any type of structure is a challenging task. A major portion of this challenge is due to the inherent uncertainty associated with the expected ground motion excitation and the post-elastic dynamic response characteristics of the structure. Another important part is due to the limitations related to the existing analysis approaches. For the case of substandard buildings these challenges are even more pronounced. Since they are often designed and constructed according to any specific design code, their resistance capacities have very high variability. Moreover, the failure modes (e.g. flexure, shear, axial) are very often hard to predict due to detailing deficiencies. It is critical to properly capture the impact of these uncertainties on the vulnerability characteristics of the substandard building stock.

While developing a vulnerability modeling scheme for substandard buildings, the following issues should be taken into account:

- There is very limited information about critical structural features (*Structural system irregularities, detailing deficiencies, poor material properties*) of these buildings.

- Developing accurate analysis models is a challenging issue (*Poor confinement, insufficient lap splices, high axial load ratios, low concrete strength*).

One strategy for tackling the first issue is to consider the stochastic character of presence and absence of various types of deficiencies. In principle, if the likelihoods of different types of uncertainties can be estimated properly, a series of analysis models can be randomly generated

and using these models, the expected variability of the vulnerability can be identified. Through such analysis, the impact of parametric uncertainty on the estimated vulnerability can be captured.

The second issue noted above, regarding the accuracy of the utilized modeling strategy is a relatively more challenging one compared to the first one. The existing analytical models available for modeling the dynamic inelastic response of RC structures, inevitably suffer from some level of inaccuracy. The uncertainty associated with the errors and biases associated with the utilized modeling approach have a direct impact on the resulting vulnerability. This source of uncertainty is difficult to assess when there are limited experimental data that can be utilized to validate the models.

Within the scope of the main research project, the vulnerability characteristics of the substandard building stock in Marmara region is being investigated. The primary characteristics that have a significant impact on the seismic vulnerability of these buildings, were considered in the investigation. These characteristics are presented in Figure 1.
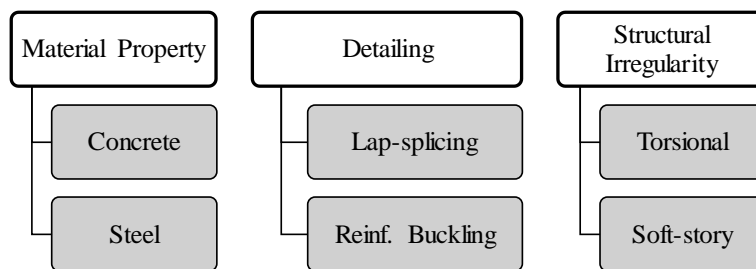

Figure 1. Structural properties that are considered in the proposed framework

In the Marmara region, two of the most common detailing deficiencies are: (1) buckling of longitudinal reinforcement due to inappropriate transverse reinforcement detailing, and (2) debonding and slipping of reinforcement due to insufficient lap-splice. As a result, a special investigation was undertaken to quantify the impact of these deficiencies on the resulting vulnerability.

The aspect ratio of the longitudinal reinforcement which can be defined as the ratio of stirrup spacing to diameter of longitudinal reinforcement is the most significant parameter that affects buckling behavior. When the spacing is large and the reinforcement diameter is small, a very slender configuration is obtained. Longitudinal reinforcing bars tend to buckle under very low levels of compressive stresses. Yalcin and Saatcioglu (2000) proposed an analytical formulation aiming to represent this buckling behavior in the fiber-section models of RC components. Their formulation is based on modification of the stress-strain model of the fibers representing longitudinal reinforcement.

For the case of lap-splice deficiency, the situation is different than the buckling deficiency because it is not easy to define the interlock mechanism between reinforcement and concrete. Additionally, most of the studies are concentrated on bond strength of reinforcements and to find required lap splice lengths instead of defining the behavior after slip occurs (Zuo and Darwin, 2000). The reinforcement type -whether it is smooth or deformed-, lap splice length, diameter of reinforcement, clear cover, confinement, distance between longitudinal reinforcements are the considered parameters to define bond stress-slip relations (Lettow and Eligehausen, 2006). The slip versus bond stress behavior can be modeled by using nonlinear springs to consider bond-slip behavior. In this project, the lap-splice model proposed by Verderame et al. (2009) was utilized. In the fragility analysis, bond-slip related deformation components were modelled by defining moment-rotation hinges at column ends.
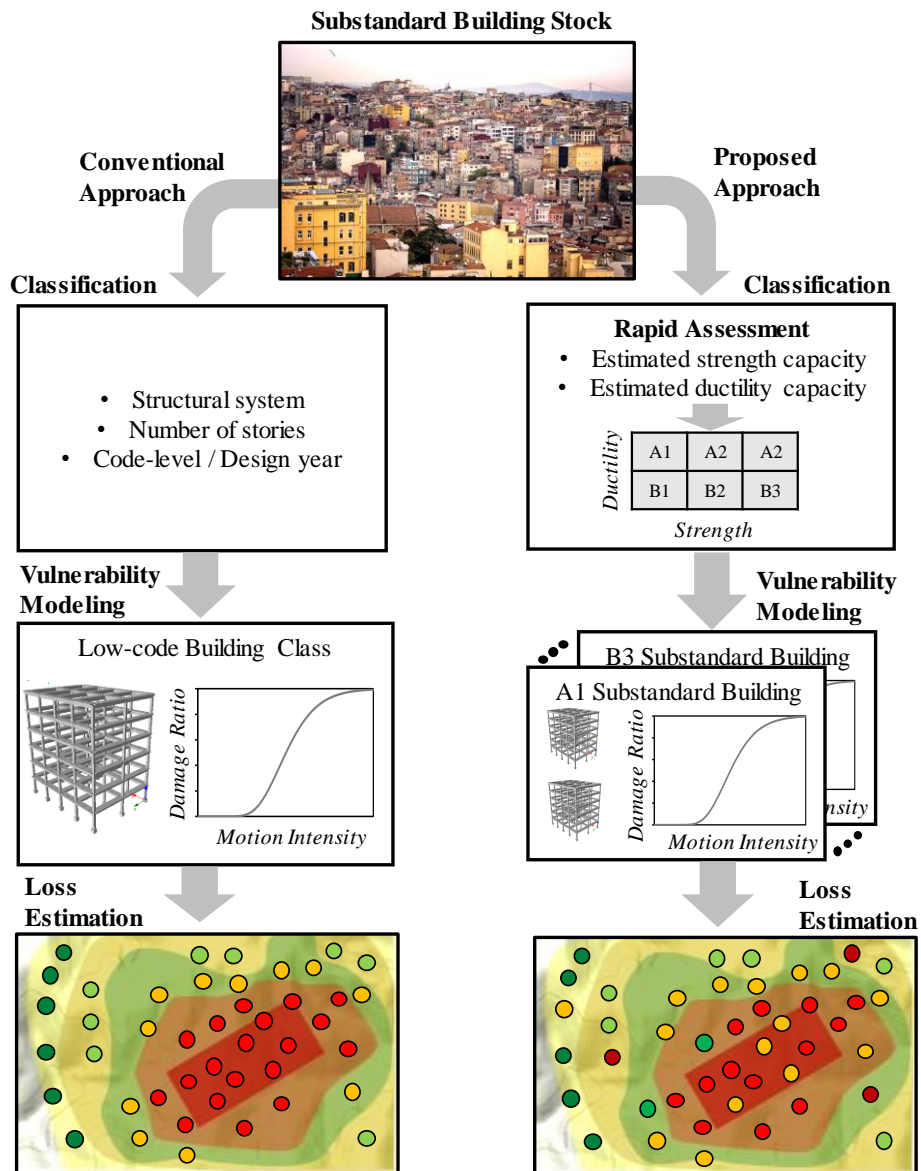
Figure 2. Classification of substandard buildings in seismic risk assessment frameworks:
Conventional approach and the proposed alternative.

Another important source of uncertainty related to vulnerability of substandard buildings is related to poor material properties. This variability will be considered by means of response surface method in the envisioned framework. Specifically, the variability of the actual concrete compressive strength and the reinforcement tensile strength, were considered. For this purpose, the statistical distributions of material properties were identified based on available databases of material test results.

One of the innovative aspects of the proposed vulnerability assessment framework is the classification of buildings into specific vulnerability subgroups (Figure 2). For the classification of substandard buildings, rapid assessment based strength and ductility properties of buildings are utilized as the basis parameters. The rapid assessment based classification followed in this study is rooted from the PERA Method (2014) developed for performance based quick seismic assessment of reinforced concrete (RC) frame buildings. Considering the vast stock of vulnerable buildings, the level of on-site investigations and structural analysis is simplified and minimized compared to code based assessment approaches. The followed linear procedure is similar to Turkish Seismic Design Code (2007) approach. Thus, the PERA method predicts the seismic

performance of existing RC buildings by estimating the damage state of the columns by considering different failure modes, drifts and demand/capacity ratios for which confinement condition and shear and axial stress levels of the columns are accounted. Original PERA method provides approximate estimates of the strength capacities of the buildings. In order to provide approximate estimates of the ductility capacities of substandard buildings, the original PERA method will be modified.

4   CONCLUSIONS

Developing accurate seismic vulnerability models for substandard buildings is a critical challenge. These buildings drive the major part of seismic risks associated with the building stocks in seismically active regions. Therefore, potential losses due to future earthquakes can only be predicted accurately if the seismic vulnerabilities of the substandard buildings are estimated accurately. There are, however, a series of existing challenging issues that must be tackled by researchers developing vulnerability models for substandard building stocks.

- Existing loss modeling frameworks utilize very coarse classification schemes for vulnerability modeling of substandard buildings. Such classifications lead to large clusters of buildings being categorized as high-risk buildings without the possibility of disaggregation of losses. Therefore the risk mitigation efforts cannot be possible.

- Analysis models that can accurately capture the seismic response of buildings with structural deficiencies, are needed. The accuracy of the resulting vulnerability modes for substandard buildings would be significantly improved when such tools become available.

- The impact of transverse reinforcement detailing deficiency and insufficient lap-splice length on the seismic vulnerability was investigated for the case of a representative substandard building. Results indicate that the estimated vulnerability is noticeably affected the presence of such deficiencies.

- Effective classification of substandard buildings is an important challenge. Quick assessment method such as PERA (Ilki et al. 2014) is going to be utilized in this regard.

- There is also a strong need for experimental data that would provide a reliable basis for understanding the impacts of the most common RC detailing deficiencies on the seismic response of substandard buildings.

- There is very limited information about the frequencies of the critical structural deficiencies within the existing substandard building stocks. It would be highly beneficial to collect the necessary information that would allow effective categorization of substandard buildings into specific vulnerability classes.

ACKNOWLEDGEMENTS

REFERENCES

Ahmad, S., Kyriakides, N., Pilakoutas, K., Neocleous, K. and Zaman, Q., 2015. Seismic fragility assessment of existing sub-standard low strength reinforced concrete structures. *Earthquake Engineering and Engineering Vibration*, 14(3):439-452.

Fahjan,Y., Kara, Fİ., and Pakdamar, F., 2013. Disaster and emergency management authority of Turkey (AFAD) and Gebze Technical University (GTU), Earthquake damage estimation system software development project final report, *Technical Report*, Kocaeli, Turkey.

Freeman, JP., 1932. *Earthquake damage and earthquake insurance*, McGraw Hill, New York.

Global Facility for Disaster Reduction and Recovery (GFDRR), 2014. Review of open source and open access software packages available to quantify risk from natural hazards, *Technical Report*, United Nations, New York.

Giovinazzi, S., 2005. Vulnerability assessment and the damage scenario in seismic risk analysis,. *Ph.D. Dissertation*, Department of Civil Engineering of the Technical University Carolo-Wilhelmina at Braunschweig and Department of Civil Engineering, University of Florence, Italy.

Grunthal G., 1998. European Macroseismic Scale. *Technical Report*, Centre Européen de Géodynamique et de Séismologie, Vol. 15, Luxembourg.

Hancilar, U., Tuzun, C., Yenidogan, C. and Erdik, M., 2010. ELER software- a new tool for urban earthquake loss assessment. *Natural Hazards and Earth System Sciences*, 10(12):2677-2696.

Ilki, A., Comert, M., Demir, C., Orakcal, K., Ulugtekin, D., Tapan, M., and Kumbasar, N., 2014. Performance based rapid seismic assessment method (PERA) for reinforced concrete frame buildings. *Advances in Structural Engineering*, 17(3):439-459.

Ilki, A., Demir, C., Ates, A.O., Demir, U., Kupçu, E., Goktug, Ü., Altinok, MA., Karakaya, B., and F., Narlitepe, 2019. Development of a framework for rapid earthquake risk assessment for substandard buildings in Turkey, *2nd International Workshop on Advanced Materials and Innovative Systems in Structural Engineering* (IWAMISSE), Istanbul, Turkey.

Khan, SA., Pilakoutas, K., Hajirasouliha, I., Guadagnini M., Mulyani, R., Ahmadi, R. and W. Elwaeli, 2012. A new framework for earthquake risk assessment in developing countries, 15th World Conference on Earthquake Engineering, Lisbon, Portugal.

Kythreoti, S., 2002. Earthquake risk assessment and management case study: Cyprus. *Doctoral Dissertation*, The University of Sheffield, Sheffield, UK.

Lettow, S., and Eligehausen, R., 2006. Formulation of application rules for lap splices in the new Model Code Bond model. Presentation, Task group 4.5, Bond models, *Technical Report*, Stuttgart, Germany.

Mau, ST, and El-Mabsout, M., 1989. Inelastic buckling of reinforcing bars. *Journal of Engineering Mechanics*, 115(1):1–17.

Orangun, CO., Jirsa, JO., and Breen, JE., 1977. A reevaluation of test data on development length and splices. *Journal of the American Concrete Institute*, 74(3):114–122.

Schneider, PJ., and Schauer, BA., 2006. HAZUS - Its development and its future, *Natural Hazards Review*, 7(2): 40-44.

Trendafiloski, G., Wyss, M. and Rosset, P., 2011. Loss estimation module in the second generation software QLARM. In *Human Casualties in Earthquakes*, Springer Netherlands.

Turkish Seismic Design Code, 2007. Ministry of Public Works and Settlement, Ankara, Turkey.

Verderame, GM., Ricci, P., De Carlo, G., and Manfredi, G., 2009. Cyclic bond behaviour of plain bars. Part I: Experimental investigation, *Construction and Building Materials*, 23:3499–3511

Whitman, RV., 1973. Damage Probability Matrices for Prototype Buildings. Structures Publication 380. Department of Civil Engineering, Massachusetts Institute of Technology, *Technical Report*, Boston, Massachusetts

Yalcin, C. and M. Saatcioglu, 2000. Inelastic analysis of reinforced concrete columns. *Computers and Structures*, 77(5):539–555.

Zuo, J., and Darwin, D., 2000. Splice strength of conventional and high relative rib area bars in normal and high-strength concrete. *ACI Structural Journal*, 97(4), 630–641.

Author Index